



# **BRNO UNIVERSITY OF TECHNOLOGY**

VYSOKÉ UČENÍ TECHNICKÉ V BRNĚ

## **FACULTY OF CIVIL ENGINEERING**

FAKULTA STAVEBNÍ

## **INSTITUTE OF COMPUTER AIDED ENGINEERING AND COMPUTER SCIENCE**

ÚSTAV AUTOMATIZACE INŽENÝRSKÝCH ÚLOH A INFORMATIKY

# **HEAT TRANSFER ANALYSIS OF PHASE-CHANGE PROCESS IN TUBULAR EXCHANGER**

ANALÝZA PŘENOSU TEPLA PŘI FÁZOVÉ ZMĚNĚ V TRUBKOVÉM VÝMĚNÍKU

## **DISSERTATION THESIS**

DISERTAČNÍ PRÁCE

### **STUDENT:**

STUDENT

**ING. TOMÁŠ FEČER**

### **SUPERVISOR:**

ŠKOLITEL

**ING. JOSEF PLÁŠEK, PH.D.**

**BRNO 2021**

## **Acknowledgement**

The special thank goes to Institute of Building Services (TZB) on Faculty of Civil Engineering at Brno University of Technology. The experimental measurement of condensation process has been supported by company E S L a.s., Spirax Sarco spol. s r.o., Teplárny Brno, a.s. and personally by prof. Ing. Jiří Hirš, CSc., Dr. Ing. Milan Kubín, and Ing. Lucie Horká. The experimental measurement of evaporation process has been supported by doc. Ing. Petr Horák, Ph.D. and Ing. Marian Formánek, Ph.D.

## **Declaration of Identical form**

This dissertation thesis with the title "*Heat transfer analysis of phase-change process in tubular exchanger*" in the submitted electronics form is identical with submitted printed form. This identical form is declared by Ing. Tomáš Fečer.

September 14<sup>th</sup>, 2021

Ing. Tomáš Fečer

## **Declaration of Original work**

This dissertation thesis with the title "*Heat transfer analysis of phase-change process in tubular exchanger*" is original work and all information sources and materials are clearly declared in references. This originality is declared by Ing. Tomáš Fečer.

September 14<sup>th</sup>, 2021

Ing. Tomáš Fečer

## **Abstract**

The system HVAC is frequently based on cyclic phase change of boiling fluid. This phase change of boiling fluid (liquid-gas or gas-liquid) is coupled with boiling heat transfer by nucleate boiling, convective boiling and pre/post dryout effect. The nucleate boiling is depended on superheat of wall (i.e. heat flux) and presence of active nucleation sites. The two-phase convection boiling with dependence on mass flux and vapour quality is performed in liquid film between superheated wall and vapour core. The pre/post dryout effect is significant, when the liquid film is consumed and superheated wall is exposed directly to vapour core. This boiling heat transfer by nucleate boiling, convective boiling and pre/post dryout effect is simplified for engineering design on boiling heat transfer coefficient. Therefore, the dissertation thesis is aimed at experimental analysis of phase-change process in advanced engineering design.

**Keywords:** evaporation; condensation; water steam; refrigerant

# Content

<b>1. Introduction .....</b>	<b>7</b>
<b>2. State of Art .....</b>	<b>8</b>
2.1. Phase Transition .....	8
2.2. System of Thermodynamic.....	11
2.2.1. <i>Open system</i> .....	12
2.2.2. <i>Isolated system</i> .....	13
2.2.3. <i>Closed system</i> .....	13
2.3. Review of Historical evolution .....	14
2.4. Review of Current state.....	25
2.4.1. <i>Effect of Mass flux and Heat flux</i> .....	25
2.4.2. <i>Effect of Inclination angle</i> .....	25
2.4.3. <i>Effect of Inner diameter</i> .....	26
2.4.4. <i>Effect of Surface modification</i> .....	27
<b>3. Research Aim.....</b>	<b>28</b>
<b>4. Condensation .....</b>	<b>29</b>
4.1. Experimental Measurement.....	31
4.1.1. <i>Loop of Cooling water</i> .....	35
4.1.2. <i>Loop of Water steam</i> .....	37
4.2. Analysis of Measurement .....	37
4.2.1. <i>Thermal Resistance method</i> .....	38
4.2.2. <i>Wilson plot method</i> .....	39
4.2.3. <i>Predicted condensation HTC</i> .....	40
<b>5. Evaporation .....</b>	<b>43</b>
5.1. Experimental Measurement.....	43

5.1.1.	<i>Loop of Heating water</i>	46
5.1.2.	<i>Loop of Refrigeration system</i>	46
5.2.	Analysis of Measurement	49
5.3.	Results	54
5.3.1.	<i>Dependence of Heat flux on Mass flux</i>	54
5.3.2.	<i>Dependence of Heat flux on Temperature difference</i>	56
5.3.3.	<i>Dependence of Boiling HTC on Vapour quality</i>	59
5.3.4.	<i>Correlation with predicted Nusselt number</i>	61
5.4.	Discussion of Evaporation	63
5.5.	Obtained knowledge	64
<b>6.</b>	<b>Conclusion</b>	<b>66</b>
<b>7.</b>	<b>References</b>	<b>67</b>
<b>8.</b>	<b>Appendix</b>	<b>79</b>
8.1.	Experimental setup for Condensation	79
8.2.	Experimental setup for Evaporation	86
<b>9.</b>	<b>Annex</b>	<b>90</b>
9.1.	List of Tables	90
9.2.	List of Figures	91
9.3.	Author Biography	93
9.4.	Author Results	96

9.4.1.	2018 (RIV-F) Utility model.....	96
9.4.2.	2018 (RIV-R) Software Výměník .....	97
9.4.3.	2018 (RIV-R) Software FireDES.....	98
9.4.4.	2018 (RIV-D) Conference paper .....	99
9.4.5.	2021 (RIV-J) Research paper .....	100
9.4.6.	2021 (RIV-J) Research paper .....	101

# 1. Introduction

The historical purpose of building is protection of peoples and animals before outdoor environment. Later, this protection function of building is extended about quality of indoor climate in the building. The indoor climate in modern building is controlled by system of Heating, Ventilation and Air-Conditioning (HVAC) and this system HVAC includes often heat exchanger. The most energy efficient heat exchanger uses boiling heat transfer. Typically, refrigeration system in building is based on cyclic phase change of refrigerant from liquid to gas (evaporation on cooling side) and reverse phase change from gas to liquid (condensation on heating side). The engineering design of system HVAC in building is simplified on boiling heat transfer coefficient, but this boiling heat transfer coefficient includes heat transfer by nucleate boiling, convective boiling and dryout effect.

The advanced engineering design of system HVAC in building is directly depended on experimental research of boiling heat transfer.

## **2. State of Art**

The refrigeration system uses cyclic phase change of boiling refrigerant. This cyclic phase change liquid-gas (evaporation) and gas-liquid (condensation) is coupled with the heat transfer by nucleate boiling, convective boiling, and pre/post-Dryout effect. The nucleate boiling is dependent on the superheated wall (i.e. heat flux), and the presence of active nucleation site. The heat transfer between the superheated wall and vapour core is performed in liquid film by convective boiling. This convective boiling is dependent on the mass flux and the vapour quality. The pre/post-Dryout effect is associated with the annular flow when the liquid film is consumed, and the superheated wall is exposed directly to the vapour core.

The engineering design of refrigeration system is simplified on the application of boiling heat transfer coefficient. This boiling heat transfer coefficient includes the combination of heat transfer by nucleate boiling, convective boiling, and pre/post-Dryout effect. Therefore, the boiling heat transfer coefficient is necessary to study by experimental research.

### **2.1. Phase Transition**

In the summer of 2016, during the last year of my master's degree, I and my friend decided to take a hike to the Italian-Swiss peak of Piz Bernina. Behind the Marinelli Bombardieri hut, we had a panoramic view of Vedretta di Scerscen Superiore glacier, through which our journey continued. Gradually, we ran out of drinking water. Therefore, we decided to prepare of drinking water from the glacier. In this moment, the interesting physical phenomena phase transitions has begun.

Thermal energy of cooker is gradually transferred by conduction, convection and radiation into the ice through inner surface of the bowl.



Inside the ice, the intensity of the oscillating motion of the particles (kinetic energy) occupying the crystal lattice increases, while the mutual cohesion of the particles decreases (intermolecular forces). Droplets of water are gradually formed in the bowl from the ice when the kinetic energy has exceeded the force of the cohesive forces. The crystal structure of the substance collapses and the substance begins to melt - it turns into a liquid. The temperature at which the melting of substance depends only on external pressure is called the melting point. As the temperature remains constant during of melting, the transferred heat is completely consumed to overcome the cohesion of the particles. It is a form of latent heat of melting, more [1], [2], [3], and [4].



**Figure 2.1** – *Collapse of ice crystal structure with the formation of water drops [5].*

Droplets have formed the liquid from the ice. Over the surface of the liquid, a certain number of excited particles are transformed into a gaseous state at any temperature. This process is called vaporization (Vaporization also occurs from the solid). Each molecule changing into wet vapour during vaporization, consumes a quantity of heat to

overcome the attractive forces and resistance of external pressure. This quantity of heat is called latent heat of vaporization.

Over the liquid, the released particles of wet vapour can be reflected from the surrounding particles and captured back into the liquid. If the ratio of released to captured wet vapour particles is balanced, the liquid and the wet vapour are in equilibrium state. Wet vapour in equilibrium state with the liquid enters a state of saturation and is referred to as saturated steam. Pressure of saturated steam of liquid depends on temperature.

The heated liquid in bowl increases its temperature and the pressure of the saturated steam of the liquid has reached ambient pressure. The saturated steam expands into the surrounding and facilitates the formation of new steam. The liquid begins to vaporize from the surface and simultaneously as well as from its entire volume. This phenomenon is called boiling. The temperature and the pressure at which it occurs is called boiling point. The process by which the liquid changes its steam at its boiling point is called evaporation, according to [1], [2], [3], and [4].



**Figure 2.2** – *Evaporation of liquid at its boiling point* [6].

## **2.2. System of Thermodynamic**

Processes of phase transitions are performed in a space, which is called a thermodynamic system. This physical system is consisting of individual parts as referred as a set of elements. Other elements, which surround the set of elements is called surroundings. However, set of elements and surroundings are separated by a boundary. There is a mutual interaction between the elements of the system - the transformation of energy and substance, and its exchange with the

surroundings. These complex interactions are macroscopically observed by thermodynamics according to laws of thermodynamics. Laws of thermodynamics define a group of physical quantities. These intensive<sup>1</sup> and extensive<sup>2</sup> state quantities express the current state of the thermodynamics system. Intensive state quantities represent a qualitative part of the thermodynamic system, i.e., unrelated to its size. Quantitative parts of thermodynamics system are made by extensive state quantities, which in contrast with qualitative parts is dependent on related to its size.

### **2.2.1. Open system**

When both particles (mass transfer) and energy (heat transfer) are exchanged with the surroundings, the thermodynamics system is referred as an open system. These parts of thermodynamics system are involved in creating the climate of Earth. Deep ocean circulation is forming between Earth's polar and equatorial regions. Vaporization of seawater, cycles of melting and freezing of polar glaciers determines of velocity flow of deep ocean currents. Deep ocean currents are driven by difference in the density of seawater, which is controlled by the temperature (thermo) and salinity (haline). This process is known as thermohaline circulation. The thermohaline circulation allow transport both energy (heat) and matter (solids, dissolved substances and gasses) around the globe, see [7] and [8].

---

<sup>1</sup> pressure ( $p$ ), temperature ( $T$ ), density ( $\rho$ )

<sup>2</sup> volume ( $V$ ), mass ( $m$ ) with number of molecules ( $N$ ), internal energy ( $U$ ), entropy ( $S$ ), free energy ( $F$ )

## Thermohaline Circulation

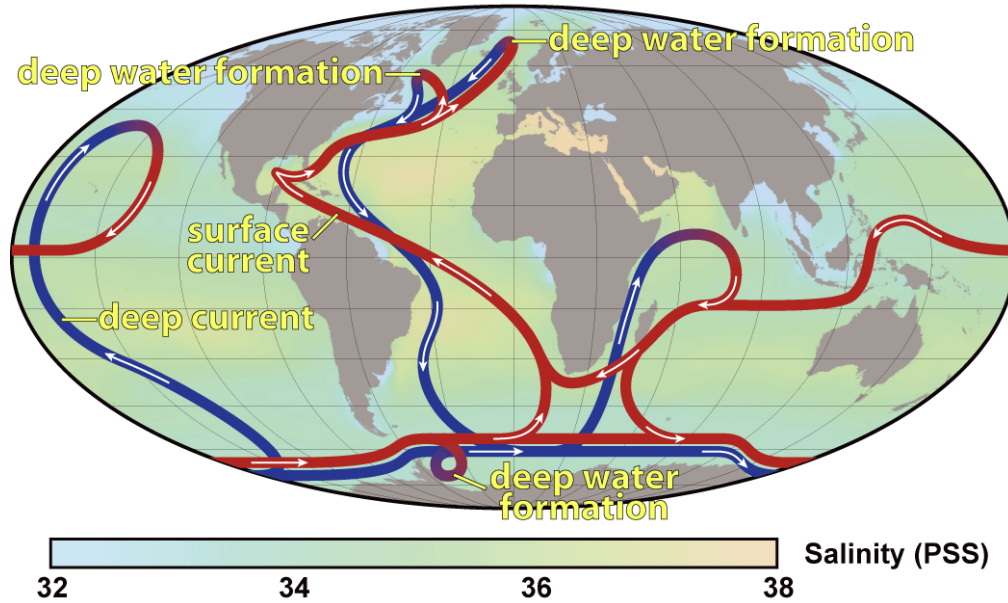


Figure 2.3 – Thermohaline circulation on the planet Earth [9].

### 2.2.2. Isolated system

The opposite of open system is an isolated system. Particles (mass transfer) and energy (heat transfer) are conserved and is not exchanged with the surroundings. According to second law of thermodynamics, the entropy of isolated system increases. Isolated systems spontaneously evolve towards thermal equilibrium—the state of maximum entropy of the system. The statistical physics describe the isolated system as micro-canonical ensemble with micro-canonical entropy, more [10], [11], [12], [13], and [14].

### 2.2.3. Closed system

The system is separated by a boundary from the surroundings and particles (mass transfer) is conserved during the exchange of energy (heat transfer). It is a middle between the isolated and the open system with is known input and output of results within specific time. This property is used for the design of engineering equipment and

is described in detail and examined in dissertation thesis, see [7], [15], [16], [17], and [18].

### **2.3. Review of Historical evolution**

At the end of the 18<sup>th</sup> century, experimental physics experienced new discoveries and descriptions of events. Units of heat is introduced, the amounts of heat needed to produce specified increases of temperature, volume, or pressure under various conditions were measured. The notion of latent heat has begun to appear [16], [19], and may perhaps be the first study of boiling is introduced by German doctor and theologian, Johan Gottlob Leidenfrost in 1756. Leidenfrost observed of repulsion between a liquid and very hot solid. Between a drop of water and hot plate was produced an insulating vapour layer. This layer kept the liquid from boiling rapidly and the droplet hovers over the surface and slowly evaporate. The phenomenon is named as Leidenfrost phenomena, see [20].

During the scientific excursion in the Alps, a trader Jean André Deluc [21], born in Geneva in 1727 investigated the melting of ice. He noticed:

*"I let freeze water in drinking glasses in which I had put thermometers whose bulbs thereby were enclosed by the ice. Thereafter I brought this little apparatus to a fire. The thermometers rose until the very moment as the ice started to melt. All fire that intruded the ice thereafter ceased to have an effect on the thermometers, because it was used to make water, while at the same time the light that freed itself from the burning particles, radiated through the ice."*

Joseph Black [22], a Scottish chemist and Professor in Glasgow and Edinburgh, born in Bordeaux in 1728, made similar observations where reported pure fact:

*"But these phenomena, though inconsistent with such a supposition, and with the old opinion of the manner in which heat produces fluidity, strongly support the one which I have proposed and can all be explained by it without difficult. They actually shew the extrication from the freezing water of that quantity of heat which is concealed in its composition so long as it retains the form of fluid. This experiment shews, that when water is cooled in a state of perfect rest, in a small vessel, it is disposed to retain this concealed heat, which I have been used to call its latent heat, a little more strongly than in ordinary circumstances."*

James Clerk Maxwell [23], a Scottish Professor of experimental physics in the University of Cambridge, born in Edinburgh in 1831 noted in his textbook in 1871:

*"DEFINITION: Latent heat is the quantity of heat which must be communicated to a body in a given state in order to convert it into another without changing its temperature."*

An analogous consideration of the process of changing the state let him finally conclude:

*"The most important cases in which heat is thus employed are-*

- 1. The conversion of solids into liquids. This is called melting' or fusion. In the reverse process of freezing or solidification heat must be allowed to escape from the body to an equal amount.*
- 2. The conversion of liquids (or solids) into the gaseous state. This is called evaporation, and its reverse condensation.*
- 3. When a gas expands, in order to maintain the temperature constant, heat must be communicated to it, and this, when properly defined, may be called the latent heat of expansion.*
- 4. There are many chemical changes during which heat is generated or disappears".*

In 1873, Van Der Waals, Johannes Diderik, Dutch physicist, defended doctoral thesis, in which he states Waals' equation of state - the first successful theory of phase transitions, more [24]. Between 1875 and 1878, Josiah Willard Gibbs, American mathematician, in his landmark paper titled On the Equilibrium of Heterogeneous Substances derived the phase rule - identifies the degree of freedom of a multiphase system, see [25].

Since 1916, the condensation of water steam on cold surface is studied by German engineer, Ernst Kraft Wilhelm Nusselt [26]. Nusselt analytically expressed dependence of boiling heat transfer coefficient on volume amount of condensed water steam on the cold wall surface. This analytical dependence assumes smooth and uniform liquid film on plane wall surface, and then condensation heat transfer coefficient is equal to inverse function of thermal resistance of condensed water steam.

However, the analytical Nusselt solution is not corresponded with experimental measurement over 20 %. Gradually, the solution is extended about sub-cooling of liquid condensate by Bromley [27], about non-linear temperature distribution in liquid film by Rohsenow [28], about momentum movement by Sparrow [29], [30], [31] and laminar downward flow of condensate by Bankoff [32] or Marschall and Lee [33]. This difference over 20 % is caused by waves on surface of liquid film, and this wave's effect improves heat transfer between vapour core and liquid film as published Kapitsa [34] in 1948.

Since 1930, after Nusselt's study, the research of boiling heat transfer begun to form of three main groups: a pool boiling, a flow boiling and a supercritical fluid, see Table 2.1.



**Table 2.1** – Chronological table of major references relating to boiling heat transfer [35].

A. D.	Pool Boiling	Flow Boiling	Supercritical Fluids
1930	(Jakob-Fritz)		( ) : Nucleate Boiling
	(Cryder-Gilland)		< > : Transition Boiling
	{Nukiyama}		[ ] : Film Boiling
35	(Jakob-Linke)		{ } : Boiling Curve
	(Jakob) (Fritz-Ende)		( ) : Forced Convection
			< > : Critical Heat Flux
			{ } : Free Convection
1940	(Insinger-Bliss)		
	(Bonilla-Perry)		
45	(Cicelli-Bonilla)		
	{Farber-Scorah}		
1950	[Bromley]	{McAdams et al}	
	(Rohsenow-Clark)	{Buchberg et al}(Gunther)	
		{Jens-Lottes}	
	(Rohsenow) (Kutateladze)		
	(Forster-Zuber) (Ellion)	{Clark-Rohsenow}	
55	(Westwater-Santangelo) (Yamagata et al)		
	(Nishikawa) (Rohsenow-Griffith)	{Dengler-Addoms}	
	(Bankoff) (Zuber) [Hsu-Westwater]	{Gambill-Green}	{Dickinson-Welch}
	(Gaertner-Westwater) (Levy)	{Zenkevich}(Lottes-Petrich-Marchaterre)	{Styrikowitsch-Milopolsky-Shitzman}
	(Bankoff-Mikesell) (Forster-Greif)		
1960	(Kurihara-Myers)	{Griffith-Wallis}(Bell)	
	(Nishikawa-Yamagata) (Berenson)		
	(Moore-Mesler) (Hsu-Graham)	{Collier et al}	{Petukov et al}(Goldmann)
		{Janssen-Levy}	
	(Hughmark) (Ishiki-Tamaki)	{Shrock-Grossman}	
	[Koh][Sparrow-Cess]	{Swenson-Carver-Szoeko}	
	(Zuber) (Séméria) (Stephan)	{Macbeth}(Tong)(Barnett)	{Fritsch-Grosh} (Shitsman)
	(Moissis-Berenson) (Cole-Shulman)		
	(Bergles-Rohsenow) (Sharp) (Merte-Clark)	{Hewitt}	
	(Siegel-Keschock)		
65	(Geartner)	{Hewitt et al}	{Nishikawa-Miyabe}
		{Bertoletti et al}	
	(Marto-Rohsenow) (van Strahlen) (Nishikawa)	{Macbeth}	{Knapp-Sabersky}
	[Nishikawa-Ito][Ito-Nishikawa]		
	(Kusuda-Nishikawa)	{Bennett}	{Grigull-Abazic}
	(Lippert-Dougal) (Katto-Yokoya)		{Goldstein-Aung}
	(Cooper-Lloyd) (Ishibashi-Nishikawa)	{Herkenrath-Mörkenstein}	{Nishikawa-Ito}
	(Bergles)		
1970	(Mikic-Rohsenow) (Czikk-Gottzmann et al)	{Hewitt-Kearsey-Collier}	{Ackerman}
	(Honda-Nishikawa)	{Collier}(Tong)	{Yamagata-Nishikawa-Hasegawa}
	[Nishikawa-Ito-Kuroki-Matsumoto]	{Nishikawa-Fujii-Yoshida}	
	(Gottzmann-O'neil-Minton)		{Nishikawa-Ito-Yamashita}
75			
		{Groeneveld-Delmore}	
	(Nishikawa-Fujita)		
	(Arai-Fukushima-Nakajima-Fujie-Nakayama)		
		{Katto}	
		{Shah}	
1980	(Stephan-Abdelsalam) (Nishikawa-Ito)	{Katto}	
	(Bergles)		
	(Cooper) (Witte-Lienhart)		
	(Nishikawa-Fujita-Obta)		
	(Nishikawa) (Webb) (Haramura-Katto)		
		{Katto}	

Regimes of pool boiling are identified by Shiro Nukiyama in his pioneering publication in 1934, see [36]. He clarified and provided an overview of the boiling phenomena using his apparatus. The Apparatus was composed of electrically heated Ni-Chrome and platinum wires immersed in liquids, see Figure 2.4.

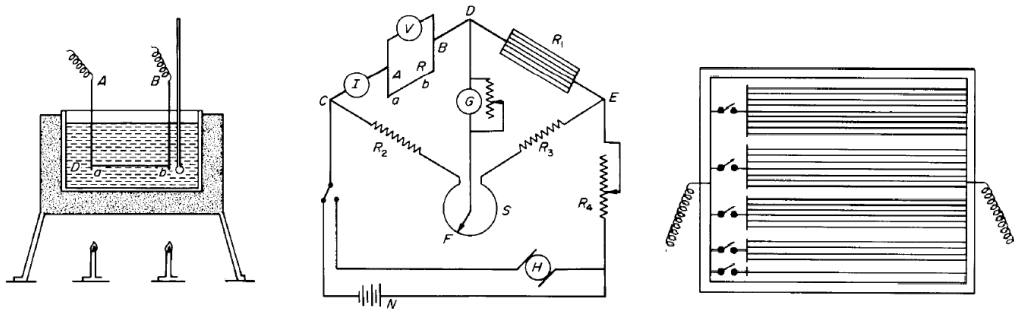


**Figure 2.4** – Equipment of Nukiyama for metal wire experiments [36].

He evaluated of temperature and heat flux from this experiment and observed:

- maximum heat flux points appear in the nucleate boiling region is diversiform
- maximum heat flux points appear in the nucleate boiling region
- minimum heat flux point appears in the film boiling region

Consequently, the pool boiling is divided according to the value of the wall superheat temperature  $\Delta T_{\text{sat}}$  [K]. This temperature is the difference between the wall temperature,  $T_{\text{wall}}$  [°C] and the saturation steam temperature of liquid,  $T_{\text{sat}}$  [°C]. Boiling regimes is divided into [37]:

- natural convection boiling  $\Delta T_{\text{sat}} < 5 \text{ K}$
- nucleate boiling  $5 \text{ K} < \Delta T_{\text{sat}} < 30 \text{ K}$
- transition boiling  $30 \text{ K} < \Delta T_{\text{sat}} < 200 \text{ K}$
- film boiling  $200 \text{ K} < \Delta T_{\text{sat}}$

After Nukiama, others researchers came across a phenomenon which is referred as a Critical Heat Flux (CHF). In 1948, another pioneering

works has come. Kutateladze addressed pool boiling of critical heat flux by using a dimensional analysis based on the similarity between critical heat flux and column flooding [38]. In 1958, ten years after Kutateladze, Novak Zuber and Myron Tribus present to an analytical expression. This analysis permits the prediction of the maximum nucleate heat flux in pool boiling of saturated or subcooled liquids, see [39]. Gradually, new studies are published and are improved the predictive of CHF, see [39], [40], [41], [42], [43], and five different of CHF mechanisms are prevalent in the literature: bubble interference, hydrodynamic instability, macro layer dryout, hot/dry spot, and interfacial lift-off, see [45].

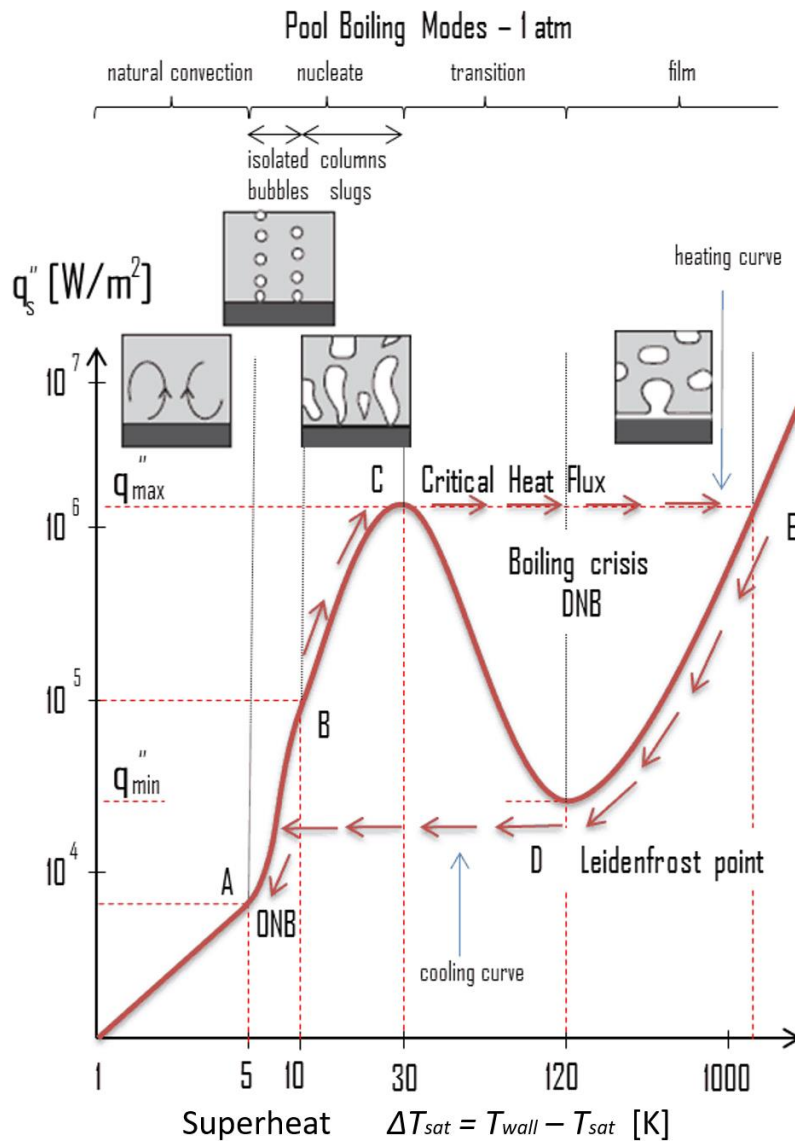


**Figure 2.5** – Pool boiling curve, according to [37].

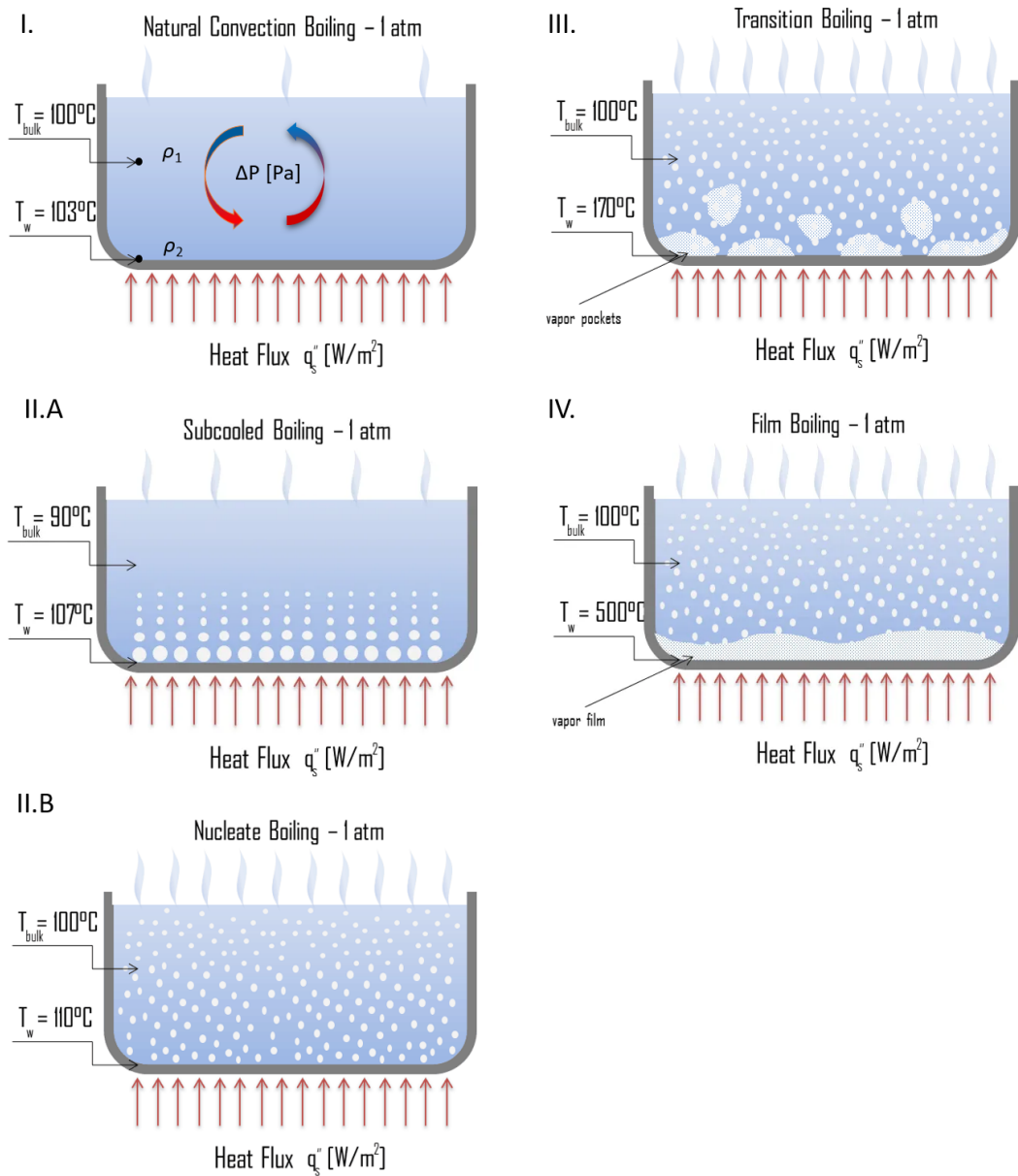


**Figure 2.6** – Regimes of pool boiling. During the transition from natural convection to nucleate boiling, sub cooling boiling occurs. The temperature of most of the liquid is below the saturation temperature and bubbles formed at the surface may condense in the liquid [37].

Gradually, several experimental studies described of flow boiling of saturated liquids, see [46], [47], [48], and [49]. The obtained results indicated to the contribution from two heat transfer mechanisms: nucleate boiling and convective boiling. When is the nucleate boiling of flow boiling dominated the heat transfer coefficient increases with

increasing heat flux and saturation pressure, and is independent of mass flux and vapour quality. In opposite case, when is dominated convective flow boiling, the heat transfer coefficient is independent of heat flux and increases with increasing mass flux and vapour quality.

In 1963, Chen proposed the first flow boiling correlation for evaporation in vertical tubes to attain widespread Use. The region of interest was range of vapour quality of approximately 1 to 70% and was strictly to defined by following conditions:

- saturated, two-phase fluid in convective flow
- vertical, axial flow
- stable flow
- no slug flow
- no liquid deficiency
- heat flux less than critical flux

The nucleate pool boiling correlation of Forster and Zuber (1955) is used to calculate the nucleate boiling heat transfer coefficient in this study. The turbulent flow correlation of Dittus-Boelter (1930) for tubular flows is used to calculate the liquid-phase convective heat transfer coefficient. The average deviation between calculated and measured boiling coefficients from ten experimental cases was  $\pm 12\%$  [50].

In 1976, Shah presented graphical form a general correlation named CHAPT and published it in 1982. The graphical correlation is focus on the estimation of heat transfer coefficients during saturated boiling at subcritical heat flux in tubes and annuli. The mean deviation of graphical correlation is 14 % with data points from 19 independent experimental studies. The correlation was shown to be applicable to both horizontal and vertical tubes [51].

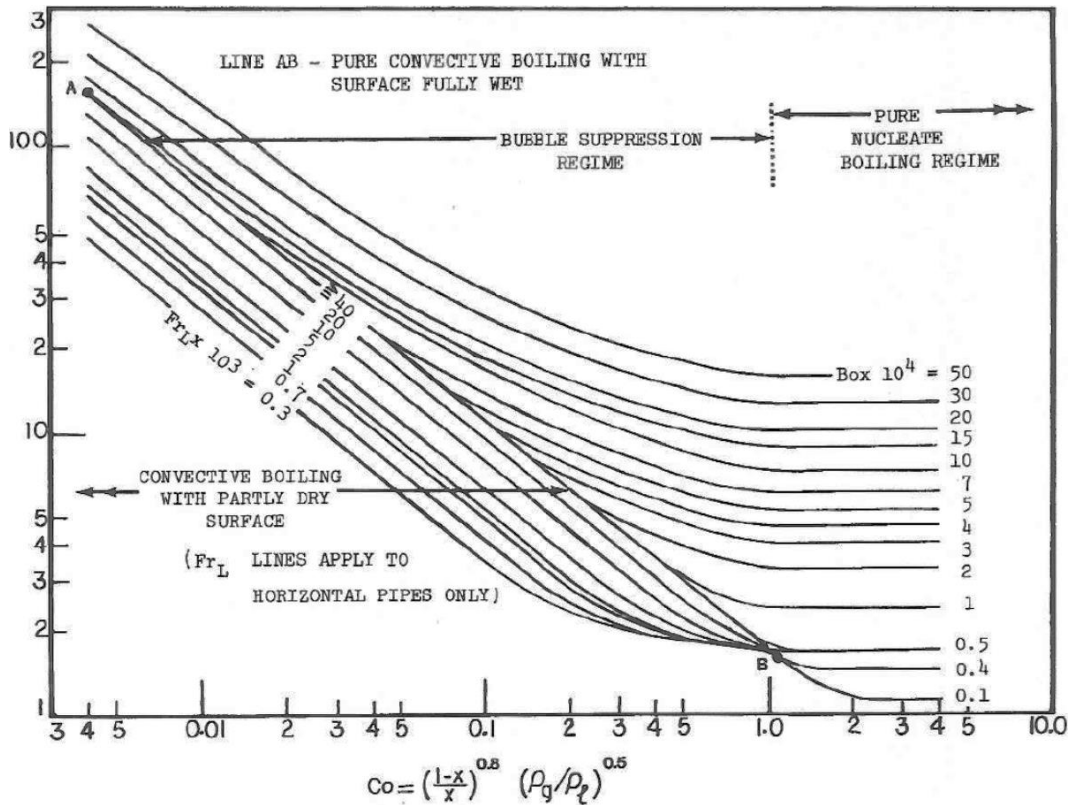


**Figure 2.7** – The chart correlation of Shah [51].

In 1986, Gungor and Winterton introduced a general correlation for forced convection boiling has been developed. The general correlation is based on data bank consists of over 4300 data points. The mean deviation between the calculated and measured boiling heat transfer coefficient is 21.4 % for saturated boiling and 25.0 % for subcooled boiling, more [52].

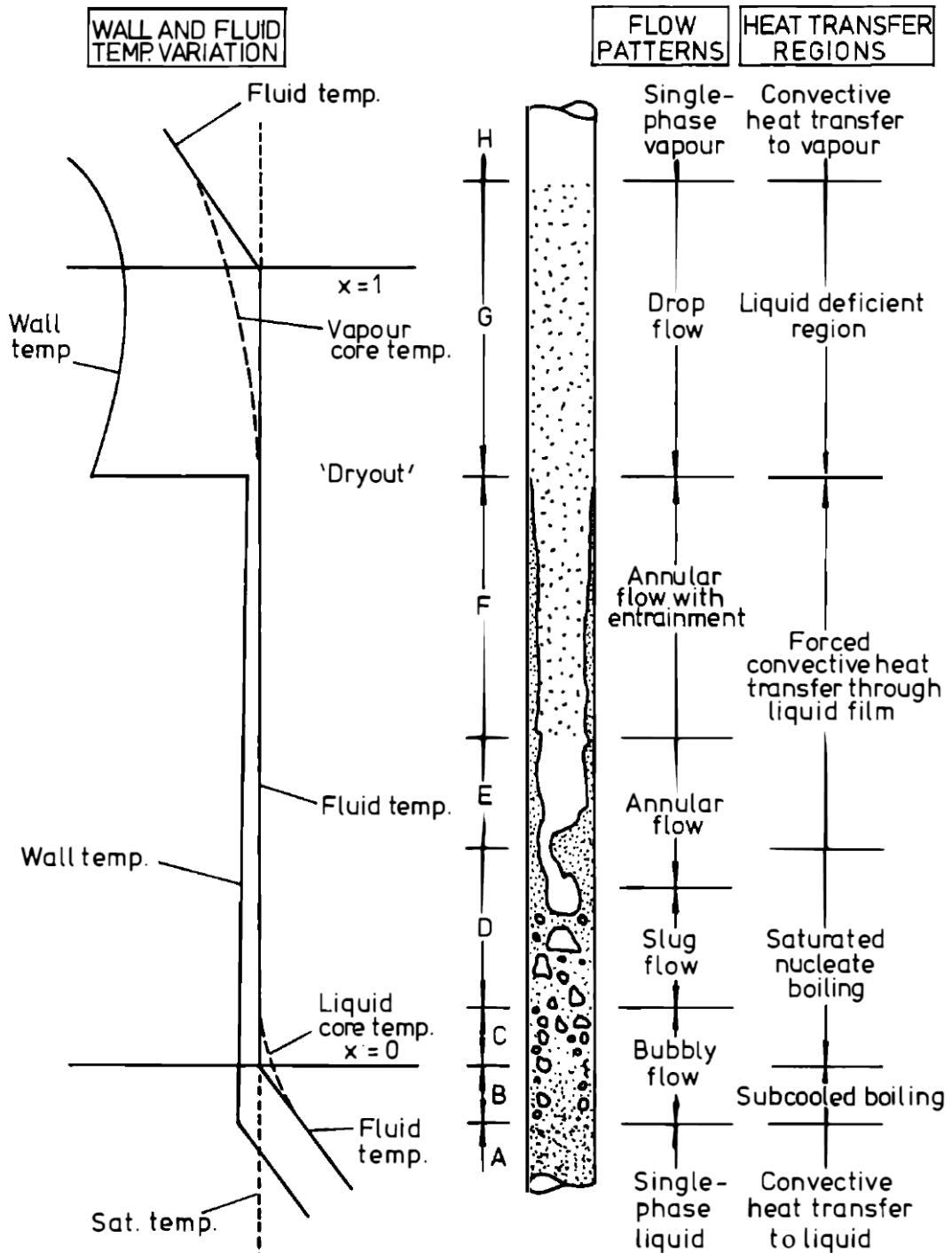


**Figure 2.8** – Heat transfer regions in convective boiling in a vertical tube, according to [53].

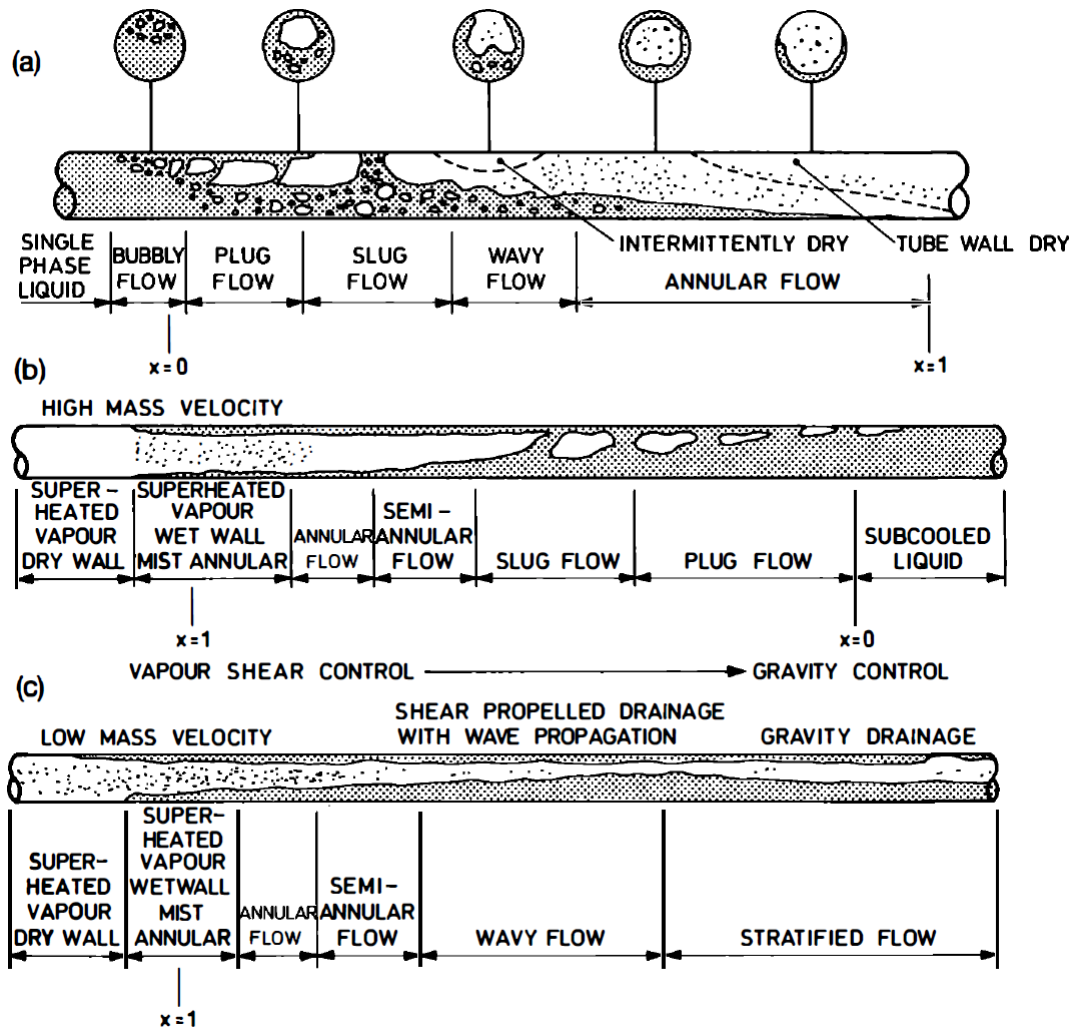


**Figure 2.9** – Two phase flow patterns in horizontal tubes: (a) evaporation, (b) condensation with high liquid loading, (c) condensation with low liquid loading, see [53].



## **2.4. Review of Current state**

The boiling heat transfer is studied since 1916. Nevertheless, the boiling heat transfer is not concluded yet. The boiling heat transfer is studied currently on mass flux, heat flux, inclination angle, inner diameter, surface modification etc.

### **2.4.1. Effect of Mass flux and Heat flux**

The dependence of boiling heat transfer coefficient on mass flux and vapour quality is published by Jung et al. [54], Bandhauer et al. [55], Arslan and Eskin [56], Adekunle et al. [57], Aroonrat and Wongwises [58] as well as Meyer et al. [59]. This dependence is decreased for lower mass flux (below or equal to  $100 \text{ kg}\cdot\text{m}^{-2}\cdot\text{s}^{-1}$ ) as reported Cavallini et al. [60]. This decreased dependence of boiling heat transfer coefficient on lower mass flux is substituted by dependence on temperature difference (superheat of wall) as reported Meyer and Ewim [61]. The dependence of boiling heat transfer coefficient on heat flux for fixed mass flux is published by Greco and Vanoli [62]. Later, Greco [63] reported about dependence of boiling heat transfer coefficient on heat flux, but only in the region with dominated nucleate boiling. The effect of low mass flux is studied by Meyer et al. [64] on value ( $50 \text{ kg}\cdot\text{m}^{-2}\cdot\text{s}^{-1}$ ), by Akhavan-Behabadi and Esmailpour [65] on value ( $46 \text{ kg}\cdot\text{m}^{-2}\cdot\text{s}^{-1}$ ), by Aprea et al. [66] on value ( $45.5 \text{ kg}\cdot\text{m}^{-2}\cdot\text{s}^{-1}$ ), by Lee and Son [67] on value ( $35.5 \text{ kg}\cdot\text{m}^{-2}\cdot\text{s}^{-1}$ ), by Dalkiliç et al. [68] on value ( $29 \text{ kg}\cdot\text{m}^{-2}\cdot\text{s}^{-1}$ ) and by Arslan and Eskin [69] on value ( $20 \text{ kg}\cdot\text{m}^{-2}\cdot\text{s}^{-1}$ ), and Hojati et al. [70] on value ( $16.5 \text{ kg}\cdot\text{m}^{-2}\cdot\text{s}^{-1}$ ).

### **2.4.2. Effect of Inclination angle**

The impact of inclination angle on boiling heat transfer coefficient is published by Akhavan-Behabadi et al. [65] in range 7 – 62 % and range

40 – 56 % by Ewim et al. [61]. The lowest boiling heat transfer coefficient is reported identically for vertical downward flow.

Meyer et al. [71], [72] published impact of inclined tube ( $\beta = -90^\circ$  to  $90^\circ$ ) on condensation R134a with mass flux ( $G = 50$  to  $600 \text{ kg}\cdot\text{m}^{-2}\cdot\text{s}^{-1}$ ), heat flux ( $q = 4.50$  to  $6.90 \text{ kW}\cdot\text{m}^{-2}$ ), vapour quality ( $x = 20$  to  $80 \%$ ) and saturation temperature ( $T = 30$  to  $50 \text{ }^\circ\text{C}$ ) in inclined smooth tube with inner diameter  $8.38 \text{ mm}$ . This boiling heat transfer coefficient for vertical downward flow is obtained in range  $900 - 1500 \text{ W}\cdot\text{m}^{-2}\cdot\text{K}^{-1}$ .

Akhavan-Behabadi et al. [65], [73] and Mohseni et al. [74], [75] reported impact of inclined tube ( $\beta = -90^\circ$  to  $90^\circ$ ) on evaporation R134a with mass flux ( $G = 46$  to  $170 \text{ kg}\cdot\text{m}^{-2}\cdot\text{s}^{-1}$ ), heat flux ( $q = 4.56$  to  $9.13 \text{ kW}\cdot\text{m}^{-2}$ ), vapour quality ( $x = 20$  to  $80 \%$ ) and saturation temperature ( $T = -26$  to  $-2 \text{ }^\circ\text{C}$ ) in inclined smooth and corrugated tube with inner diameter  $8.9 \text{ mm}$ . This boiling heat transfer coefficient for vertical downward flow is obtained in range  $600 - 2500 \text{ W}\cdot\text{m}^{-2}\cdot\text{K}^{-1}$ . This effect of inclination angle is increased for lower mass flux as reported Akhavan-Behabadi et al. [73], Mohseni et al. [75] and Meyer et al. [59].

### **2.4.3. Effect of Inner diameter**

The impact of inner diameter on boiling heat transfer coefficient is coupled with the capillary effect and flow pattern map (since size mesoscale between macro-channel and micro-channel) as noted Thome et al. [76]. The classification of channel is based on hydraulic diameter and Mehendale et al. [77] offered classification on conventional channel ( $D > 6 \text{ mm}$ ), macro-channel ( $6 \text{ mm} \geq D > 1 \text{ mm}$ ), meso-channel ( $1 \text{ mm} \geq D > 100 \text{ }\mu\text{m}$ ) and micro-channel ( $100 \text{ }\mu\text{m} \geq D > 1 \text{ }\mu\text{m}$ ). Later, Kandlikar and Grande [78] proposed classification on conventional channel ( $D > 3 \text{ mm}$ ), mini-channel ( $3 \text{ mm} \geq D > 200 \text{ }\mu\text{m}$ ) and micro-channel ( $200 \text{ }\mu\text{m} \geq D > 10 \text{ }\mu\text{m}$ ).

This impact of inner diameter on boiling heat transfer coefficient is reported by Yan and Lin [79] (the boiling heat transfer coefficient with inner diameter 2.0 mm is about 30 – 80 % higher than for larger pipe  $D \geq 8.0$  mm), Huo et al. [80] (the boiling heat transfer coefficient in tube with inner diameter 2.01 mm is higher than in tube with inner diameter 4.26 mm) and Bandhauer et al. [55] (the boiling heat transfer coefficient increases with mass flux and vapour quality, but decrease with inner diameter).

#### **2.4.4. Effect of Surface modification**

The impact of surface modification on boiling heat transfer coefficient is summarized by Cavallini et al. in review [81]. Yu et al. [82] reported about increased boiling heat transfer coefficient in horizontal micro-fin tube up to 200 % in comparison with horizontal smooth tube. Aroonrat and Wongwises [58] published about dimpled tube enhances the Nusselt number about 1.3 - 1.4 times in comparison with smooth tube. Solanki and Kumar [83] reported about increased boiling heat transfer coefficient about 18 – 32 % for dimpled helically coiled tube in comparison with smooth helically coiled tube, as well as increasing about 51 – 61 % in comparison with smooth straight tube. Woodcock et al. [84] published about surface modification by Piranha Pin-Fin (PPF) and (MECH-X) for ultra-high heat flux (up to  $10 \text{ MW}\cdot\text{m}^{-2}$ ) in electronics devices. The increased boiling heat transfer coefficient in tube with corrugated surface is reported by Akhavan-Behabadi and Esmailpour [65], Aroonrat and Wongwises [76], Laohalertdecha et al. [85] and Dalkiliç et al. [86].

### 3. Research Aim

The dissertation thesis is focused on heat transfer analysis of phase change process in a tubular exchanger. This phase change of fluid from liquid to gas (evaporation) or reverse phase change from gas to liquid (condensation) is applied in heating/cooling system, air-conditioning, etc. This phase change process is experimentally analysed for water steam (condensation) and refrigerants (evaporation).

- ❖ **Condensation** of water steam in tubular heat exchanger with 55 spiral micro tubes with inner diameter 3.0 mm.
- ❖ **Evaporation** of refrigerant R134a, R404a, and R407c with low mass flux in vertical smooth tube with inner diameter 32 mm.

The main result of dissertation thesis is extension of current state of knowledge about boiling heat transfer and dissemination of obtained knowledge in scientific journal.

## 4. Condensation

The condensation of water steam in copper spiral micro tube with total length  $1300 \pm 2$  mm and inner diameter  $3.0 \pm 0.01$  mm is lower than critical inner diameter 5.05 mm. This small inner diameter increases interaction of water steam with copper surface of tube. This thermodynamics interaction is caused by surface tension in fluid. The impact of surface tension on condensation heat transfer is analysed experimentally in the bundle of 55 spiral micro tubes, see Fig. 4.1. Number of waves on one tube is 28. The outer surface area of spiral micro tube is  $15\,904$  mm<sup>2</sup> with inner surface area  $11\,928$  mm<sup>2</sup>. Total outer surface area of 55 tubes is  $874\,703$  mm<sup>2</sup> with total inner surface area  $656\,028$  mm<sup>2</sup>, see Fig. 4.2 and Fig. 4.3.

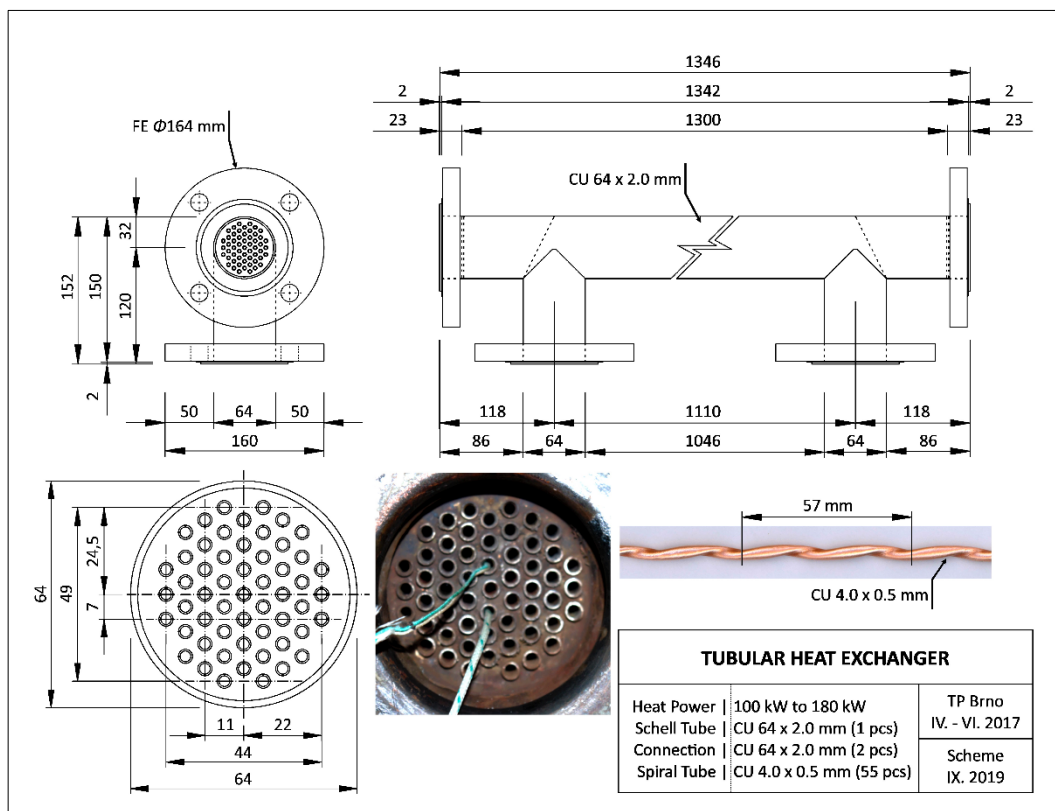


**Figure 4.1** – Scheme of tubular heat exchanger with 55 spiral micro tubes.

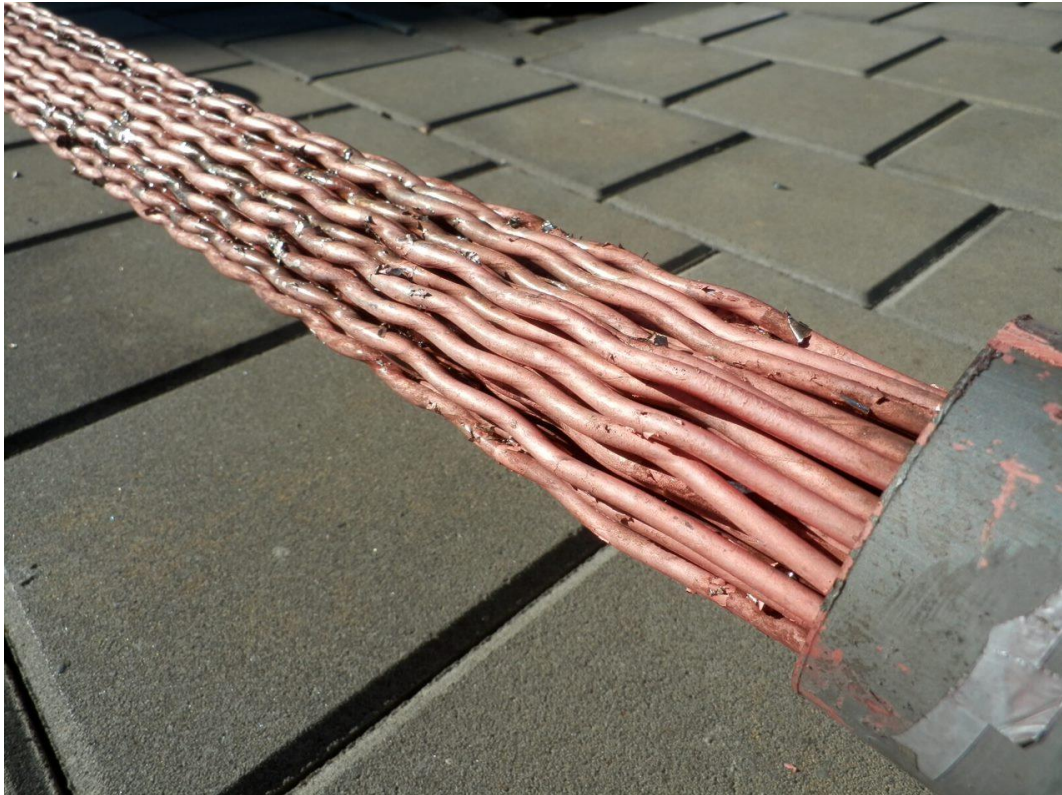


**Figure 4.2** – *Bundle of 55 spiral micro tubes for water steam.*



**Figure 4.3** – *Detail of spiral micro tubes with inner diameter 3.0 mm.*

## 4.1. Experimental Measurement

This experimental measurement is performed with mass flux of water steam in range from 0 to  $1000 \text{ kg}\cdot\text{m}^{-2}\cdot\text{s}^{-1}$  and the heat flux is obtained in range from 0 to  $300 \text{ kW}\cdot\text{m}^{-2}$ . The vapour quality is measured in range from 0 % (total condensation) to 92% (mixture of liquid water with vapour water). The condensation of water steam in 55 spiral micro tubes is measured for vertical parallel-flow (11 252 data points = 15.6 hours), vertical counter-flow (12 949 data points = 17.9 hours), inclined parallel-flow (11 807 data points = 16.4 hours) and inclined counter-flow (17 171 data points = 23.8 hours), see Fig. 4.4 and Appendix 8.1.



**Figure 4.4** – *Experimental setup of tubular heat exchanger.*

The shell of heat exchanger is insulated by Rockwool 800 76/50 mm with thermal conductivity  $\lambda = 0.04 \text{ W}\cdot\text{m}^{-1}\cdot\text{K}^{-1}$ . The surface temperature of shell tube below the insulation is monitored by 27 pcs thermocouples in the distance from 95 to  $1209 \pm 1 \text{ mm}$ . Thermocouples are ALMEMO AHLBORN NiCr-Ni type T190-0 and T 190-1 (temperature range -25 to  $400 \text{ }^\circ\text{C}$ ), T 190-2 (temperature range -10 to  $105 \text{ }^\circ\text{C}$ ) and T 190-3

(temperature range -45 to 200 °C). Sensitivity of thermocouples is  $\pm 0.10$  K, see Fig. 4.5. Thermocouples on the copper surface of shell tube are glued in ultra-high thermal conductivity MasterGEL and fixed by aluminium tape. The surface temperature of shell tube is recorded by ALMEMO Multi-function data logger type 5590 in time step 5 seconds, see Fig. 4.6. The experimental measurement is processed by co-author software application, see Fig. 4.7 – 4.9.

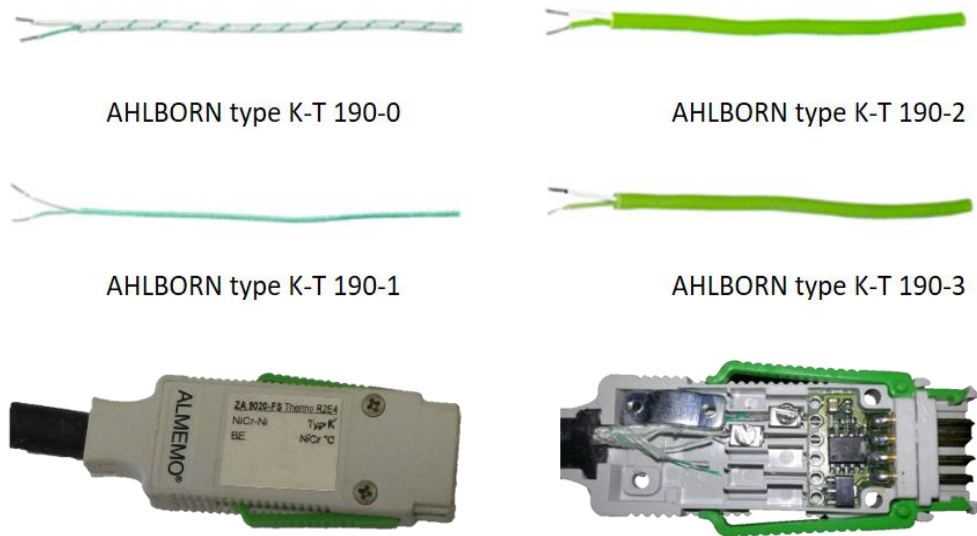


**Figure 4.5** – AHLBORN thermocouple wires with ALMEMO connector.

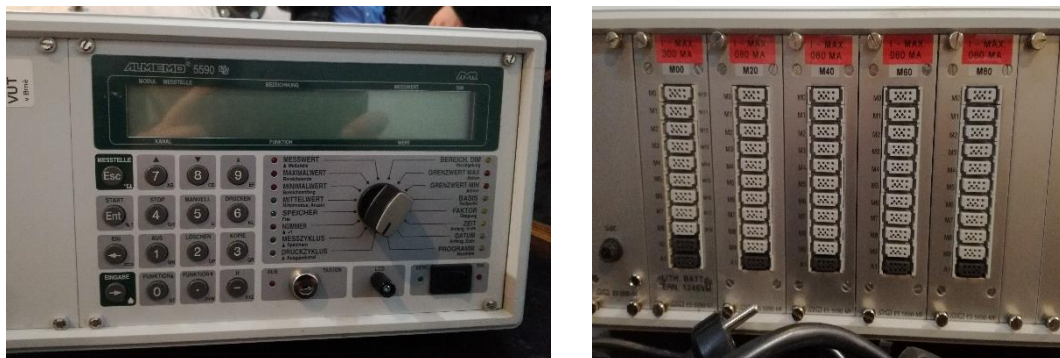


**Figure 4.6** – ALMEMO Multi-function data logger 5590.



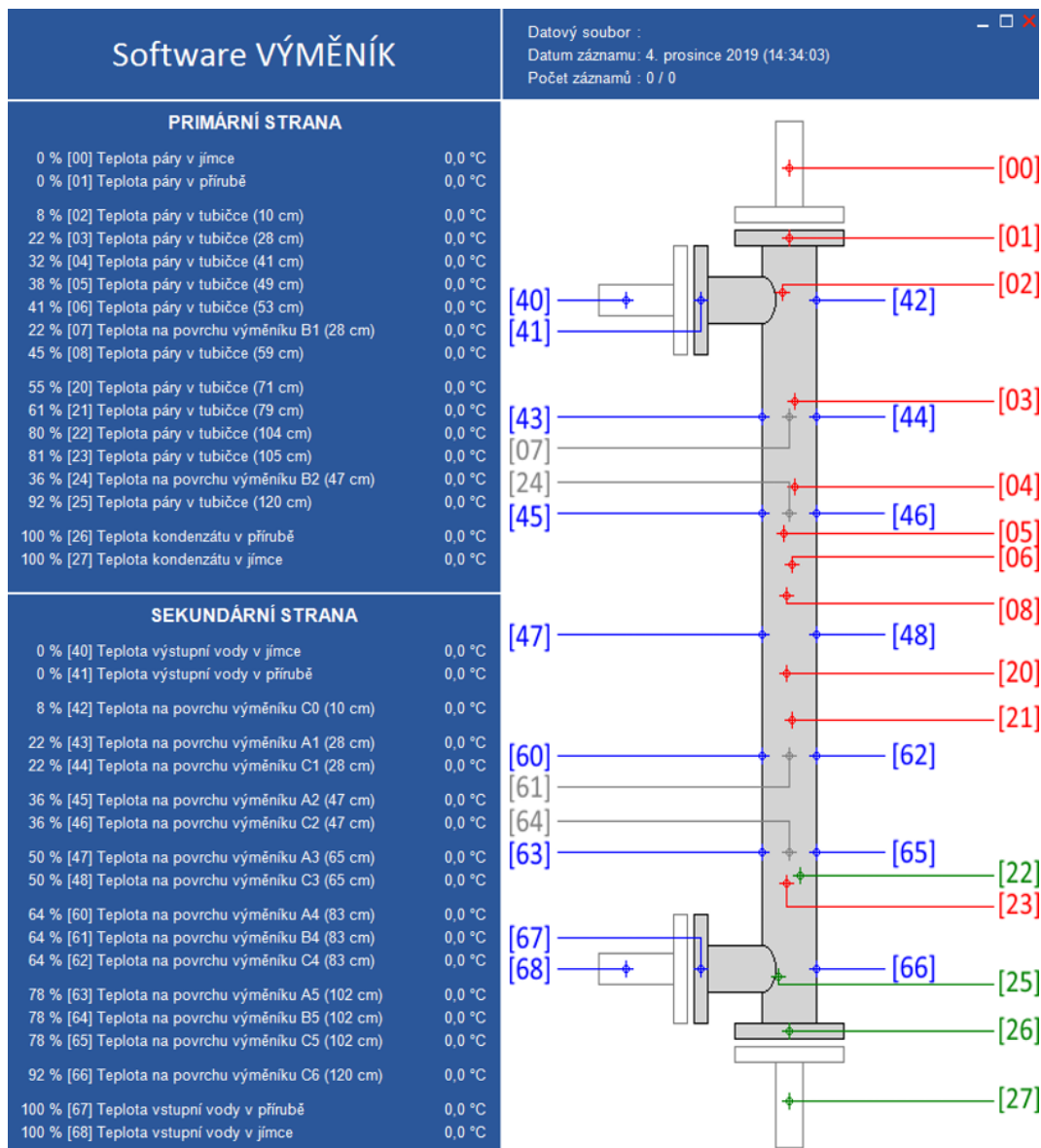


**Figure 4.7** – Condensation in the parallel-flow with inclination 45°.

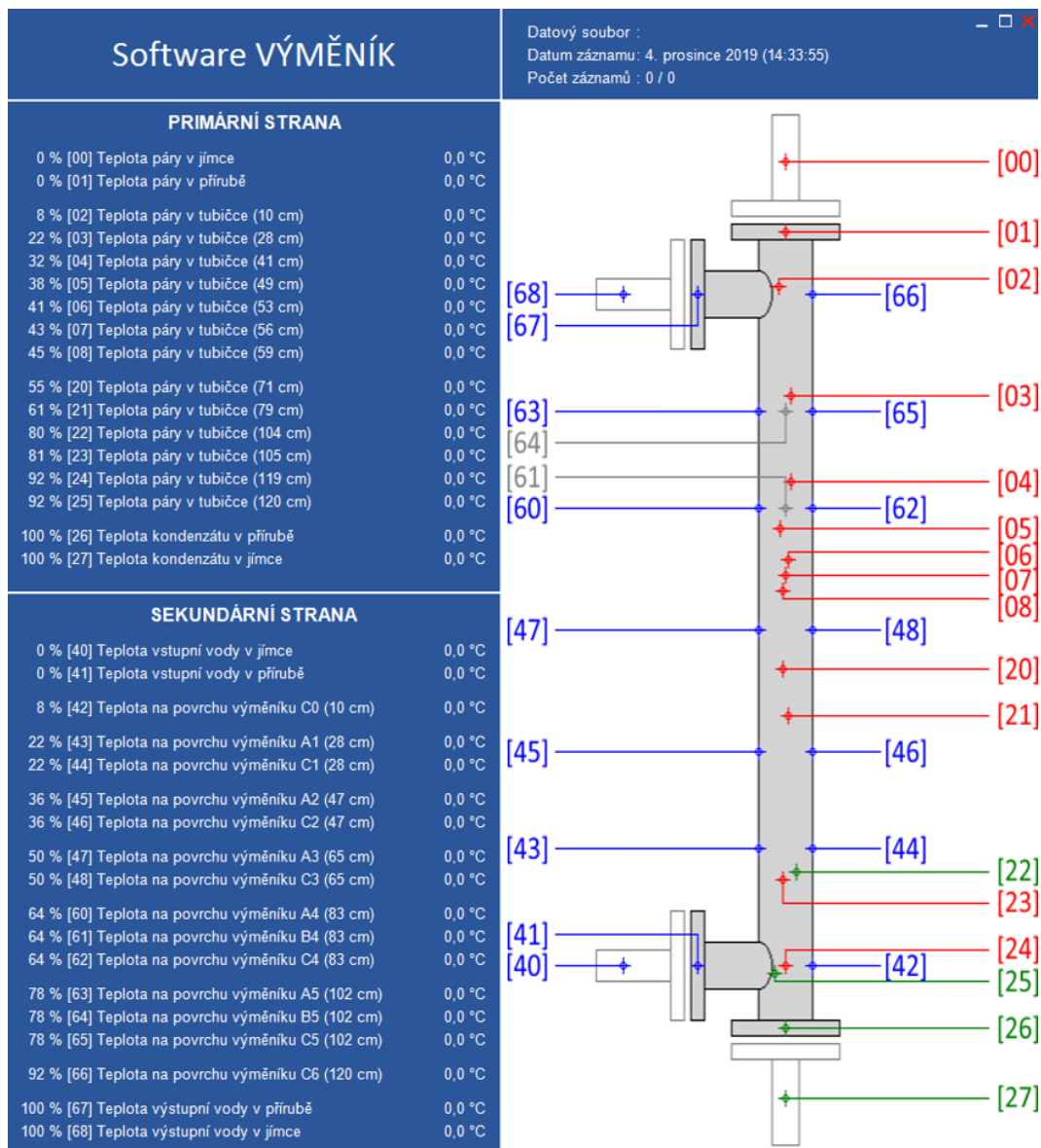


**Figure 4.8** – Condensation in the counter-flow with inclination 45°.

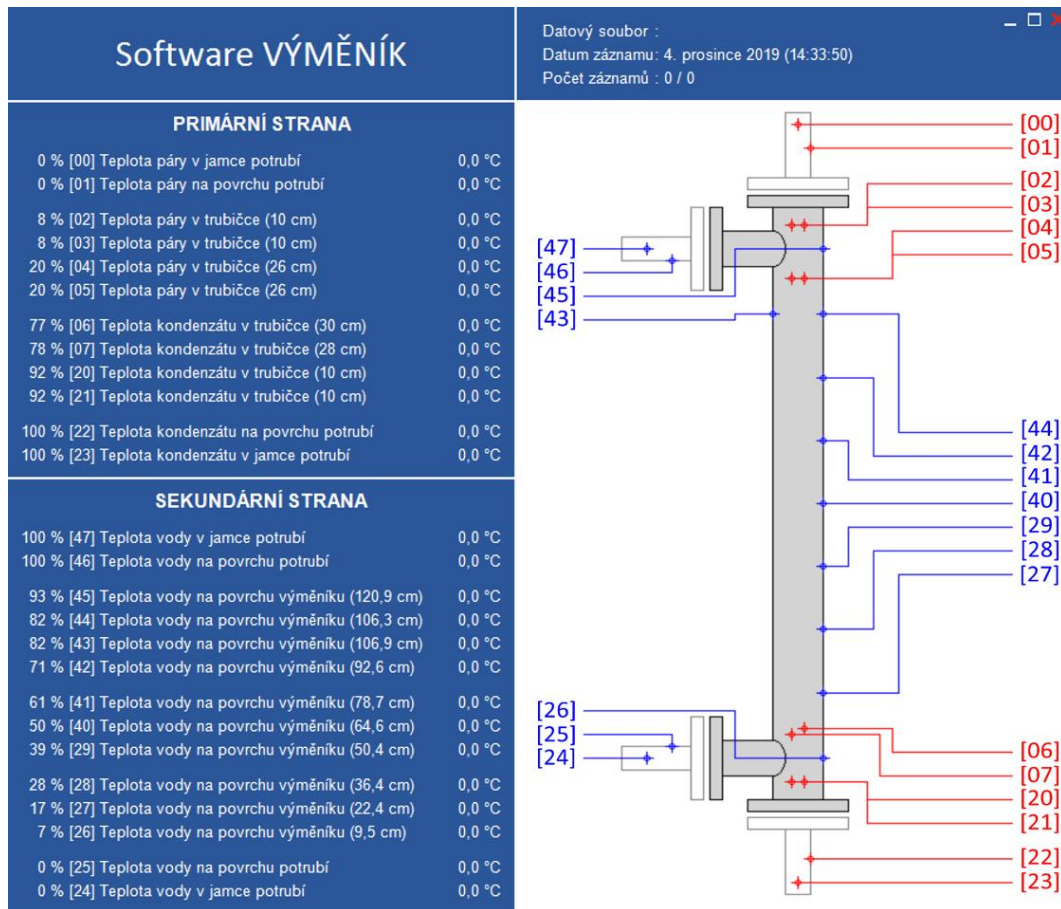


Figure 4.9 – Vertical condensation in the parallel/counter-flow.

#### 4.1.1. Loop of Cooling water

The primary cooling water loop is composed of water pump Grundfos Magna UPE 40 -120/F with a variable mass flow rate and with the maximum flow rate  $22 \text{ m}^3 \cdot \text{hour}^{-1}$ . The volume flow rate of cooling water is measured by water meter G. GIOANOLA, IARC/25 R80, class T90 (reading accuracy  $0.0001 \text{ m}^3$ ) with recording system AMiNi 4 DW2, see Fig. 4.10. The volume flow rate of cooling water is assigned by a manual valve on the constant value at the beginning of measurement. The stable source of cooling water is a clean tap water. The secondary cooling water loop is composed of insulated water tank with a total volume  $1.0 \text{ m}^3$  and is connected with primary cooling water loop by

a manual three-way valve, see Fig. 4.11. The secondary cooling water loop is used for thermocouples calibration.



**Figure 4.10** – Water meter G. GIOANOLA, IARC/25 R80, Class T90 with MaR recording system.



**Figure 4.11** – Manual three-way valve.

### 4.1.2. Loop of Water steam

The water steam of the supply pipe is reduced by pressure regulating valve Spirax Sarco BRV73 from 9.0 bar/400 °C to 3.5 bar/183 °C, see Fig. 4.12. Furthermore, the water steam flow is regulated by a manual valve according to pressure manometer. Behind the manual valve is desludging loop with a ball valve for capture and condensate drain. These parts are insulated by Rockwool 800 76/50 mm with thermal conductivity  $\lambda = 0.04 \text{ W}\cdot\text{m}^{-1}\cdot\text{K}^{-1}$ . The condensate of the heat exchanger is measured by mass flow and it is returned to the heating plant.



Figure 4.12 – Manual valve for pressure regulating by Spirax Sarco BRV73.

### 4.2. Analysis of Measurement

The transferred condensation heat  $Q_v$  [W] between water steam and cooling water is calculated from (Eq. 4.1), where specific enthalpy of water steam condensate is  $h_{c,out} = 419.10 \text{ kJ/kg}$  and condensation

temperature is  $t_{v,out} = 100$  °C. The logarithmic mean temperature difference  $\Delta T$  [K] for counter-flow involvement is determined from (Eq. 4.2). The one-dimensional state steady overall heat transfer coefficient  $k$  [W/(m·K)] for cylindrical wall in condensing zone is calculated by (Eq. 4.3). Finally, the condensation heat transfer coefficient  $\alpha_v$  [W/(m<sup>2</sup>·K)] is determined by Thermal resistance method and Wilson plot method.

$$Q_v = m_v \cdot (h_{v,in} - h_{c,out}) \quad (\text{Eq. 4.1})$$

$$\Delta T = \frac{(t_{v,in} - t_{w,out}) - (t_{v,out} - t_{w,in})}{\ln\left(\frac{t_{v,in} - t_{w,out}}{t_{v,out} - t_{w,in}}\right)} \quad (\text{Eq. 4.2})$$

$$k = \frac{Q_v}{n_T \cdot (L - H) \cdot \Delta T} \quad (\text{Eq. 4.3})$$

#### 4.2.1. Thermal Resistance method

The overall heat transfer coefficient  $k$  [W/(m·K)] of cylindrical wall includes inverted sum of thermal resistance of solid tube wall  $R_T$  [m·K/W] and two unknown surface thermal resistances on internal  $R_v$  [m·K/W] and external surface  $R_w$  [m·K/W] of tube, see (Eq. 4.4). The external thermal resistance  $R_w$  [m·K/W] of tube on cooling water site can be estimated by average heat transfer coefficient  $\alpha_w$  [W/(m<sup>2</sup>·K)] from (Eq. 4.5). The Nusselt number  $Nu_w$  [-] in for cooling water flow along the tube is calculated from (Eq. 4.5), according to Gröber [88]. Subsequently the condensation heat transfer coefficient  $\alpha_v$  [W/(m<sup>2</sup>·K)] on inner surface of tube can be obtained from (Eq. 4.6).

$$\frac{1}{k} = \frac{1}{\pi \cdot D_i \cdot \alpha_v} + \frac{\ln(D_e / D_i)}{2 \cdot \pi \cdot \lambda_T} + \frac{1}{\pi \cdot D_e \cdot \alpha_w} = R_v + R_T + R_w \quad (\text{Eq. 4.4})$$

$$Nu_w = 1.86 \cdot \left( Re_w \cdot Pr_w \cdot \frac{D_e}{L} \right)^{0.33} \quad (\text{Eq. 4.5})$$

$$\alpha_w = \frac{Nu_w \cdot \lambda_w}{D_e} \quad (\text{Eq. 4.6})$$

### 4.2.2. Wilson plot method

The Wilson plot method is suitable for determination of heat transfer coefficient in case where two fluids are separated by solid wall, in detail [89]. The condensation heat transfer coefficient  $\alpha_v$  [W/(m<sup>2</sup>·K)] on internal surface of tube is expressed by exponential function (Eq. 4.7). The equation (Eq. 4.7) substituted to (Eq. 4.4) is rewritten to linear equation ( $y = A \cdot x + B$ ) where parameter  $x = q_v^{-0.80}$  and  $y = k^{-1}$ , see (Eq. 4.8). The unknown parameters  $A$  [m<sup>-1</sup>] (Eq. 4.9) and  $B$  [m·K/W] (Eq. 4.10) of linear regress function are determined by least square method. The obtained parameters  $A$  [m<sup>-1</sup>] and  $B$  [m·K/W] are used for calculation of heat transfer coefficient  $\alpha_w$  [W/(m<sup>2</sup>·K)] and condensation heat transfer coefficient  $\alpha_v$  [W/(m<sup>2</sup>·K)].

$$\alpha_v = C \cdot q_v^{0.80} \quad (\text{Eq. 4.7})$$

$$\frac{1}{k} = \left( \frac{1}{\pi \cdot D_i \cdot C} \right) \cdot q_v^{-0.80} + \left( \frac{\ln(D_e / D_i)}{2 \cdot \pi \cdot \lambda_T} + \frac{1}{\pi \cdot D_e \cdot \alpha_w} \right) \quad (\text{Eq. 4.8})$$

$$A = \frac{1}{\pi \cdot D_i \cdot C} \quad (\text{Eq. 4.9})$$

$$B = \frac{\ln(D_e / D_i)}{2 \cdot \pi \cdot \lambda_T} + \frac{1}{\pi \cdot D_e \cdot \alpha_w} \quad (\text{Eq. 4.10})$$

### 4.2.3. Predicted condensation HTC

The condensation heat transfer coefficient (HTC)  $\alpha_v$  [W/(m<sup>2</sup>·K)] can be predicted by equations obtained by theoretical or experimental way. The first chosen equation is theoretically determined by Nusselt [26] in 1916. The Nusselt equation (Eq. 4.11) is expressed from amount of condensate and thermal resistance of laminar film condensate on surface wall.

$$\alpha_v = 0.9428 \cdot \left[ \frac{g \cdot \rho_c \cdot l_{23} \cdot \lambda_c^3}{\nu_c \cdot (t_v - t_T) \cdot L} \right]^{0.25} \quad (\text{Eq. 4.11})$$

The Nusselt equation (Eq. 4.11) is valid for stationary steam because flowing steam in tube causes waves on condensate surface. The wave's effect increases condensation heat transfer about 20.6 % as published Whitham [90] in (Eq. 4.12).

$$\alpha_v = 1.137 \cdot \left[ \frac{g \cdot \rho_c \cdot l_{23} \cdot \lambda_c^3}{\nu_c \cdot (t_v - t_T) \cdot L} \right]^{0.25} \quad (\text{Eq. 4.12})$$

Next chosen equation (Eq. 4.13) is theoretically determined for calculation of condensation heat transfer coefficient and includes the wave's effect, too. This equation is chosen for comparison because the equation is often applied in engineering tasks. The equation (Eq. 4.13) published by Hobler [91] is valid for many kind of fluids with pressure  $0.07 < p_v$  [MPa]  $< 17$  and specific heat flux  $1.0 < q_v$  [kW/m<sup>2</sup>]  $< 1\ 000$ .

$$\alpha_v = 0.00252 \cdot \left( \frac{\rho_v \cdot l_{23}}{\rho_c - \rho_v} \cdot \frac{\rho_c}{\sigma_c} \right)^{0.33} \cdot \frac{\lambda_c^{0.8} \cdot q_v^{0.7}}{\mu_c^{0.5} \cdot c_c^{0.167} \cdot T_v^{0.37}} \cdot p_v^{\frac{10}{T_v - 273.15}} \quad (\text{Eq. 4.13})$$

Another chosen equation (Eq. 4.14) determined by experimental way is formulated in typical exponential function  $\alpha = C \cdot q^n$  similar as substitution in Wilson plot method, see (Eq. 4.7). The base of function is specific heat flux  $q$  [W/m<sup>2</sup>] and prefix constant  $C = 1.537$  depends



on kind of surface and fluid properties, more Kutateladze [92]. The exponent of function takes into account boundary conditions and for constant boil temperature without impact of radiation heat transfer is  $n = 0.75$ .

$$\alpha_v = 1.537 \cdot q_v^{0.75} \quad (\text{Eq. 4.14})$$

The last chosen equation (Eq. 4.15) for comparison is determined by experimental way and predict minimal value of Nusselt number  $Nu_{\min}$  [-] depending on fluid properties included in Prandtl number  $Pr_c$  [-]. The characteristics length  $d$  [m] in Nusselt number  $Nu_{\min}$  [-] is  $d = (0.125 \cdot v_c^2)^{0.33}$ , according to Hausen [93].

$$Nu_{\min} = 0.16 \cdot Pr_c^{0.61} \quad (\text{Eq. 4.15})$$

**Table 4.1** – *The correlation of obtained results with other studies*

Experimental study	Material	$D_i$ [mm]	$L$ [mm]	$p_{v,in}$ [kPa]	$t_{v,in}$ [°C]	$\alpha_v$ $W \cdot m^{-2} \cdot K^{-1}$	$\epsilon$ [%]
Kubín et al. [94]	Cu	2.00	1285	102.2 to 185.8	100.2 to 117.9	7229	100.0
Shammari et al. [95]	Cu	28.2	3000	16.0 to 22.0	56.6 to 63.18	6502	89.9
Urban et al. [96]	Fe	6.50	1036	226.3	134.9	7285	100.8
Ma et al. [97]	Cu	30.0	410	100.0	100.0	6151	85.1
Kim el al. [98]	Fe	46.2	1800	300 to 7500	130 to 300	5443	75.3
Goodykoonz et al. (page 19) [99]	Fe	15.9	2133	111.7	102.2	7008	96.9
Goodykoonz et al. (page 20) [99]	Fe	15.9	2133	166.9	114.4	6650	92.0
Goodykoonz et al. (page 25) [99]	Fe	15.9	2133	266.8	129.4	8455	117.0
Goodykoonz et al. (page 29) [99]	Fe	15.9	2133	116.5	103.3	8920	123.4
Goodykoonz et al. (page 31) [99]	Fe	15.9	2133	244.1	126.7	6639	91.8
Goodykoonz et al. (page 32) [99]	Fe	15.9	2133	243.4	126.7	8160	112.9

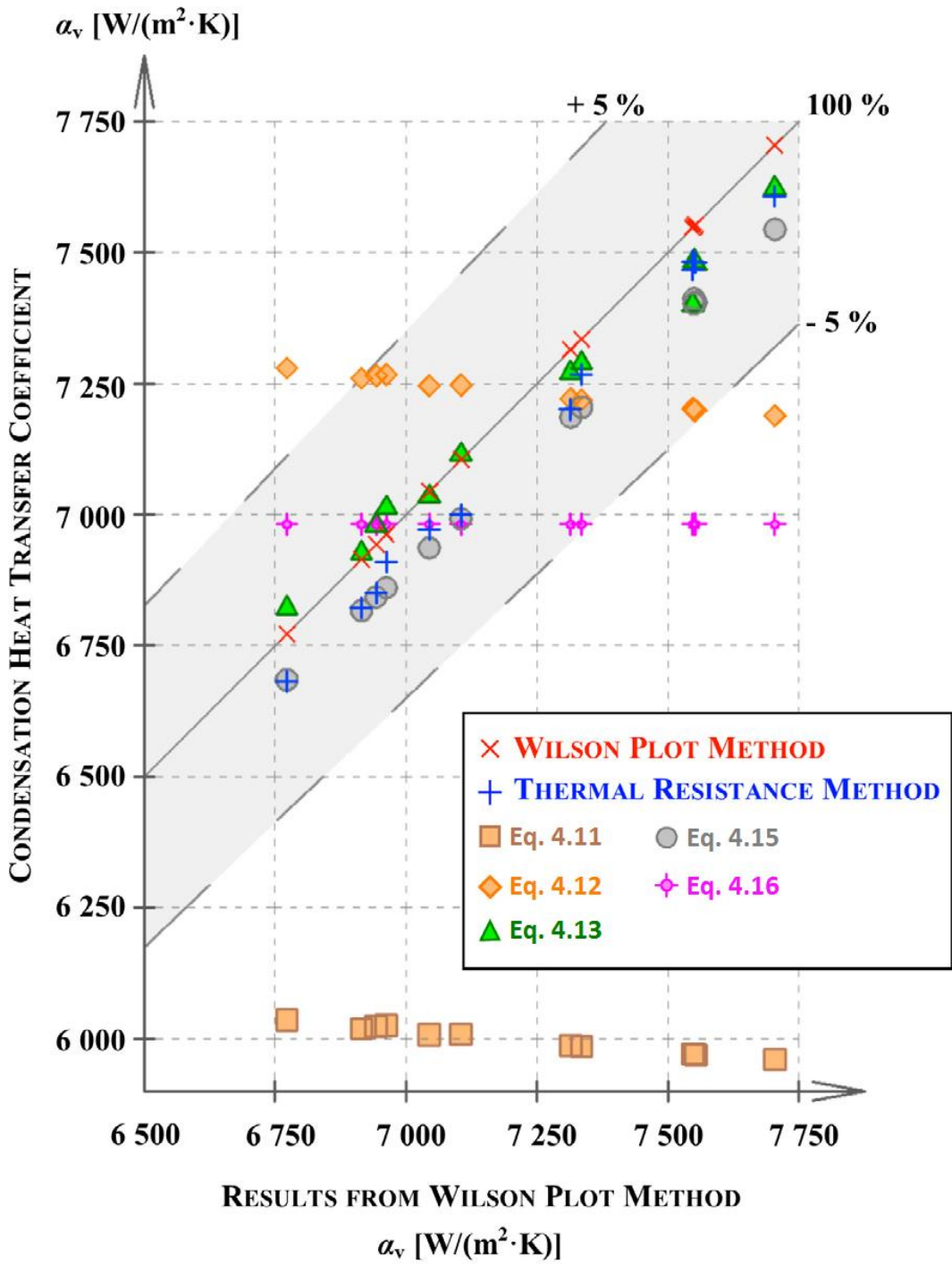


Figure 4.13 – Comparison of tested equations related to Wilson plot method.

## 5. Evaporation

The experimental measurement is based on the energy balance between the refrigerant R134a, R404A and R407C with the low mass flux and the heating water in parallel/counter flow. The laminar flow of heating water in the annular space is the simplification of numerical analysis on the analytical solution. This analytical solution of annular temperature distribution in the fully developed laminar velocity profile is known as the Graetz-Nusselt problem. The analytical solution allows the calculation of local inner surface temperature of evaporator tube and subsequent solution of local boiling heat transfer coefficient. The total energy balance on the evaporator tube is necessary for the calculation of local phase change of refrigerant. This steady-state of energy balance is performed over 34.7 hours for refrigerant R134a (24 951 data points), 32.2 hours for refrigerant R404A (23 215 data points), and 30.7 hours for refrigerant R407C (22 096 data points).

### 5.1. Experimental Measurement

The experimental vertical evaporator tube is created from smooth copper tube Cu 35 x 1.5 mm with an inner diameter  $32.0 \pm 0.01$  mm in total length  $2030 \pm 2$  mm. The upper inlet of refrigerant to vertical evaporator tube is expansion valve Honeywell AEL 222200 with manual adjusting pressure 1 – 7 bar. The bottom outflow of refrigerant from the vertical evaporator tube guarantees downward flow with natural gravity. This vertical evaporator tube is surrounded by an outer shell copper tube Cu 42 x 1.5 mm with an inner diameter  $39.0 \pm 0.01$  mm. The annular space with thickness  $2.0 \pm 0.01$  mm between centred tubes (pipe-in-pipe) is used for the laminar flow of heating water. This heating water in the annular space is studied in parallel/counter flow with the steady downward flow of refrigerant. The connection of heating water

to the annular space is on one side. The shell tube is insulated by Armacell HT 042/19 mm with thermal conductivity  $\lambda = 0.039 \text{ W}\cdot\text{m}^{-1}\cdot\text{K}^{-1}$ . The surface temperature of shell tube below the insulation is monitored by 32 pcs thermocouples in the distance from 80 to  $105 \pm 1 \text{ mm}$ , see Fig. 5.1. The thermocouple is ALMEMO type NiCr-Ni with a sensitivity  $\pm 0.10 \text{ K}$  in the temperature range from  $-25$  to  $400 \text{ }^\circ\text{C}$ . The thermocouple on the copper surface of shell tube is glued in the ultra-high thermal conductivity MasterGEL and fixed by aluminium tape. The surface temperature of shell tube is recorded by ALMEMO Multi-function data logger type 5690 in time step 5 seconds, see Appendix 8.2.

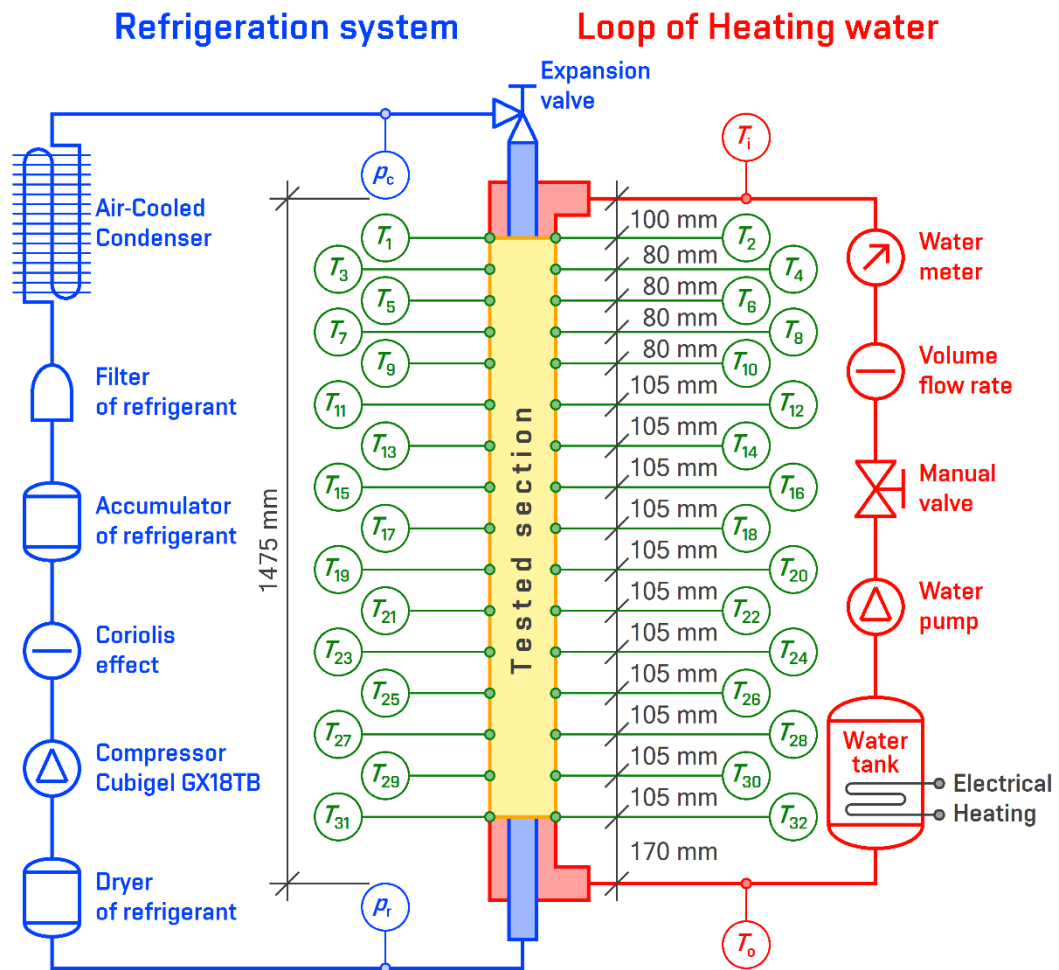


Figure 5.1 – Scheme of sensor location [100].

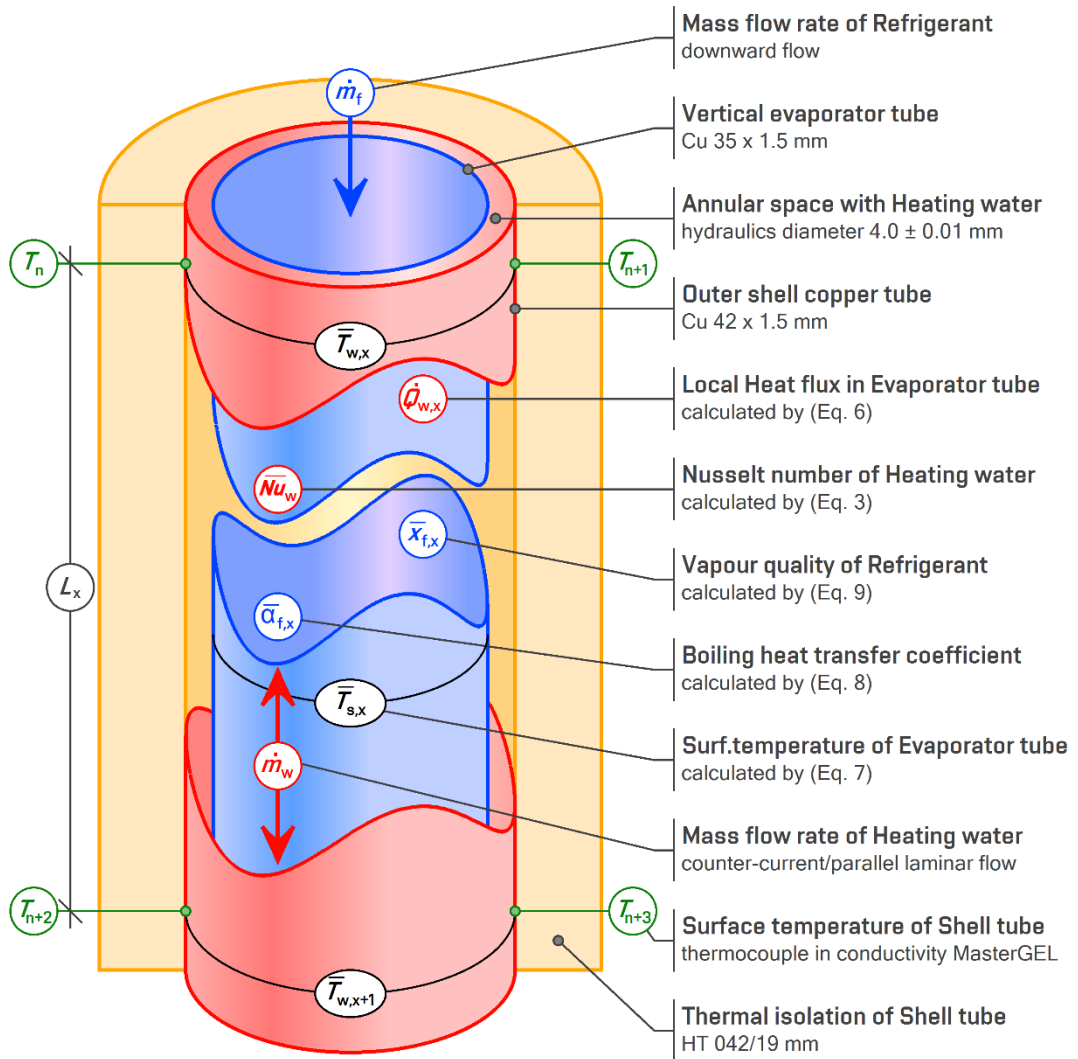


Figure 5.2 – Scheme of calculation part [100].



Figure 5.3 – Compressor unit (left photo) and expansion valve (right photo).

### 5.1.1. Loop of Heating water

The heating water loop is composed of water pump GRUNDFOS UPS 25/70 with a variable mass flow rate in the range from 0.0283 to 0.0600  $\text{m}^3\cdot\text{hour}^{-1}$ . The volume flow rate of heating water is monitored by Kamstrup Multical 402 and controlled by the water meter. The volume flow rate of heating water is assigned by a manual valve on the constant value at the beginning of measurement. The stable source of heating water is a water tank with a total volume 0.400  $\text{m}^3$ . The heating water in the water tank is heated electrically at setpoint temperature up to 56  $^{\circ}\text{C}$ .

### 5.1.2. Loop of Refrigeration system

The refrigeration system is based on compressor Cubigel GX18TB VE09 with a cooling capacity from 286 to 2568 W, and the mass flow rate of refrigerant in a range from 8.48 to 92.88  $\text{g}\cdot\text{s}^{-1}$ . The compressor is lubricated by oil ISO VG 46 ESTER. This POE oil is separated by accumulator of refrigerant, dryer of refrigerant, and vertical piping with a height difference over 2.30 m.

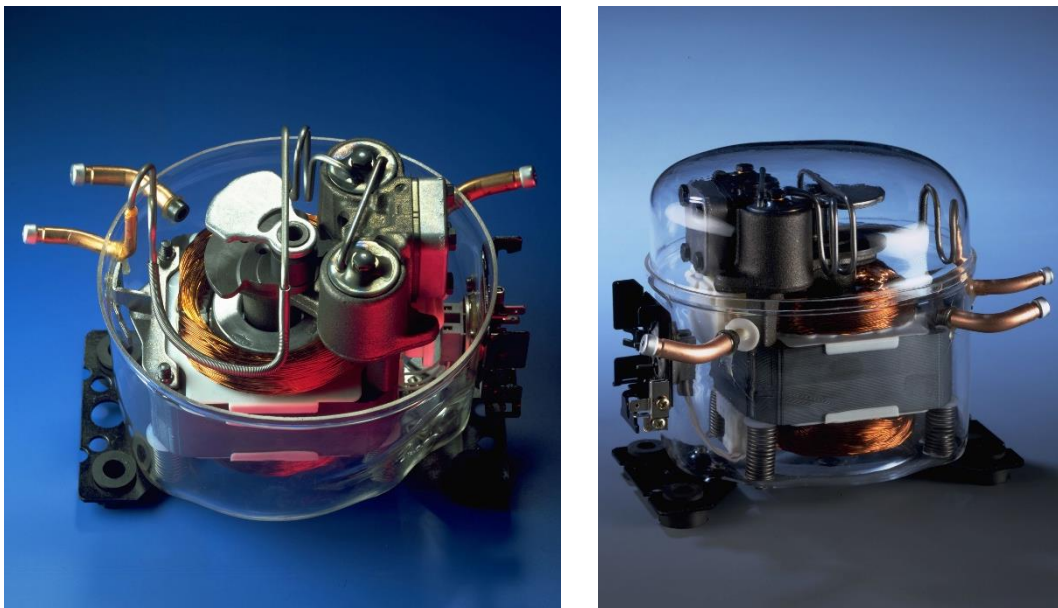


**Figure 5.4** – *Compressor Cubigel GX18TB VE09.*

The saturation temperature of refrigerant is monitored as refrigerant pressure by certificated data logger Testo 450. The mass flow rate of refrigerant is measured by Coriolis effect. The filter of refrigerant before the compressor is used to dampen fluctuation and protection of compressor before liquid hammer. The air-condenser is cooled by axial ventilator ELCO with 1340 RPM used to dampen fluctuation and protection of compressor before liquid hammer.

The applied refrigerant is homogenous refrigerant R134a without temperature glide, near-azeotrope refrigerant R404A (44 % of R125, 52 % of R143a, and 4 % of R134a by weight) with temperature glide 0.80 K, and zeotrope refrigerant R407C (23 % of R32, 25 % of R125, and 52 % of R134a by weight) with temperature glide 7.10 K. The refrigerant is immiscible with the POE oil and compatible with a metals and alloys in the compressor. The refrigerant purity is certificated and the copper surface of evaporator tube is cleaned. The electronics equipment is calibrated and certificated for the elimination of uncertainties, see Table 5.1.

**Table 5.1** – Accuracy and uncertainties of experimental measurement.

Measurement	Variable	Instrument	Range	Accuracy	Uncertainty
Temperature of Heating water	$T_w$ [°C]	Thermocouple ALMEMO NiCr-Ni	5.2 to 55.7	±0.1 K	±1.7 %
Mass flow of Heating water	$m_w$ [kg·s <sup>-1</sup> ]	Kamstrup Multical 402	0.0078 to 0.0167	±0.0003 kg·s <sup>-1</sup>	±3.9 %
Pressure of Refrigerant	$p_f$ [kPa]	Datalogger Testo 450	326 to 2246	±0.1 kPa	±0.3 %
Mass flow of Refrigerant	$G_f$ [kg·m <sup>-2</sup> ·s <sup>-1</sup> ]	Corriolis effect	8.63 to 9.13	±0.07 kg·m <sup>-2</sup> ·s <sup>-1</sup>	±0.8 %
Heat flow from Heating water	$Q_w$ [W]	calculated by (Eq. 6)	616 to 2356	±31 W	±4.8 %
Surface temperature of Evaporator tube	$T_s$ [°C]	calculated by (Eq. 7)	-0.1 to 50.9	±0.5 K	±2.1 %
Boiling heat transfer coefficient	$\alpha_f$ [W·m <sup>-2</sup> ·K <sup>-1</sup> ]	calculated by (Eq. 8)	234 to 1008	±75 W·m <sup>-2</sup> ·K <sup>-1</sup>	±13.1 %
Vapour quality of Refrigerant	$X_f$ [-]	calculated by (Eq. 9)	0.01 to 0.98	±0.05	±5.2 %

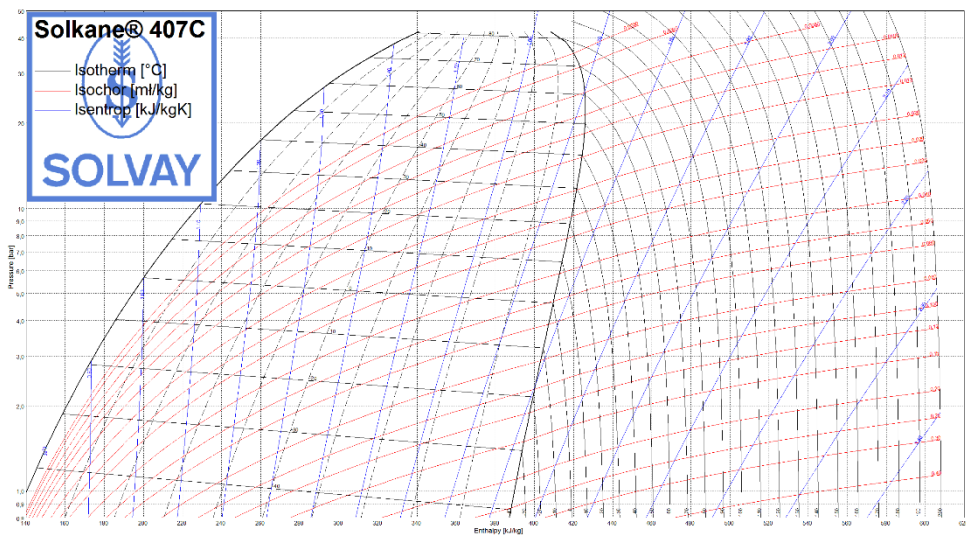
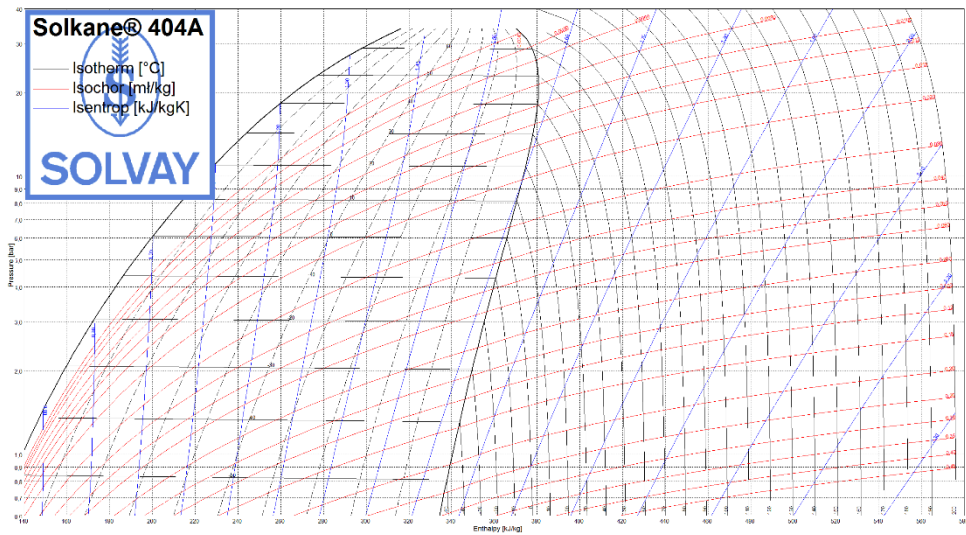
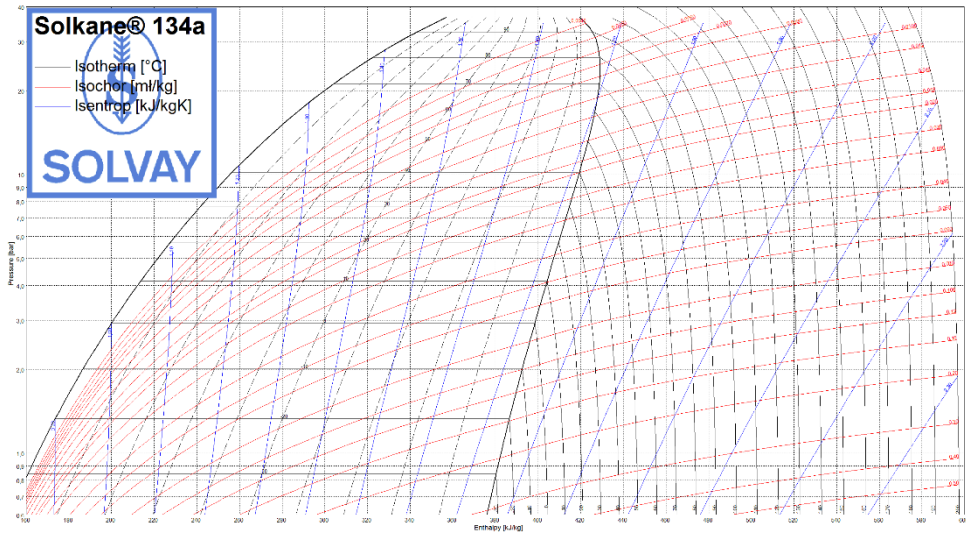


**Figure 5.5** – Pressure-Enthalpy diagram of refrigerant R134a, R404A, and R407C.



The variable parameter of experimental measurement is the tested refrigerant, the inlet temperature of heating water, the volume flow rate of heating water, and the connection of heating water in parallel/counter flow, see Table 2. Before the start, the heating water is connected in the parallel/counter flow with the tested refrigerant. The heating water is run on the constant volume flow rate and constant inlet temperature. The refrigeration system is run in the last step. The energy balance between the refrigeration system and the heating water loop is steady-state when the temperature difference of outlet temperature of heating water is lower than 0.3 K in the last 5 minutes (60 time-steps ago). All assigned parameters are stable for a whole day of measurement (over 3 hours). The manual expansion valve is assigned in the stable position for all refrigerants.

**Table 5.2** – *Range of variable parameter of experimental measurement.*

Variable 1.	Variable 2.	Variable 3.	Variable 4.
Refrigerant	Flow direction	Volume flow rate of Heating water [ $\text{m}^3 \cdot \text{hour}^{-1}$ ]	Inlet temperature of Heating water [ $^{\circ}\text{C}$ ]
R134a	parallel	0.0505 to 0.0600	43.6 to 51.5
	counter	0.0409 to 0.0533	42.8 to 48.1
R404A	parallel	0.0497 to 0.0586	30.2 to 51.6
	counter	0.0493 to 0.0600	35.8 to 55.7
R407C	parallel	0.0283 to 0.0514	34.5 to 48.5
	counter	0.0438 to 0.0554	38.8 to 50.2

## 5.2. Analysis of Measurement

The hydrodynamics analysis of heating water in the annular space is based on the volume flow rate of heating water in the range from 0.0283 to 0.0600  $\text{m}^3 \cdot \text{hour}^{-1}$ . The calculated Reynolds number in a range from 135.4 to 286.7 shows the laminar flow ( $Re < 2300$ ) with the average velocity from 0.0339 to 0.0717  $\text{m} \cdot \text{s}^{-1}$ . The parabolic velocity profile in the annular space is described by Hagen-Poiseuille law. The critical

hydraulics length for stabilization of velocity profile is  $L_h = 0.033$  m, see (Eq. 5.1). The critical thermic length for stabilization of temperature profile is  $L_t = 0.040$  m, see (Eq. 5.2). The critical distance between the connection of heating water to annular space and first/last thermocouple is fulfilled by distance 0.100 m (upper edge) and 0.170 m (bottom edge), see Fig. 5.1. This entry imperfection is idealised on the fully developed laminar flow in the annular space. The entry imperfection is caused by change of hydraulic cross-section, change of velocity flow, change of temperature distribution, etc. Nevertheless, this entry imperfection is idealised on the fully developed laminar flow in the annular space.

$$\frac{L_h}{D_h} = 0.02875 \cdot Re \quad (\text{Eq. 5.1})$$

$$\frac{L_t}{D_h} = 0.050 \cdot Re \cdot Pr \quad (\text{Eq. 5.2})$$

The uncertainty is possible to obtain for example from the change of velocity. The heat transfer coefficient of heating water in the annular space is calculated by equation (Eq. 5.3) in the range from 745 to 869  $\text{W}\cdot\text{m}^{-2}\cdot\text{K}^{-1}$  for the velocity in a range from 0.0339 to 0.0717  $\text{m}\cdot\text{s}^{-1}$ . The velocity in the circular connection pipe is calculated in a range from 0.0066 to 0.0140  $\text{m}\cdot\text{s}^{-1}$ . The lowest velocity of heating water is near to the pipe connection.

The heat transfer coefficient for this low velocity is obtained in a range from 686 to 689  $\text{W}\cdot\text{m}^{-2}\cdot\text{K}^{-1}$ . The hydraulics uncertainty is calculated by ratio of the fully developed laminar flow to the low entry velocity. The entry imperfection is calculated in a range from 1.09 to 1.26. This entry imperfection is valid for the distance 0.033 m related to 0.100 m (upper edge) and 0.170 m (bottom edge). The hydraulics uncertainty of entry imperfection recalculated by length shows a range from 3 to 9 % for the upper edge and the range from 2 to 5 % for the bottom edge.

The thermodynamics analysis of heating water in the annular space is based on the surface temperature of shell tube below the insulation. The temperature distribution in the concentric annular space with the laminar flow is known as the Graetz-Nusselt problem. The analytical solution of annular temperature distribution in a fully developed laminar velocity profile is solved by asymptotic function as “Third kind”, see Reynolds et al. [100], [102], and [103]. This asymptotic function for constant inner temperature (saturation temperature of refrigerant) and adiabatic outer wall (thermal insulation on shell tube) is proposed by Gnielinski [104] in Bennett T.D. [105] as the Nusselt number of heating water in the annular space, see (Eq. 5.3). The heat transfer coefficient of heating water on the outer surface of evaporator tube  $aw$  [ $W \cdot m^{-2} \cdot K^{-1}$ ] is obtained from (Eq. 5.3) in a range from 745 to 869  $W \cdot m^{-2} \cdot K^{-1}$ .

Hydro-dynamically developed laminar flow

$$Nu_w = \sqrt[3]{(Nu_t)^3 + (Nu_{\infty 1,i})^3} \quad (\text{Eq. 5.3})$$

$$Nu_t = 1.615 \cdot (1 + 0.14 \cdot \eta^{-0.50}) \cdot \sqrt[3]{Gz} \quad (\text{Eq. 5.4})$$

Inner surface heated

$$Nu_{\infty 1,i} = 3.66 + 1.20 \cdot \eta^{-0.80} \quad (\text{Eq. 5.5})$$

Outer surface heated

$$Nu_{\infty 1,o} = 3.66 + 1.20 \cdot \eta^{0.5} \quad (\text{Eq. 5.6})$$

Both surfaces heated at equal wall temperatures

$$Nu_{\infty 1,b} = 3.66 + \left[ 4 - \frac{0.102}{\eta + 0.02} \right] \cdot \eta^{0.04} \quad (\text{Eq. 5.7})$$

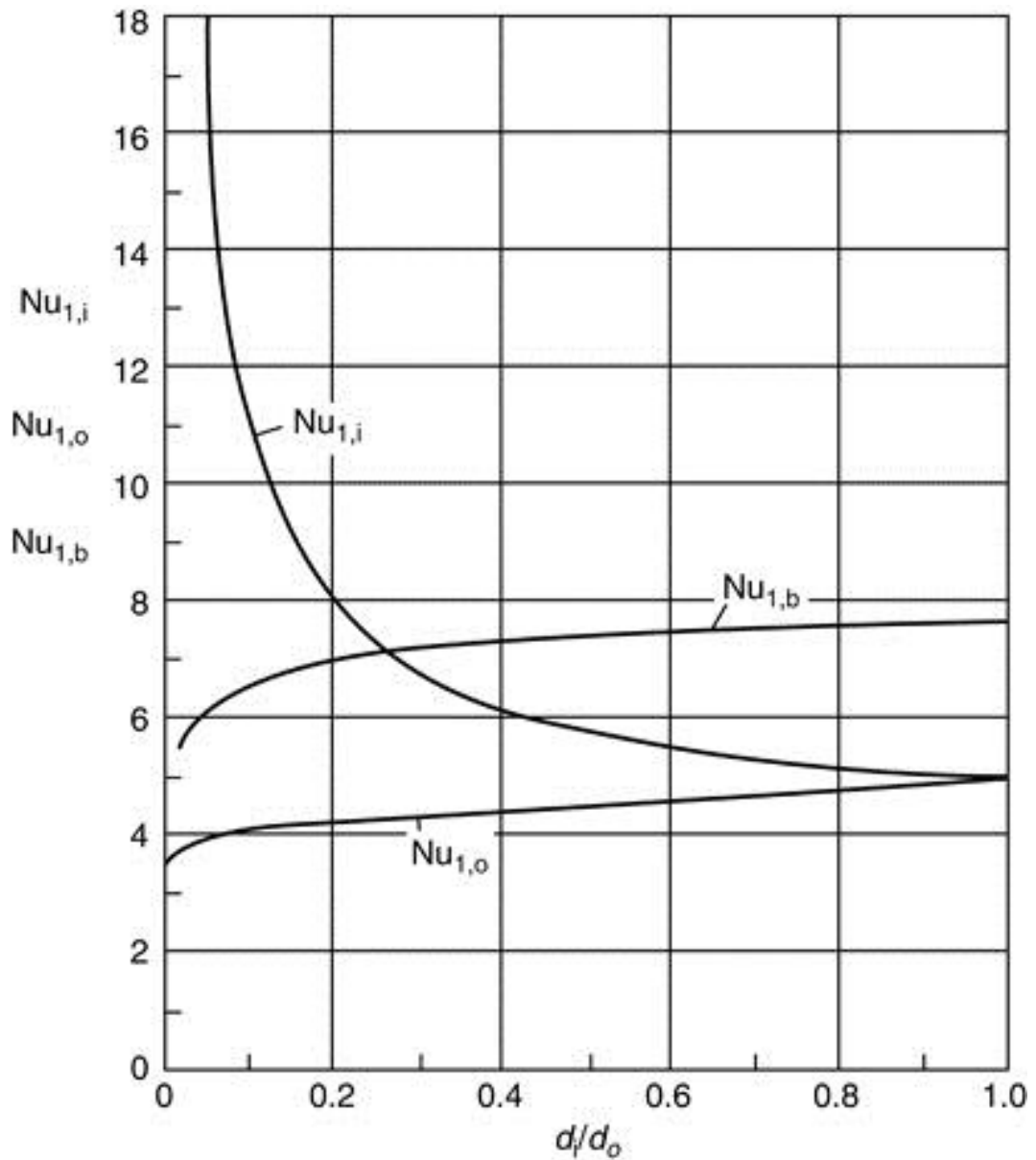


**Figure 5.6** - Graphical nomogram (Eq. 5.5), (Eq. 5.6), and (Eq. 5.7) for the determination of  $Nu_{\infty}$  as a function of  $(D_i/D_o)$  ratio for the three boundary conditions [104].

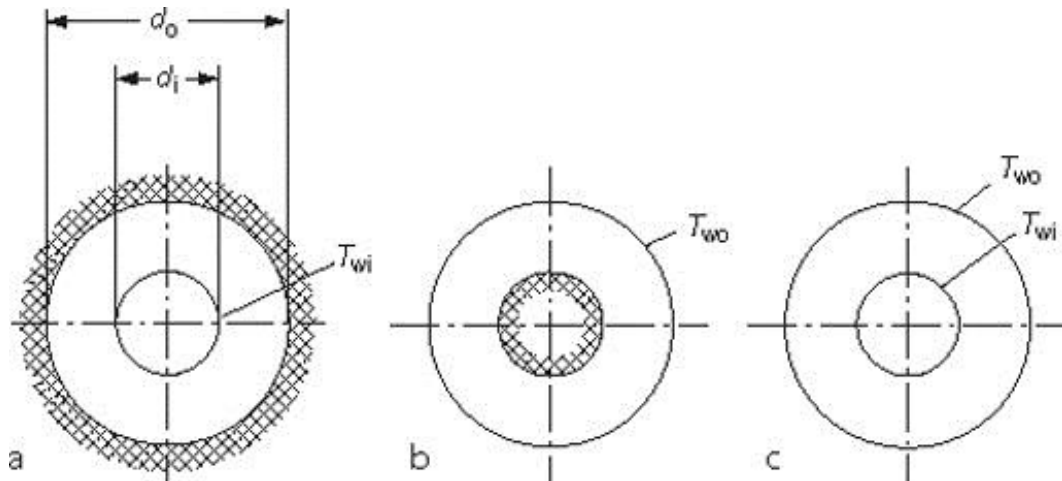


**Figure 5.7** - Boundary conditions for heat transfer in an annular gap.  
 1. Heat transferred at the inner tube (subscript *i*); the outer tube insulated  
 2. Heat transferred at the outer tube (subscript *o*); the inner tube insulated  
 3. Heat transferred at both tubes (subscript *b*); the walls of each are at the same temperature  $T_{wi}=T_{wo}$  [104].

The analysis of experimental measurement assumes the energy balance between the heating water in annular space and the refrigerant in evaporator tube. The heat flow in the thermal insulation from the heating water to the laboratory is neglected. The local heat flow  $Q_{w,f}$  [W] in the wall of evaporator tube is obtained from the mass flow of heating water  $m_w$  [ $\text{kg}\cdot\text{s}^{-1}$ ] and the local temperature difference of heating water ( $T_{w,x} - T_{w,x+1}$ ) [K], see (Eq. 5.8). The heat transfer coefficient of heating water  $\alpha_w$  [ $\text{W}/(\text{m}^2\cdot\text{K})$ ] (see Eq. 5.3) and the local heat flow in the wall of evaporator tube  $Q_{w,f}$  [W] is used for the calculation of local inner surface temperature of evaporator tube  $T_{s,x}$  [ $^{\circ}\text{C}$ ], see (Eq. 5.9). The local boiling heat transfer coefficient  $\alpha_{f,x}$  [ $\text{W}/(\text{m}^2\cdot\text{K})$ ] is calculated from the local heat flow  $Q_{w,f}$  [W] and the local temperature difference ( $T_{s,x} - T_{f,x}$ ) [K] between the inner surface temperature of evaporator tube and the saturation temperature of refrigerant, see (Eq. 5.10). The local vapour quality of refrigerant  $X_x$  [-] is obtained from the total energy balance on the evaporator tube. The calculation of local vapour quality is based on the

energy ratio of the temperature change of heating water and the phase change of refrigerant, see (Eq. 5.11).

$$\dot{Q}_{w,x} = \dot{m}_w \cdot c_w \cdot (T_{w,x} - T_{w,x+1}) \quad (\text{Eq. 5.8})$$

$$\bar{T}_{s,x} = T_{w,x} - \frac{\dot{Q}_{w,x}}{\pi \cdot L_x} \cdot \left( \frac{1}{2 \cdot \lambda} \cdot \ln \frac{D_e}{D_i} + \frac{1}{D_e \cdot \alpha_w} \right) \quad (\text{Eq. 5.9})$$

$$\bar{\alpha}_{f,x} = \left[ \frac{\pi \cdot L_x \cdot D_i \cdot (T_{w,x} - T_{f,x})}{\dot{Q}_{w,x}} - \frac{D_i}{2 \cdot \lambda} \cdot \ln \frac{D_e}{D_i} - \frac{D_i}{D_e \cdot \alpha_w} \right]^{-1} \quad (\text{Eq. 5.10})$$

$$\bar{x}_x = \frac{\dot{m}_w \cdot c_w \cdot (T_{w,x} - T_{w,in})}{\dot{m}_f \cdot (i_l - i_g)} \quad (\text{Eq. 5.11})$$

### 5.3. Results

The experimental analysis shows the evaporation of downward flow refrigerant R134a, R404A and R407C in the smooth vertical tube with an inner diameter 32 mm. The mass flux about  $9 \text{ kg} \cdot \text{m}^{-2} \cdot \text{s}^{-1}$  in parallel/counter flow with the heating water shows suppressed dependence of heat flux on the mass flux, significant dependence of heat flux on the temperature difference, and dependence of boiling heat transfer coefficient on the vapour quality. This obtained boiling heat transfer coefficient is correlated as Nusselt numbers with the predicted Nusselt numbers.

#### 5.3.1. Dependence of Heat flux on Mass flux

The dependence of local heat flux  $q_{f,x}$  [ $\text{kW} \cdot \text{m}^{-2}$ ] on the mass flux  $G_f$  [ $\text{kg} \cdot \text{m}^{-2} \cdot \text{s}^{-1}$ ] is plotted for refrigerant R134a, R404A and R407C, see Fig. 5.8.

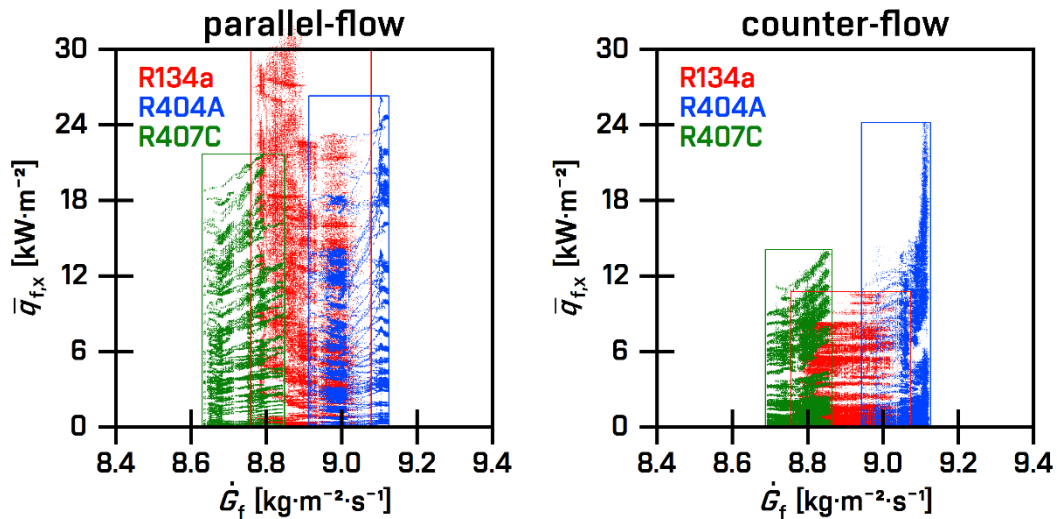


**Figure 5.8** - The dependence of heat flux on the mass flux is suppressed [100].

The refrigerant R134a in the parallel flow shows median mass flux  $8.877 \pm 0.071 \text{ kg}\cdot\text{m}^{-2}\cdot\text{s}^{-1}$  in a range from  $8.759$  to  $9.079 \text{ kg}\cdot\text{m}^{-2}\cdot\text{s}^{-1}$  and local heat flux up to  $32.09 \text{ kW}\cdot\text{m}^{-2}$ . The refrigerant R134a in the counter flow shows median mass flux  $8.877 \pm 0.064 \text{ kg}\cdot\text{m}^{-2}\cdot\text{s}^{-1}$  in a range from  $8.756$  to  $9.073 \text{ kg}\cdot\text{m}^{-2}\cdot\text{s}^{-1}$  and local heat flux up to  $10.75 \text{ kW}\cdot\text{m}^{-2}$ . The refrigerant R404A in the parallel flow shows median mass flux  $9.004 \pm 0.059 \text{ kg}\cdot\text{m}^{-2}\cdot\text{s}^{-1}$  in a range from  $8.913$  to  $9.125 \text{ kg}\cdot\text{m}^{-2}\cdot\text{s}^{-1}$  and local heat flux up to  $26.34 \text{ kW}\cdot\text{m}^{-2}$ . The refrigerant R404A in the counter flow shows median mass flux  $9.084 \pm 0.025 \text{ kg}\cdot\text{m}^{-2}\cdot\text{s}^{-1}$  in a range from  $8.943$  to  $9.127 \text{ kg}\cdot\text{m}^{-2}\cdot\text{s}^{-1}$  and local heat flux up to  $24.20 \text{ kW}\cdot\text{m}^{-2}$ . The refrigerant R407C in the parallel flow shows median mass flux  $8.752 \pm 0.050 \text{ kg}\cdot\text{m}^{-2}\cdot\text{s}^{-1}$  in a range from  $8.630$  to  $8.848 \text{ kg}\cdot\text{m}^{-2}\cdot\text{s}^{-1}$  and local heat flux up to  $21.70 \text{ kW}\cdot\text{m}^{-2}$ . The refrigerant R407C in the counter flow shows median mass flux  $8.788 \pm 0.042 \text{ kg}\cdot\text{m}^{-2}\cdot\text{s}^{-1}$  in a range from  $8.688$  to  $8.865 \text{ kg}\cdot\text{m}^{-2}\cdot\text{s}^{-1}$  and local heat flux up to  $14.10 \text{ kW}\cdot\text{m}^{-2}$ .

The stable position of manual expansion valve induced the comparable low mass flux of refrigerant over measurements. This low mass flux of refrigerant in the parallel flow and counter flow is comparable on 99.991 % for R134a, 99.120 % for R404A, and 99.583 % for R407C. The small fluctuation of mass flux is the effect of mechanical spring of valve

in the seat. The wide range of local heat flux for the stable mass flux is influenced by local surface temperature of evaporator tube. The temperature distribution on the inner surface of evaporator tube is driven by volume flow rate and inlet temperature of heating water in the annular space. The dependence of heat flux on the mass flux is suppressed.

### **5.3.2. Dependence of Heat flux on Temperature difference**

The dependence of local heat flux  $q_{f,x}$  [ $\text{kW}\cdot\text{m}^{-2}$ ] on the temperature difference  $(T_{s,x} - T_{f,x})$  [K] between the inner surface temperature of evaporator tube  $T_{s,x}$  [ $^{\circ}\text{C}$ ] and the saturation temperature of refrigerant  $T_{f,x}$  [ $^{\circ}\text{C}$ ] is plotted for refrigerant R134a, R404A and R407C, see Fig. 5.9.

The refrigerant R134a with the saturation temperature  $T_{f,x} \in [3.7 \text{ }^{\circ}\text{C}, 4.8 \text{ }^{\circ}\text{C}]$  shows temperature difference  $(T_{s,x} - T_{f,x})$  in a range from 3.4 K to 44.9 K for the temperature of heating water  $T_{w,x} \in [19.8 \text{ }^{\circ}\text{C}, 51.5 \text{ }^{\circ}\text{C}]$  in parallel flow. The linear regression of obtained result correlates on 96 % in the range from 3.4 K to 29.8 K, and the absolute difference is lower than  $\pm 5.2 \text{ kW}\cdot\text{m}^{-2}$ . The refrigerant R134a with the saturation temperature  $T_{f,x} \in [3.1 \text{ }^{\circ}\text{C}, 4.7 \text{ }^{\circ}\text{C}]$  shows temperature difference  $(T_{s,x} - T_{f,x})$  in a range from 7.3 K to 19.9 K for the temperature of heating water  $T_{w,x} \in [17.1 \text{ }^{\circ}\text{C}, 48.1 \text{ }^{\circ}\text{C}]$  in counter flow. The linear regression of obtained result correlates on 90 % in the range from 7.3 K to 19.9 K, and the absolute difference is lower than  $\pm 4.3 \text{ kW}\cdot\text{m}^{-2}$ .



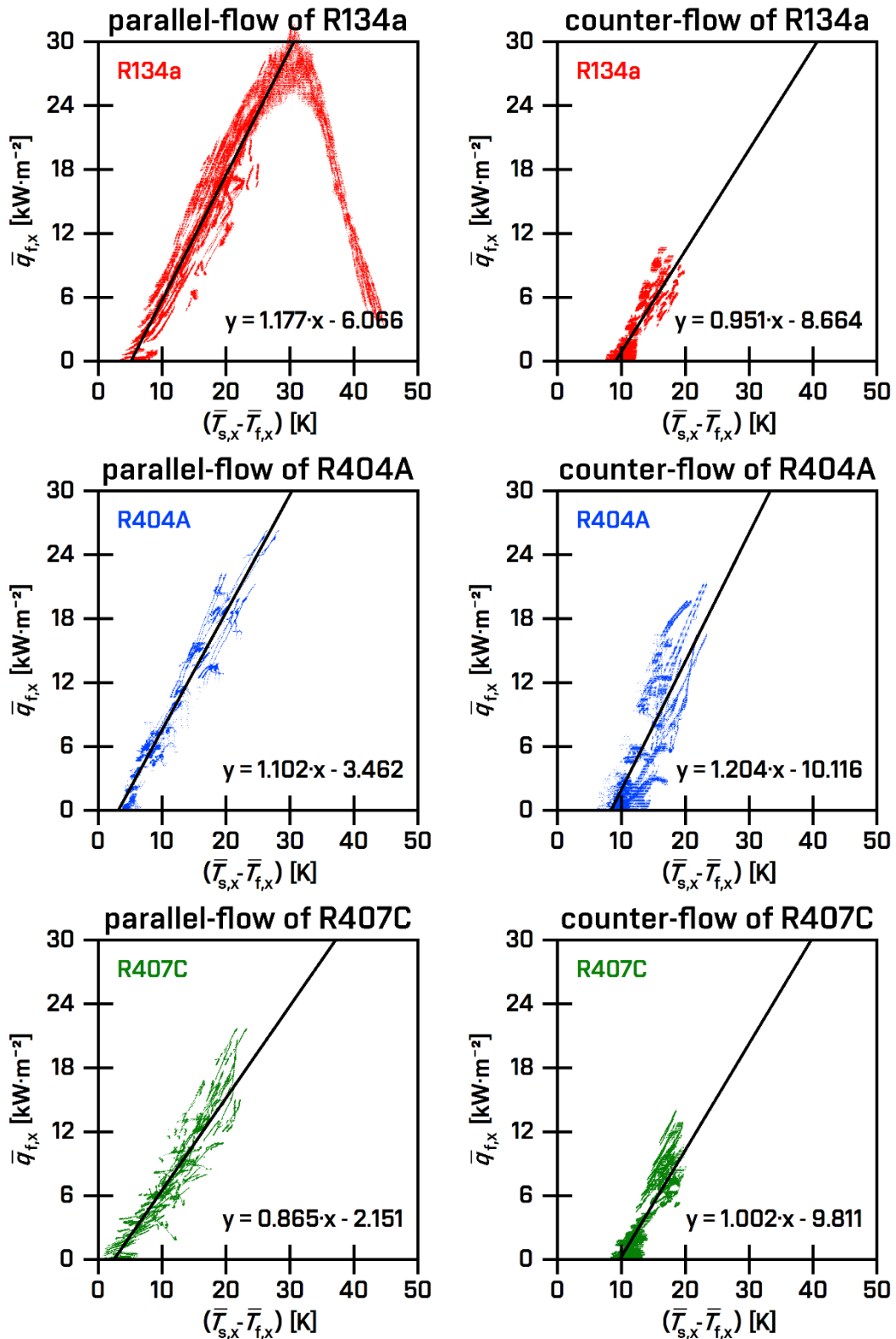


Figure 5.9 - The heat flux is driven by the temperature difference [100].

The refrigerant R404A with the saturation temperature  $T_{f,x} \in [-0.5 \text{ }^\circ\text{C}, 4.4 \text{ }^\circ\text{C}]$  shows temperature difference ( $T_{s,x} - T_{f,x}$ ) in a range from 3.5 K to 28.3 K for the temperature of heating water  $T_{w,x} \in [14.8 \text{ }^\circ\text{C}, 51.6 \text{ }^\circ\text{C}]$  in parallel flow. The linear regression of obtained result correlates on 97 % in the range from 3.5 K to 28.3 K, and the absolute difference is lower than  $\pm 5.1 \text{ kW}\cdot\text{m}^{-2}$ . The refrigerant R404A with the saturation temperature  $T_{f,x} \in [2.1 \text{ }^\circ\text{C}, 4.3 \text{ }^\circ\text{C}]$  shows temperature difference ( $T_{s,x} - T_{f,x}$ ) in a range from 6.1 K to 23.4 K for the temperature of heating water  $T_{w,x} \in [15.6 \text{ }^\circ\text{C}, 55.7 \text{ }^\circ\text{C}]$  in counter flow. The linear regression of obtained result correlates on 90 % in the range from 6.1 K to 23.4 K, and the absolute difference is lower than  $\pm 8.2 \text{ kW}\cdot\text{m}^{-2}$ .

The refrigerant R407C with the saturation temperature  $T_{f,x} \in [-0.1 \text{ }^\circ\text{C}, 5.5 \text{ }^\circ\text{C}]$  shows temperature difference ( $T_{s,x} - T_{f,x}$ ) in a range from 0.9 K to 23.3 K for the temperature of heating water  $T_{w,x} \in [5.2 \text{ }^\circ\text{C}, 48.5 \text{ }^\circ\text{C}]$  in parallel flow. The linear regression of obtained result correlates on 95 % in the range from 0.9 K to 23.3 K, and the absolute difference is lower than  $\pm 5.7 \text{ kW}\cdot\text{m}^{-2}$ . The refrigerant R407C with the saturation temperature  $T_{f,x} \in [4.0 \text{ }^\circ\text{C}, 6.7 \text{ }^\circ\text{C}]$  shows temperature difference ( $T_{s,x} - T_{f,x}$ ) in a range from 8.3 K to 20.5 K for the temperature of heating water  $T_{w,x} \in [14.8 \text{ }^\circ\text{C}, 50.2 \text{ }^\circ\text{C}]$  in counter flow. The linear regression of obtained result correlates on 91 % in the range from 8.3 K to 20.5 K, and the absolute difference is lower than  $\pm 6.2 \text{ kW}\cdot\text{m}^{-2}$ .

This dependence of local heat flux on the temperature difference (superheated wall) is obtained by the stable low mass flux of refrigerant in combination with the variable volume flow rate of heating water with the variable inlet temperature. The obtained dependence of heat flux on the temperature difference is significant, and the dependence for the parallel flow of R134a is comparable with the Boiling curve. The variable width of dependence is the impact of measurement uncertainty. This

measurement uncertainty is suppressed for the increased temperature difference.

### **5.3.3. Dependence of Boiling HTC on Vapour quality**

The dependence of boiling heat transfer coefficient  $\alpha_{f,x}$  [ $\text{W}\cdot\text{m}^{-2}\cdot\text{K}^{-1}$ ] on the vapour quality  $X_{f,x}$  [-] is plotted for refrigerant R134a, R404A and R407C, see Fig. 5.10.

The refrigerant R134a in parallel flow with vapour quality from 1 % to 96 % shows the boiling heat transfer coefficient  $609 \pm 129 \text{ W}\cdot\text{m}^{-2}\cdot\text{K}^{-1}$  in a range from 366 to  $1008 \text{ W}\cdot\text{m}^{-2}\cdot\text{K}^{-1}$ . The linear regression correlates with the obtained result of 71 %, and the relative deviation is lower than  $\pm 29$  %. The refrigerant R134a in counter flow with vapour quality from 68 % to 98 % shows the boiling heat transfer coefficient  $518 \pm 105 \text{ W}\cdot\text{m}^{-2}\cdot\text{K}^{-1}$  in a range from 234 to  $743 \text{ W}\cdot\text{m}^{-2}\cdot\text{K}^{-1}$ . The linear regression correlates with the obtained result of 76 %, and the relative deviation is lower than  $\pm 25$  %.

The refrigerant R404A in parallel flow with vapour quality from 22 % to 92 % shows the boiling heat transfer coefficient  $636 \pm 139 \text{ W}\cdot\text{m}^{-2}\cdot\text{K}^{-1}$  in a range from 396 to  $992 \text{ W}\cdot\text{m}^{-2}\cdot\text{K}^{-1}$ . The linear regression correlates with the obtained result of 73 %, and the relative deviation is lower than  $\pm 28$  %. The refrigerant R404A in counter flow with vapour quality 30 % to 94 % shows the boiling heat transfer coefficient  $499 \pm 106 \text{ W}\cdot\text{m}^{-2}\cdot\text{K}^{-1}$  in a range from 278 to  $794 \text{ W}\cdot\text{m}^{-2}\cdot\text{K}^{-1}$ . The linear regression correlates with the obtained result of 68 %, and the relative deviation is lower than  $\pm 36$  %.

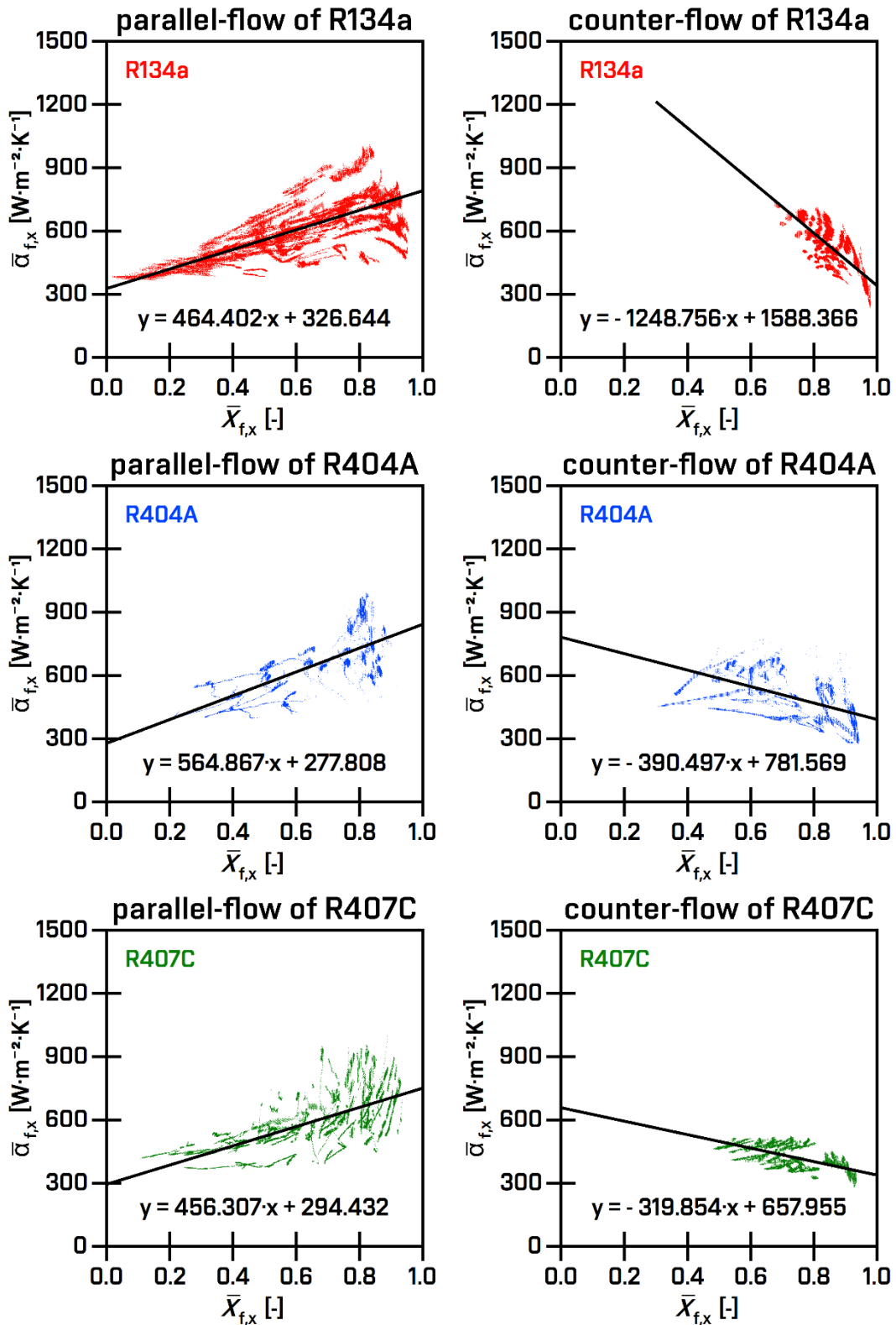


**Figure 5.10** - The boiling heat transfer coefficient is dependent on the vapour quality [100].

The refrigerant R407C in parallel flow with vapour quality from 11 % to 93 % shows the boiling heat transfer coefficient  $573 \pm 132 \text{ W}\cdot\text{m}^{-2}\cdot\text{K}^{-1}$  in a range from 366 to  $998 \text{ W}\cdot\text{m}^{-2}\cdot\text{K}^{-1}$ . The linear regression correlates with the obtained result of 65 %, and the relative deviation is lower than  $\pm 37$  %. The refrigerant R407C in counter flow with vapour quality from 48 % to 93 % shows the boiling heat transfer coefficient  $411 \pm 56 \text{ W}\cdot\text{m}^{-2}\cdot\text{K}^{-1}$  in a range from 281 to  $524 \text{ W}\cdot\text{m}^{-2}\cdot\text{K}^{-1}$ . The linear regression correlates with the obtained result of 76 %, and the relative deviation is lower than  $\pm 21$  %.

The boiling heat transfer coefficient is dependent on the vapour quality. The correlation quality of linear regression is decreased with the increased vapour quality. The dispersion of local boiling heat transfer coefficient is the complex effect of liquid drops in the vapour core, phase change of refrigerant, regime of flow, etc. The obtained dependence of local boiling heat transfer coefficient on the vapour quality is increased for the parallel flow of heating water, see Fig. 5.10.

#### **5.3.4. Correlation with predicted Nusselt number**

The obtained boiling heat transfer coefficient  $\alpha_{f,x}$  [ $\text{W}\cdot\text{m}^{-2}\cdot\text{K}^{-1}$ ] is compared as experimental Nusselt number  $Nu_{\text{exp}}$  [-] with the predicted Nusselt number  $Nu_{\text{pre}}$  [-], see Fig. 5.11.

The refrigerant R134a shows the experimental Nusselt number in the range from 1.08 to 324.1 for parallel flow and the range from 0.93 to 197.5 for counter flow. This experimental Nusselt number correlates with the predicted Nusselt number by Fang et al. [106] on 92.2 %, Kim and Mudawar [107] on 81.1 %, and Sun and Mishima [108] on 91.1 %.

The refrigerant R404A shows the experimental Nusselt number in the range from 1.51 to 397.8 for parallel flow and the range from 0.95 to

358.4 for counter flow. This experimental Nusselt number correlates with the predicted Nusselt number by Fang et al. [106] on 92.4 %, Kim and Mudawar [107] on 86.5 %, and Sun and Mishima [108] on 89.1 %.

The refrigerant R407C shows the experimental Nusselt number in the range from 1.12 to 197.0 for parallel flow and the range from 1.02 to 187.7 for counter flow. This experimental Nusselt number correlates with the predicted Nusselt number by Fang et al. [106] on 83.2 %, Hamdar et al. [109] on 78.6 %, and Li and Wu [110] on 81.6 %.

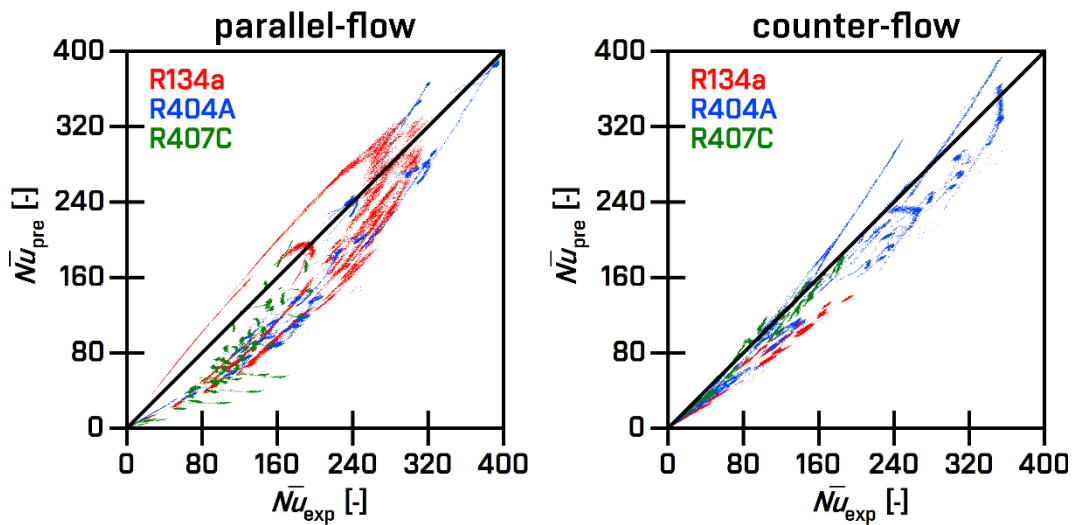


**Figure 5.11** - The correlation quality of experimental Nusselt number with the predicted Nusselt numbers by Fang et al. [106]

The correlation quality of experimental Nusselt number with the predicted Nusselt number is dependent on the experimental analogy (inner diameter, mass flux, heat flux, and vapour quality). The lowest correlation on 78.6 % for R407C is obtained for the inner diameter 1.0 mm and mass flux over  $200 \text{ kg}\cdot\text{m}^{-2}\cdot\text{s}^{-1}$  published by Hamdar et al. [109]. Oppositely, the highest correlation on 92.2 % for R134a and 92.4 % for R404A is obtained for the inner diameter up to 32 mm and mass flux since  $10 \text{ kg}\cdot\text{m}^{-2}\cdot\text{s}^{-1}$  published by Fang et al. [106].

**Table 5.3** – *The correlation quality of experimental Nusselt number with the predicted Nusselt number.*

Source	$D$ [mm]	$G$ [kg·m <sup>-2</sup> ·s <sup>-1</sup> ]	$q$ [kW·m <sup>-2</sup> ]	$X$ [-]	R134a	R404A	R407C
Sun and Mishima [108]	0.21 to 6.05	44 to 1500	5 to 109	-	91.1 %	89.1 %	-
Hamdar et al. [109]	1.0	200 to 600	10 to 60	0 to 1	-	-	78.6 %
Li and Wu [110]	0.19 to 3.1	20.3 to 1500	0 to 715	0.1 to 1	-	-	81.6 %
Kim, Mudawar [107]	0.19 to 6.5	19 to 1608	-	0 to 1	81.1 %	86.5 %	-
Fang et al. [106]	0.207 to 32.0	10 to 1782	0.2 to 4788	0.0001 to 0.998	92.2 %	92.4 %	83.2 %

## 5.4. Discussion of Evaporation

The suppressed dependence of heat flux on the low mass flux (see 5.3.1), but the significant dependence of heat flux on the temperature difference (see 5.3.2) is predicted by Cavallini et al. [81], and Meyer and Ewim [64].

The various dependence slope of local boiling heat transfer coefficient on the vapour quality for parallel/counter flow (see 5.3.3) is the complex effect of liquid drops in the vapour core, phase change of refrigerant, regime of flow, etc. However, the local boiling heat transfer coefficient in the parallel flow is increased significantly and the maximal local boiling heat transfer coefficient is obtained for the vapour quality of about 80 - 90 %. This dependence of boiling heat transfer coefficient on the vapour quality is published by Klimenko [111] for vapour quality of about 80 %, Wojtan et al. [112] in a range from 68 % to 92 %, and Lee and Mudawar [113] in a range from 55 % to 100 %.

The obtained boiling heat transfer coefficient of refrigerant R134a in the range from 234 to 1008 W·m<sup>-2</sup>·K<sup>-1</sup> (see 3.3) is comparable with the result 900 – 1500 W·m<sup>-2</sup>·K<sup>-1</sup> for mass flux since 50 kg·m<sup>-2</sup>·s<sup>-1</sup> published by

Meyer et al. [59], Ewim et al. [61], and Lips et al. [71], [72]. The comparable result  $600 - 2500 \text{ W}\cdot\text{m}^{-2}\cdot\text{K}^{-1}$  for mass flux since  $46 \text{ kg}\cdot\text{m}^{-2}\cdot\text{s}^{-1}$  is published by Akhavan-Behabadi et al. [65], [73], and Mohseni et al. [74], and [75].

The correlation quality of obtained Nusselt number with the predicted Nusselt number (see 5.3.4) is affected by the experimental analogy (inner diameter of tube, mass flux of refrigerant, heat flux, vapour quality, etc.). Therefore, the highest correlation of Nusselt number up to 92 % is obtained for the mass flux  $10 \text{ kg}\cdot\text{m}^{-2}\cdot\text{s}^{-1}$  published by Fang et al. [114].

## 5.5. Obtained knowledge

The downward flow of refrigerant R134a, R404a and R407c with low mass flux ( $G = 8.63$  to  $9.13 \text{ kg}\cdot\text{m}^{-2}\cdot\text{s}^{-1}$ ), maximal heat flux ( $q = 21.70$  to  $32.09 \text{ kW}\cdot\text{m}^{-2}$ ), vapour quality ( $x = 0.7$  to  $97.8 \%$ ) and evaporation temperature ( $T = -2.1$  to  $6.7 \text{ }^\circ\text{C}$ ) in vertical smooth tube is summarized to following points.

- The convective boiling is suppressed by low mass flux, downward flow, vertical orientation of evaporator tube, wide inner diameter of evaporator tube and thin thickness of liquid film due to natural gravity, see Fig. 5.8.
- The nucleate boiling is obtained as well-known Boiling curve. The critical heat flux is obtained for refrigerant R134a on value  $32.09 \text{ kW}\cdot\text{m}^{-2}$  for superheat of wall  $29.8 \text{ K}$ . This low mass flux with dominant nucleate boiling is driven by temperature difference, see Fig. 5.9.
- The boiling heat transfer coefficient with significant post-dryout effect is depended on vapour quality, see Fig. 5.10. The boiling heat



transfer coefficient in range from 363 to 1523  $\text{W}\cdot\text{m}^{-2}\cdot\text{K}^{-1}$  correlates up to 92 % with predicted Nusselt number, see Fig. 5.11.

Summary, this experimentally obtained result for untypically low mass flux (about  $9 \text{ kg}\cdot\text{m}^{-2}\cdot\text{s}^{-1}$ ) is comparable with current knowledge for low mass flux (over  $10 \text{ kg}\cdot\text{m}^{-2}\cdot\text{s}^{-1}$ ).

## 6. Conclusion

This dissertation thesis deals with heat and mass transfer in technical applications. The research point is an experimental analysis of heat transfer with the phase-change process in the tubular exchanger. The phase-change of fluid from liquid to gas (evaporation) or reverse phase change from gas to liquid (condensation) is used in advanced technical applications very often and therefore, this research point includes experimental analysis of condensation and evaporation process.

- ❖ **Condensation** process is studied in the tubular heat exchanger with 55 spiral micro-tubes with an inner diameter of 3.0 mm. The research method of Thermal resistance and Wilson plot is useful for analysis of experimental measurement. The boiling heat transfer coefficient is determined by theoretical, experimental, and semi-experimental prediction.
- ❖ **Evaporation** process is analysed by the low mass flux about  $9 \text{ kg}/(\text{m}^2\cdot\text{K})$  of refrigerant R134a, R404A, and R407C in the vertical smooth tube with an inner diameter of 32 mm. The obtained knowledge shows suppressed dependence of heat flux on the low mass flux, significant dependence of heat flux on the temperature difference, dependence of boiling heat transfer coefficient on the vapour quality, and correlation quality up to 92 % with the predicted Nusselt number.

Finally, this experimentally obtained knowledge of heat and mass transfer is applied in technical issues and disseminated by scientific papers, see Annex 9.4.

## 7. References

- [1] GAŽO, Ján, ed.; Všeobecná a anorganická chémia: učebnica pre vysoké školy na Slovensku. Bratislava: Alfa, 1978.
- [2] KASATKIN, Andrej Georgijevič; Základní pochody a zařízení chemické technologie: celostátní vysokoškolská učebnice. 2. vyd. Praha: Státní nakladatelství technické literatury, 1957. Řada energetické literatury.
- [3] BRDIČKA, Rudolf a Jiří DVOŘÁK; Základy fyzikální chemie: vysokoškolská učebnice. 2., přeprac. vyd. Praha: Academia, 1977.
- [4] MOORE, Walter J.; Fyzikální chemie. 2. vyd. Praha: SNTL, 1981.
- [5] [cit. 2021-21-09]. Available under license Free for commercial use at WWW: <<https://www.pxfuel.com/en/free-photo-oqpop>>
- [6] [cit. 2021-21-09]. Invert color of picture Water boiling in a glass pot for Personal use: <<https://www.alamy.com/water-boiling-in-a-glass-pot-image4786801.html>>
- [7] PAPON, Pierre, Jacques LEBLOND a Paul H. E. MEIJER; The physics of phase transitions: concepts and applications. Second revised edition. Přeložil S. L. SCHNUR. Berlin: Springer, [2006]. ISBN 3-540-33389-4.
- [8] RAHMSTORF, S.; Thermohaline Circulation. Reference Module in Earth Systems and Environmental Sciences. Elsevier, 2015, 2015. ISBN 9780124095489. Available at: doi:10.1016/B978-0-12-409548-9.09514-2.
- [9] [cit. 2021-21-09]. Available under license Public Domain at <[https://en.wikipedia.org/wiki/Thermohaline\\_circulation#/media/File:Thermohaline\\_Circulation\\_2.png](https://en.wikipedia.org/wiki/Thermohaline_circulation#/media/File:Thermohaline_Circulation_2.png)>
- [10] FRANZOSI, Roberto; 2018. Microcanonical entropy for classical systems. Physica A: Statistical Mechanics and its Applications [online]. 494, 302-307 [cit. 2021-9-21]. ISSN 03784371. Available at: doi: 10.1016/j.physa.2017.12.059.

- [11] MATTY, Michael, Lachlan LANCASTER, William GRIFFIN a Robert H.; SWENDSEN, 2017. Comparison of canonical and microcanonical definitions of entropy. *Physica A: Statistical Mechanics and its Applications* [online]. 467, 474-489 [cit. 2021-9-21]. ISSN 03784371. Available at: doi: 10.1016/j.physa.2016.10.030.
- [12] GROSS, D.H.E.; 2006. Negative heat-capacity at phase-separations in microcanonical thermostatics of macroscopic systems with either short or long-range interactions. *Physica A: Statistical Mechanics and its Applications* [online]. 365(1), 138-141 [cit. 2021-9-21]. ISSN 03784371. Available at: doi: 10.1016/j.physa.2006.01.010.
- [13] SEKERKA, Robert Floyd; *Thermal physics: thermodynamics and statistical mechanics for scientists and engineers*. Elsevier, 2015.
- [14] OLLA, Piero; *An Introduction to Thermodynamics and Statistical Physics*. Springer International Publishing, 2015.
- [15] ONUKI, Akira; *Phase transition dynamics*. Cambridge University Press, 2002.
- [16] ANSERMET, Jean-Philippe; BRECHET, Sylvain D. *Principles of thermodynamics*. Cambridge University Press, 2019.
- [17] FAGHRI, Amir; ZHANG, Yuwen; *Transport phenomena in multiphase systems*. Elsevier, 2006.
- [18] COLLIER, John G.; THOME, John R.; *Convective boiling and condensation*. Clarendon Press, 1994.
- [19] TRUESDELL, Clifford; *The tragicomical history of thermodynamics, 1822–1854*. Springer Science & Business Media, 2013.
- [20] LEIDENFROST, Johann Gottlob. On the fixation of water in diverse fire. *International Journal of Heat and Mass Transfer*, 1966, 9.11: 1153-1166
- [21] Deluc, Jean-André; *Recherche sur les modifications de l'atmosphère*, vol. 2, Genève, (1772).
- [22] BLACK, Joseph; *Lectures on the Elements of Chemistry: Delivered in the University of Edinburgh*. Mathew Carey, 1807.

- [23] MAXWELL, James Clerk; RIPLXWELL, M. A. Theory of Heat. Longmans, Green and Company, 1897.
- [24] VAN DER WAALS, Johannes Diderik; Over de Continuïteit van den Gas-en Vloeistofoestand. Sijthoff, 1873.
- [25] GIBBS, Josiah Willard; ART. LII.--On the Equilibrium of Heterogeneous Substances. American Journal of Science and Arts (1820-1879), 1878, 16.96: 441.
- [26] Nußelt W.; Oberflächenkondensation des Wasserdampfes; Zeitschrift des Vereins Dtsch. Ingenieure. Band 60 (1916) 569-575
- [27] Bromley L.A.; Effect of heat capacity of condensate; Industrial and Engineering Chemistry 44 (152) 2966-2969
- [28] Rohsenow W.M.; Heat transfer and temperature distribution in laminar film condensation; Trans. ASME 78 (1956) 1645-1648
- [29] Sparrow E.M., Gregg J.L.; Laminar free convection from a vertical plate with uniform surface heat flux; Trans. ASME 78 (1956) 435-440
- [30] Sparrow E.M., Gregg J.L.; A boundary layer treatment of laminar film condensation; J. Heat Transfer; Trans. ASME 81 (1959) 13-18
- [31] Sparrow E.M., Marschall E.; Binary gravity-flow film condensation; J. Heat Transfer; Trans. ASME 91 (1969) 205-211
- [32] Bankoff S.G.; Stability of liquid flow down a heated inclined plane; Int. J. Heat Mass Transfer 14 (1971) 377-385
- [33] Marschall E., Lee C.Y.; Stability of condensate flow down a vertical wall; Int. J. Heat Mass Transfer 95 (1973) 41-48
- [34] Kapitsa P.L., Eksperim Zh.; Wave flow of thin layers of a viscous fluid; Teor. Fiz. 18 (1948) 3
- [35] NISHIKAWA, Kaneyasu. Historical developments in the research of boiling heat transfer. JSME international journal, 1987, 30.264: 897-905
- [36] NUKIYAMA, Shiro. The maximum and minimum values of the heat  $Q$  transmitted from metal to boiling water under

atmospheric pressure. *International Journal of Heat and Mass Transfer*, 1966, 9.12: 1419-1433.

- [37] Nuclear Power, s.v. "Shutdown Margin – SDM,": [online]. [cit. 2021-9-21]. Available <https://www.nuclear-power.com/nuclear-engineering/heat-transfer/boiling-and-condensation/pool-boiling-boiling-curve/>
- [38] Kutateladze, S. S., 1948, "On the Transition to Film Boiling under Natural Convection," *Kotloturbostroenie*, No. 3, pp. 10–12.
- [39] Y.-P. Chang, An analysis of the critical conditions and burnout in boiling heat transfer, Report No. TID-14004, University of Notre Dame, Notre Dame, 1961.
- [40] Y. Haramura, Y. Katto, A new hydrodynamic model of critical heat flux, applicable widely to both pool and forced convection boiling on submerged bodies in saturated liquids, *Int. J. Heat Mass Transfer* 26 (1983) 389–399.
- [41] A.A. Watwe, A. Bar-Cohen, Modeling of conduction effects on pool boiling CHF of dielectric liquids, in: *Proceedings of the 32nd National Heat Transfer Conference*, Baltimore, USA, 1997.
- [42] Y.A. Kirichenko, P.S. Chernyakov, Determination of the first critical thermal flux on flat heaters, *J. Eng. Phys. Thermophys.* 20 (1971) 699–703.
- [43] V.M. Borishanskii, On the Problem of Generalizing Experimental Data on the Cessation of Bubble Boiling in Large Volume of Liquids, Report No. Ts. K.I.T 28, Moscow, Soviet Union, 1955.
- [44] ZUBER, N.; TRIBUS, M. Further Remarks on the Stability of Boiling Heat Transfer. Report 58-5. California. Univ., Los Angeles. Dept. of Engineering, 1958.
- [45] LIANG, Gangtao; MUDAWAR, Issam. Pool boiling critical heat flux (CHF)–Part 1: Review of mechanisms, models, and correlations. *International Journal of Heat and Mass Transfer*, 2018, 117: 1352-1367.
- [46] KENNING, D. B. R.; COOPER, M. G. Saturated flow boiling of water in vertical tubes. *International Journal of Heat and Mass Transfer*, 1989, 32.3: 445-458.

- [47] COOPER, M. G. Flow boiling—the ‘apparently nucleate’ regime. *International journal of heat and mass transfer*, 1989, 32.3: 459-464.
- [48] DHIR, V. K. Nucleate and transition boiling heat transfer under pool and external flow conditions. *International journal of heat and fluid flow*, 1991, 12.4: 290-314.
- [49] WEBB, RALPH L.; GUPTA, NEELKANTH S. A critical review of correlations for convective vaporization in tubes and tube banks. *Heat Transfer Engineering*, 1992, 13.3: 58-81.
- [50] CHEN, John C. Correlation for boiling heat transfer to saturated fluids in convective flow. *Industrial & engineering chemistry process design and development*, 1966, 5.3: 322-329.
- [51] SHAH, M. Mohammed. Chart correlation for saturated boiling heat transfer: equations and further study. *ASHRAE transactions*, 1982, 88.
- [52] GUNGOR, Kernal Ersin; WINTERTON, R. H. S. A general correlation for flow boiling in tubes and annuli. *International Journal of Heat and Mass Transfer*, 1986, 29.3: 351-358.
- [53] COLLIER, John G.; THOME, John R. *Convective boiling and condensation*. Clarendon Press, 1994.
- [54] Jung D., Kim C-B., Hwang S-M., Kim K-K.; Condensation heat transfer coefficients of R22, R407C, and R410A on a horizontal plain, low fin, and turbo-C tubes; *International Journal of Refrigeration* 26 (2003) 485-491; [doi: 10.1016/S0140-7007(02)00161-5]
- [55] Bandhauer T.M., Agarwal A., Garimella S.; Measurement and modeling of condensation heat transfer coefficients in circular microchannels; *ASME* 128 (2006) 1050-1059; [doi: 10.1115/1.2345427]
- [56] Arslan G., Eskin N.; Heat transfer characteristics for condensation of R134a in a vertical smooth tube; *Experimental Heat Transfer* 28 (2015) 430-445; Publisher ELSEVIER © 2015 [doi: 10.1080/08916152.2014.926430]

- [57] Adelaja A.O., Dirker J., Meyer J.P.; Convective condensation heat transfer of R134a in tubes at different inclination angles; *International journal of Green Energy* 13 (2016) 812-821; [doi: 10.1080/15435075.2016.1161633]
- [58] Aroonrat K., Wongwises S.; Experimental study on two-phase condensation heat transfer and pressure drop of R-134a flowing in a dimpled tube; *International Journal of Heat and Mass Transfer* 106 (2017) 437-448; Publisher ELSEVIER © 2017 [doi: 10.1016/j.ijheatmasstransfer.2016.08.046]
- [59] Meyer J.P., Dirker J., Adelaje A.O.; Condensation heat transfer in smooth inclined tubes for R134a at different saturation temperatures; *International Journal of Heat and Mass Transfer* 70 (2014) 515-525; Publisher ELSEVIER © 2014 [doi: 10.1016/j.ijheatmasstransfer.2013.11.038]
- [60] Cavallini A., Censi G., Del Col D., Doretto L., Longo G.A., Rossetto L.; Experimental investigation on condensation heat transfer and pressure drop of new HFC refrigerants (R134a, R125, R32, R410a, R236ea) in a horizontal smooth tube; *International Journal of Refrigeration* 24 (2001) 73-87; [PII: S0140-7007(00)00070-0]
- [61] Ewim D.R.E., Meyer J.P., Noori Rahim Abadi S.M.A.; Condensation heat transfer coefficients in an inclined smooth tube at low mass fluxes; *International Journal of Heat and Mass Transfer* 123 (2018) 455-467; [doi: 10.1016/j.ijheatmasstransfer.2018.02.091]
- [62] Greco A., Vanoli G.P.; Flow-boiling of R22, R134a, R507, R404a and R410a inside a smooth horizontal tube; *Journal of Refrigeration* 28 (2005) 872-880; ELSEVIER © 2005 [doi: 10.1016/j.ijrefrig.2005.01.008]
- [63] Greco A.; Convective boiling of pure and mixed refrigerants: An experimental study of the major parameters affecting heat transfer; *Journal of Heat and Mass Transfer* 51 (2008) 896-909; [doi: 10.1016/j.ijheatmasstransfer.2007.11.002]
- [64] Meyer J.P., Ewim D.R.E.; Heat transfer coefficients during the condensation of low mass fluxes in smooth horizontal tubes;



- International Journal of Multiphase Flow 99 (2018) 485-499; [doi: 10.1016/j.ijmultiphaseflow.2017.11.015]
- [65] Akhavan-Behabadi M.A., Esmailpour M.; Experimental study of evaporation heat transfer of R-134a inside a corrugated tube with different tube inclinations; International Communications in Heat and Mass Transfer 55 (2014) 8-14; [doi: 10.1016/j.icheatmasstransfer.2014.03.003]
- [66] Aprea C., Greco A., Vanoli G.P.; Condensation heat transfer coefficients for R22 and R407C in gravity driven flow regime within a smooth horizontal tube; International Journal of Refrigeration 26 (2003) 393-401; [doi: 10.1016/S0140-7007(02)00151-2]
- [67] Lee Ho-Saeng, Son Chang-Hyo; Condensation heat transfer and pressure drop characteristics of R-290, R-600a, R-134a and R-22 in horizontal tubes; Heat Mass Transfer 46 (2010) 571-584; [doi: 10.1007/s00231-010-0603-9]
- [68] Dalkılıç A.S., Yildiz S., Wongwises S.; Experimental investigation of convective heat transfer coefficient during downward laminar flow condensation of R134a in a vertical smooth tube; International Journal of Heat and Mass Transfer 52 (2009) 142-150; [doi: 10.1016/j.ijheatmasstransfer.2008.05.035]
- [69] Arslan G., Eskin N.; Heat Transfer Characteristics for Condensation of R134a in a Vertical Smooth Tube; Journal of Experimental Heat Transfer 28 (2015) 430-445; [doi: 10.1080/08916152.2014.926430]
- [70] A. Hojati, M.A. Akhavan-Behabadi, P. Hanafizadeh, M.M. Ahmadpour, Effect of geometrical parameters on entropy generation during R134a boiling flow inside unique internally grooved tubes: experimental approach, Int. J. Therm. Sci. 163 (2021) 106845, <https://doi.org/10.1016/j.ijthermalsci.2021.106845>.
- [71] Lips S., Meyer J.P.; Experimental study of convective condensation in an inclined smooth tube. Part I: Inclination effect on flow pattern and heat transfer coefficient;

- International Journal of Heat and Mass Transfer 55 (2012) 395-404; [doi: 10.1016/j.ijheatmasstransfer.2011.09.033]
- [72] Lips S., Meyer J.P.; Stratified flow model for convective condensation in an inclined tube; International Journal of Heat and Fluid Flow 36 (2012) 83-91; [doi: 10.1016/j.ijheatfluidflow.2012.03.005]
- [73] Akhavan-Behabadi M.A., Mohseni S.G., Razavinasab S.M.; Evaporation heat transfer of R-134a inside a microfin tube with different tube inclinations; Experimental Thermal and Fluid Science 35 (2011) 996-1001; [doi: 10.1016/j.expthermflusci.2011.01.020]
- [74] Mohseni S.G., Akhavan-Behabadi M.A., Saedinia M.; Flow pattern visualization and heat transfer characteristics of R-134a during condensation inside a smooth tube with different tube inclinations; International Journal of Heat and Mass Transfer 60 (2013) 598-602; [doi: 10.1016/j.ijheatmasstransfer.2013.01.023]
- [75] Mohseni S.G., Akhavan-Behabadi M.A.; Flow pattern visualization and heat transfer characteristics of R-134a during evaporation inside a smooth tube with different tube inclinations; International Communications in Heat and Mass Transfer 59 (2014) 39-45; [doi: 10.1016/j.icheatmasstransfer.2014.10.018]
- [76] Thome J.R., El Hajal J., Cavallini A.; Condensation in horizontal tubes, part 2: new heat transfer model based on flow regimes; International Journal of Heat and Mass Transfer 46 (2003) 3365-3387; [doi: 10.1016/S0017-9310(03)00140-6]
- [77] Mehendale S.S., Jacobi A.M., Shah R.K.; Fluid flow and heat transfer at micro- and meso-scales with application to heat exchanger design; Appl. Mech. Rev. 53 (2000) 175-193; ASME Reprint No AMR290 \$18
- [78] Kandlikar S.G., Grande W.J.; Evolution of microchannel flow passages—Thermohydraulic performance and fabrication technology; Heat Transfer Engineering 24(2003) 3-17; [doi: 10.1080/01457630390116077]

- [79] Yan Y-Y., Lin T-F.; Evaporation heat transfer and pressure drop of refrigerant R-134a in a small pipe; *International Journal of Heat and Mass Transfer* 30 (1998) 4183-4194; [PII: S0017-9310(98)00127-6]
- [80] Huo X., Chen L., Tian Y.S., Karayiannis T.G.; Flow boiling and flow regimes in small diameter tubes; *Applied Thermal Engineering* 24 (2004) 1225-1239; Publisher ELSEVIER © 2004 [doi: 10.1016/j.applthermaleng.2003.11.027]
- [81] Cavallini A., Censi G., Del Col D., Doretti L., Longo G.A., Rossetto L., Zilio C.; Condensation inside and outside smooth and enhanced tubes — a review of recent research; *International Journal of Refrigeration* 26 (2003) 373-392; [doi: 10.1016/S0140-7007(02)00150-0]
- [82] Yu M., Lin T., Tseng C.; Heat transfer and flow pattern during two-phase flow boiling of R-134a in horizontal smooth and microfin tubes; *International Journal of Refrigeration* 25 (2002) 789-798; [PII: S0140-7007(01)00075-5]
- [83] Solanki A.K., Kumar R.; Condensation of R-134a inside dimpled helically coiled tube-in-shell type heat exchanger; *Applied Thermal Engineering* 129 (2018) 535-548; [doi: 10.1016/j.applthermaleng.2017.10.026]
- [84] Woodcock C., Ng'oma C., Sweet M., Wang Y., Peles Y., Plawsky J.; Ultra-high heat flux dissipation with Piranha Pin Fins; *International Journal of Heat and Mass Transfer* 128 (2019) 504-515; [doi: 10.1016/j.ijheatmasstransfer.2018.09.030]
- [85] Laohalertdecha S., Dalkiliç A.S., Wongwises S.; Correlations for evaporation heat transfer coefficient and two-phase friction factor for R-134a flowing through horizontal corrugated tubes; *International Communications in Heat and Mass Transfer* 38 (2011) 1406-1413; [doi: 10.1016/j.icheatmasstransfer.2011.08.014]
- [86] Dalkiliç A.S., Çebi A., Acikgoz O., Wongwises S.; Prediction of frictional pressure drop of R134a during condensation inside smooth and corrugated tubes; *International Communications in*

- Heat and Mass Transfer 88 (2017) 183-193; [doi: 10.1016/j.icheatmasstransfer.2017.08.011]
- [87] Aroonrat K., Wongwises S.; Evaporation heat transfer and friction characteristics of R-134a flowing downward in a vertical corrugated tube; *Experimental Thermal and Fluid Science* 35 (2011) 20-28; [doi: 10.1016/j.expthermflusci.2010.08.002]
- [88] H. Gröber, S. Erk, U. Grigull, *Die Grundgesetze der Wärme Übertragung*, Springer Verlag, Berlin, 1963.
- [89] J.W. Rose, Heat-transfer coefficients, Wilson plots and accuracy of thermal measurements, *Exp. Therm. Fluid Sci.* 28 (2004) 77–86, [http://dx.doi.org/10.1016/S0894-1777\(03\)00025-6](http://dx.doi.org/10.1016/S0894-1777(03)00025-6).
- [90] G.B. Whitham, *Linear and Nonlinear Waves*, Wiley, New York, 1974.
- [91] T. Hobbler, *Heat Transfer and Heat Exchangers*, Publishing House of Chemical Literature, Leningrad, 1961.
- [92] S. Kutateladze, *Theory of Heat Transfer*, Novosibirsk, 1970.
- [93] Hausen H, *Wärmeübertragung im Gegenstrom und Kreuzstrom*, Berlin, 1950.
- [94] Kubín M., Hirš J., Plášek J.; Experimental analysis of steam condensation in vertical tube with small diameter; *International Journal of Heat and Mass Transfer* 94 (2016) 403–410; [doi: <http://dx.doi.org/10.1016/j.ijheatmasstransfer.2015.11.022>]
- [95] S.B. Al-Shammari, D.R. Webb, P. Heggs, Condensation of steam with and without the presence of non-condensable gases in a vertical tube, *Desalination* 169 (2004) 151–160, [doi: <http://dx.doi.org/10.1016/j.desal.2003.11.006>]
- [96] Urban F., Kubín M, Kučák L., Experiments on the heat exchangers with the tubes of small diameters, *AIP Conf. Proc.* 1608 (1) (2014) 245–248, <http://dx.doi.org/10.1063/1.4892743>.
- [97] X.-H. Ma, X.-D. Zhou, Z. Lan, Y.-M. Li, Y. Zhang, Condensation heat transfer enhancement in the presence of non-condensable gas using the interfacial effect of dropwise condensation, *Int. J. Heat Mass Transfer* 51 (2008) 1728–1737.

- [98] S.J. Kim, H.C. No, Turbulent film condensation of high pressure steam in a vertical tube, *Int. J. Heat and Mass Transfer* 43 (2000) 4031–4042 (PII: S0017- 9310(00)00015-6).
- [99] J.H. Goodykoontz, R.G. Dorsch, Local heat-transfer coefficients for condensation of steam in vertical downflow within a 5/8 inch diameter tube, National Aeronautics and Space Administration, Lewis Research Center (NASA), Technical Note (NASA TN D-3326), United States, Washington, D.C. 1966, [online: [ntrs.nasa.gov/archive/nasa/casi.ntrs.nasa.gov/19660008881.pdf](https://ntrs.nasa.gov/archive/nasa/casi.ntrs.nasa.gov/19660008881.pdf)]
- [100] Horák P., Formánek M., Fečer T., Plášek J.; Evaporation of refrigerant R134a, R404A and R407C with low mass flux in smooth vertical tube. *International journal of Heat and Mass transfer* 181 (2021) 121845 (page 1-8); ISSN: 0017-9310; [doi: <https://doi.org/10.1016/j.ijheatmasstransfer.2021.121845>]
- [101] W.C. Reynolds, R.E. Lundberg, P.A. McCuen, Heat transfer in annular passages. General formulation of the problem for arbitrarily prescribed wall temperatures or heat fluxes, *Int. J. Heat Mass Transf.* 6 (1963) 4 83–4 93 Pergamon Press 1963. Printed in Great Britain.
- [102] R.E. Lundberg, P.A. McCuen, W.C. Reynolds, Heat transfer in annular passages. Hydrodynamically developed laminar flow with arbitrarily prescribed wall temperatures or heat fluxes, *Int. J. Heat Mass Transf.* 6 (1963) 495–529 Pergamon Press 1963. Printed in Great Britain.
- [103] H.S. Heaton, W.C. Reynolds, W.M. Kays, Heat transfer in annular passages. Simulations development of velocity and temperature fields in laminar flow, *Int. J. Heat Mass Transf.* 7 (1964) 763–781 Pergamon Press 1964. Printed in Great Britain.
- [104] V. Gnielinski, in: *Heat Transfer in Concentric Annular and Parallel Plate Ducts*; VDI-Heat Atlas, Springer Press, 1993, pp. 701–708. 1993. Printed in Berlin, Germany.
- [105] T.D. Bennett, Fully developed transport constants of annular tubes, with application to the entrance region, *J. Therm. Sci. Eng. Appl.* 12 (2020) 1–7, doi: 10.1115/1.4045697.

- [106] X. Fang, Q. Wu, Y. Yuan, A general correlation for saturated flow boiling heat transfer in channels of various sizes and flow directions, *Int. J. Heat Mass Transf.* 107 (2017) 972–981, doi: 10.1016/j.ijheatmasstransfer.2016.10.125.
- [107] S-M. Kim, I. Mudawar, Universal approach to predicting saturated flow boiling heat transfer in mini/micro-channels – Part II. Two-phase heat transfer coefficient, *International Journal of Heat Mass Transfer* 64 (2013) 1239–1256, doi: 10.1016/j.ijheatmasstransfer.2013.04.014.
- [108] L. Sun , K. Mishima , An evaluation of prediction methods for saturated flow boiling heat transfer in mini-channels, *Int. J. Heat Mass Transf.* 52 (2009) 5323–5329.
- [109] M. Hamdar , A. Zoughaib , D. Clodic , Flow boiling heat transfer and pressure drop of pure HFC-152a in a horizontal mini-channel, *Int. J. Refrig.* 33 (2010) 566–577.
- [110] W. Li , Z. Wu , A general criterion for evaporative heat transfer in mi- cro/mini-channels, *Int. J. Heat Mass Transf.* 53 (2010) 1967–1976.
- [111] V.V. Klimenko, A generalizes correlation for two-phase forced flow heat trans- fer, *Int. J. Heat Mass Transf.* 31 (1988) 541–552 [0017-9310/88 \$03.0 0 + 0.0 0.
- [112] L. Wojtan, T. Ursenbacher, J.R. Thome, Investigation of flow boiling in horizon- tal tubes: Part I—a new adiabatic two-phase flow pattern map, *Int. J. Heat Mass Transf.* 48 (2005) 2955–2969, doi: 10.1016/j.ijheatmasstransfer.2004.12. 012.
- [113] J. Lee, I. Mudawar, Two-phase flow in high-heat-flux micro-channel heat sink for refrigeration cooling applications: Part II— heat transfer characteristics, *Int. J. Heat Mass Transf.* 48 (2005) 941–955, doi: 10.1016/j.ijheatmasstransfer.2004. 09.019.
- [114] X. Fang, Z. Fengting, C. Chuang, W. Qi, C. Yanyu, C. Yuanyuan, H. Yan, Saturated flow boiling heat transfer: review and assessment of prediction methods, *Heat and Mass Transfer* 55 (2019) 197–222, doi: 10.10 07/s0 0231- 018- 2432- 1.

## 8. Appendix

### 8.1. Experimental setup for Condensation

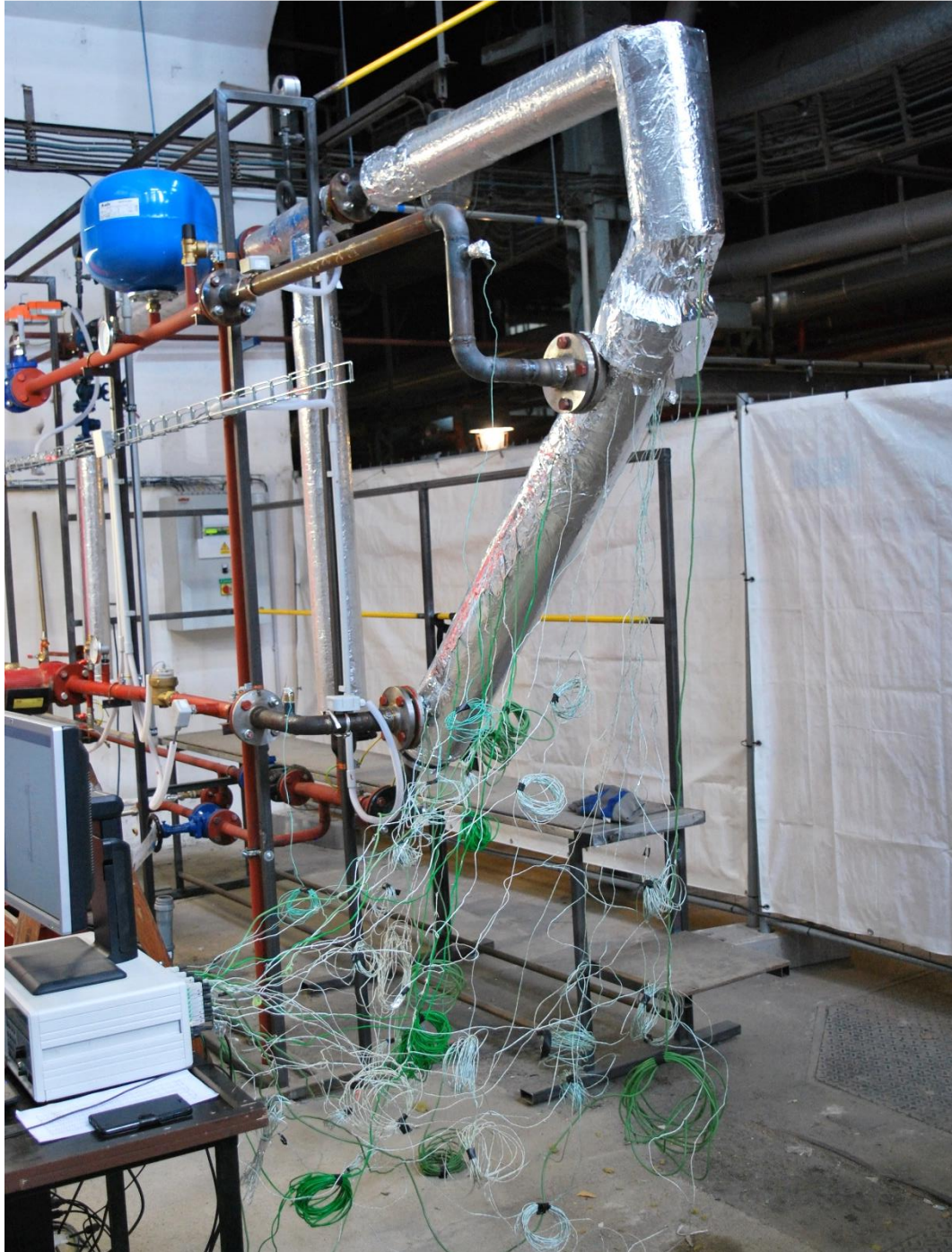


**Figure 8.1A** – *Photo of vertical heat exchanger in counter-flow at 11<sup>th</sup> April 2017.*

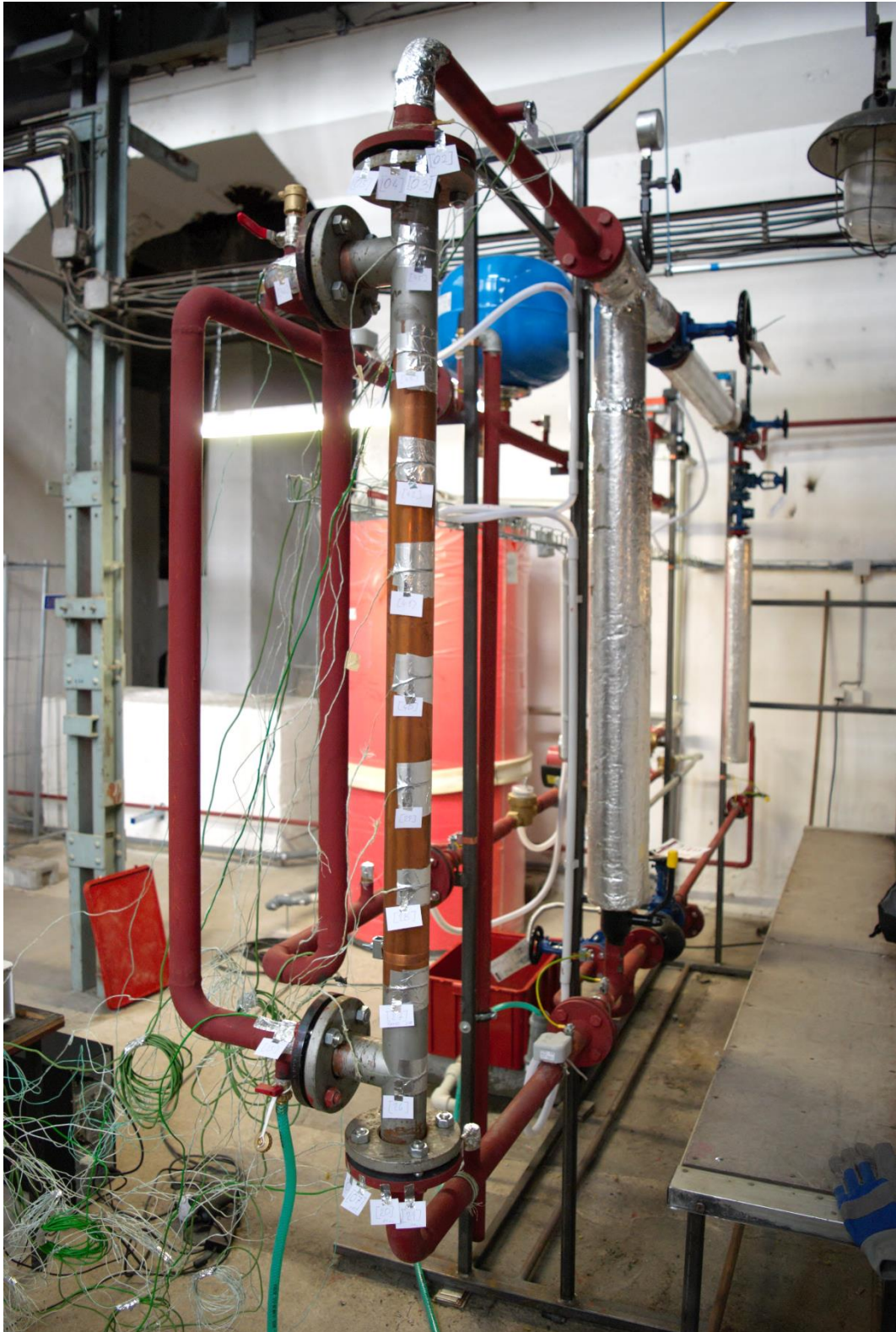


**Figure 8.1B** – *Photo of vertical heat exchanger in parallel-flow at 4<sup>th</sup> May 2017.*





**Figure 8.1C** – *Photo of inclined heat exchanger in counter-flow at 30<sup>th</sup> April 2017.*



**Figure 8.1D** – *Photo of vertical heat exchanger in parallel-flow at 20<sup>th</sup> June 2017.*



**Figure 8.1E** – *Photo of experimental measurement at 20<sup>th</sup> June 2017.*



**Figure 8.1F** – *Photo of experimental setup at 11<sup>th</sup> April 2017.*

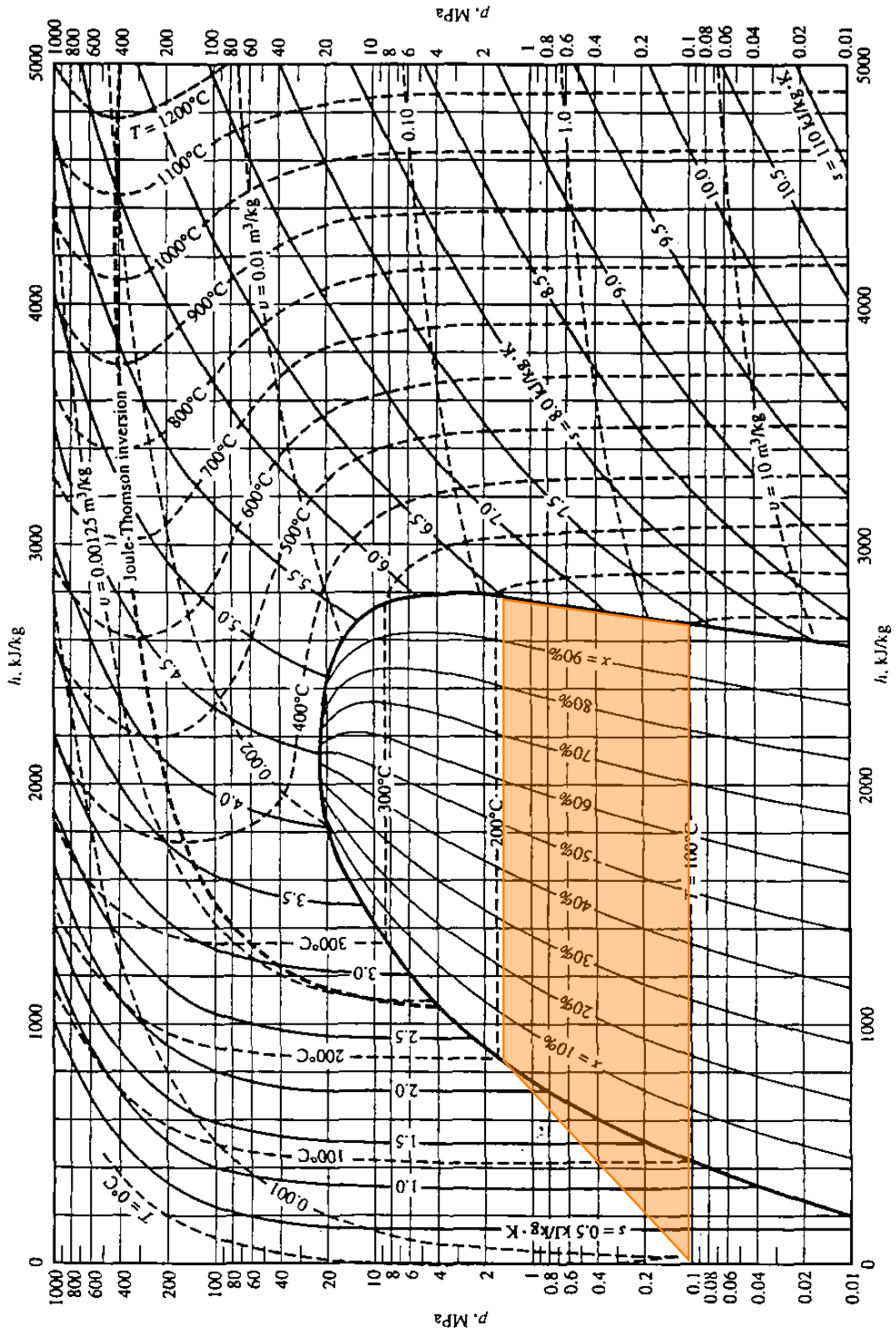


**Figure 8.1G** – Pressure-Enthalpy diagram of water steam with the scheme of measured area.

## 8.2. Experimental setup for Evaporation



**Figure 8.2A** – *Photo of experimental setup in laboratory TZB at 6<sup>th</sup> April 2017.*



**Figure 8.2B** – *Photo of evaporator tube at 6<sup>th</sup> April 2017.*



**Figure 8.2C** – Photo of expansion valve to evaporator tube and upper connection of heating water at 6<sup>th</sup> April 2017.





**Figure 8.2D** – *Photo of compressor section (left down) and bottom outflow of refrigerant from evaporator tube at 6<sup>th</sup> April 2017.*

# 9. Annex

## 9.1. List of Tables

**Table 2.1** Chronological table of major references relating to boiling heat transfer [35].

**Table 4.1** The correlation of obtained results with other studies

**Table 5.1** Accuracy and uncertainties of experimental measurement.

**Table 5.2** Range of variable parameter of experimental measurement.

## 9.2. List of Figures

- Figure 2.1** Collapse of ice crystal structure with the formation of water drops [5].
- Figure 2.2** Evaporation of liquid at its boiling point [6].
- Figure 2.3** Thermohaline circulation on the planet Earth [9].
- Figure 2.4** Equipment of Nukiyama for metal wire experiments [36].
- Figure 2.5** Pool boiling curve, according to [37].
- Figure 2.6** Regimes of pool boiling. During the transition from natural convection to nucleate boiling, sub cooling boiling occurs. The temperature of most of the liquid is below the saturation temperature and bubbles formed at the surface may condense in the liquid [37].
- Figure 2.7** The chart correlation of Shah [51].
- Figure 2.8** Heat transfer regions in convective boiling in a vertical tube, according to [53].
- Figure 2.9** Two phase flow patterns in horizontal tubes:  
(a) evaporation,  
(b) condensation with high liquid loading,  
(c) condensation with low liquid loading, see [53].
- Figure 4.1** Scheme of tubular heat exchanger with 55 spiral micro tubes.
- Figure 4.2** Bundle of 55 spiral micro tubes for water steam.
- Figure 4.3** Detail of spiral micro tubes with inner diameter 3.0 mm.
- Figure 4.4** Experimental setup of tubular heat exchanger.
- Figure 4.5** AHLBORN thermocouple wires with ALMEMO connector.
- Figure 4.6** ALMEMO Multi-function data logger 5590.
- Figure 4.7** Condensation in the parallel-flow with inclination 45°.
- Figure 4.8** Condensation in the counter-flow with inclination 45°.
- Figure 4.9** Vertical condensation in the parallel/counter-flow.

- Figure 4.10** Water meter G. GIOANOLA, IARC/25 R80, Class T90 with MaR recording system.
- Figure 4.11** Manual three-way valve.
- Figure 4.12** Manual valve for pressure regulating by Spirax Sarco BRV73.
- Figure 4.13** Comparison of tested equations related to Wilson plot method.
- Figure 5.1** Scheme of sensor location.
- Figure 5.2** Scheme of calculation part.
- Figure 5.3** Compressor unit (left photo) and expansion valve (right photo).
- Figure 5.4** Compressor Cubigel GX18TB VE09.
- Figure 5.5** Pressure-Enthalpy diagram of refrigerant R134a, R404A, and R407C.
- Figure 5.6** Graphical nomogram (Eq. 5.5), (Eq. 5.6), and (Eq. 5.7) for the determination of  $Nu^\infty$  as a function of  $(D_i/D_o)$  ratio for the three boundary conditions.
- Figure 5.7** Boundary conditions for heat transfer in an annular gap.
1. Heat transferred at the inner tube (subscript  $i$ ); the outer tube insulated
  2. Heat transferred at the outer tube (subscript  $o$ ); the inner tube insulated
  3. Heat transferred at both tubes (subscript  $b$ ); the walls of each are at the same temperature  $T_{wi} = T_{wo}$ .
- Figure 5.8** The dependence of heat flux on the mass flux is suppressed.
- Figure 5.9** The heat flux is driven by the temperature difference.
- Figure 5.10** The boiling heat transfer coefficient is dependent on the vapour quality.
- Figure 5.11** The correlation quality of experimental Nusselt number with the predicted Nusselt numbers by Fang et al. [92]

## 9.3. Author Biography



**Ing. Tomáš Fečer**

[135414@vutbr.cz](mailto:135414@vutbr.cz)

### Experience

2017 – 2018

#### **Junior Researcher**

Brno University of Technology, Research Centre AdMAS

### Education

since 2017

#### **Doctoral study programme**

Brno University of Technology, Faculty of Civil Engineering,  
Institute of Computer Aided Design and Informatics (AIU),  
Theme: Heat transfer analysis of phase-change process  
in tubular exchanger,  
Mentor: Ing. Josef Plášek, Ph.D.

2015 – 2017

#### **Master study programme**

Brno University of Technology, Faculty of Civil Engineering,  
Institute of Building services (TZB),  
Theme: Energy evaluation of apartment building,  
Mentor: Ing. Pavel Adam, Ph.D.

2010 – 2015

#### **Bachelor study programme**

Brno University of Technology, Faculty of Civil Engineering,  
Institute of Building services (TZB),  
Theme: Ventilation of wooden apartment building  
Mentor: Ing. Pavel Adam, Ph.D.

### Internship

2017 – 2022

#### **Norwegian University of Science and Technology (NTNU)**

Experimental measurement of Indoor climate,  
09/2020 – 02/2022 (6 months)  
10/2019 – 08/2020 (11 months)  
11/2018 – 12/2018 (24 days)  
05/2017 (3 days)  
Mentor: prof. Guangyu Cao

2017

#### **Technical University of Kosice (TUKE)**

Experimental measurement of Thermal conductivity,  
05/2017 (6 days), Mentor: Ing. František Vranay, Ph.D.

## Teaching

- 2017 – 2018 BU001 – Informatics  
2018 BU091 - CAD system in 2D

## Results

- (RIV-J<sub>imp</sub>)** 2021 Aganovic A., Cao G., **Fečer T.**, Ljungqvist B., Lytsy B., Radtke A., Reinmüller B., Traversari R.; Ventilation design conditions associated with airborne bacteria levels within the wound area during surgical procedures: a systematic review; Journal of Hospital infection 113 (2021) 85-95; ISSN: 0195-6701; Elsevier **(IF = 3.926)** [<https://doi.org/10.1016/j.jhin.2021.04.022>]
- (RIV-J<sub>imp</sub>)** 2021 Horák P., Formánek M., **Fečer T.**, Plášek J.; Evaporation of refrigerant R134a, R404A, and R407C with low mass flux in smooth vertical tube; International Journal of Heat and Mass Transfer 181 (2021) 121845; ISSN: 0017-9310; **(IF = 5.584)** [<https://doi.org/10.1016/j.ijheatmasstransfer.2021.121845>]
- (RIV-D)** 2018 Čekon M., Plášek J., Slávik R., **Fečer T.**, Juráš P.; An experimental and numerical model of a solar facade prototype with transparent insulation and selective absorber; Conference proceeding by ASHRAE 2018; Chicago, USA: 2018; 398-405; ISSN: 2577-0446.
- (RIV-R)** 2018 Apeltauer T., Apeltauer J., Mishuk A., **Fečer T.**, Plášek J.; Software FireDES version 1.0 at Brno University of Technology (FAST); [[www.fce.vutbr.cz/AIU/plasek.j/firedes.htm](http://www.fce.vutbr.cz/AIU/plasek.j/firedes.htm)]
- (RIV-R)** 2018 Hirš J., Kubín M., Horká L., **Fečer T.**, Plášek J.; Software Výměník; [[www.fce.vutbr.cz/AIU/plasek.j/vymenik.htm](http://www.fce.vutbr.cz/AIU/plasek.j/vymenik.htm)]
- (RIV-F)** 2018 Horák P., Uher P., Plášek J., Formánek M., **Fečer T.**; Výměník tepla; Vysoké učení technické v Brně; Užitélný vzor 2018 (číslo patentu 32502)

## Projects

- 2019 – 2020 **Specific research at BUT (FAST-J-19-6082)**  
Fečer T., Plášek J.; Interakce vnitřního prostředí s povrchem stěny v historické budově, zahájení: 01.03.2019, ukončení: 28.02.2020
- 2018 – 2019 **Specific research at BUT (FAST-J-18-5574)**  
Fečer T., Plášek J.; Numerická analýza vnitřního prostředí v historické budově, zahájení: 01.03.2018, ukončení: 28.02.2019
- 2018 – 2019 **Specific research at BUT (FAST-S-18-5327)**

Podroužek J., Apeltauer T., Fečer T., Krč R., Okřinová P., Plášek J.;  
Analýza progresivních stavebních struktur a materiálů, zahájení:  
01.03.2018, ukončení: 28.02.2019

2017 – 2018 **Junior GA CR (GJ 16-02430Y)**  
Čekon M., Plášek J., Slávik R., Fečer T., Struhala K.; Novodobé  
koncepty klimaticky aktivních solárních fasád integrujících  
pokročilá materiálová řešení; Juniorský GA ČR.

2017 – 2018 **Specific research at BUT (FAST-J-17-4275)**  
Plášek J., Apeltauer T., Fečer T., Horák J., Krč R., Okřinová P.,  
Podroužek J., Stančík A., Uher L.; Numerické modelování  
inženýrských úloh ve stavebnictví, zahájení: 01.03.2017,  
ukončení: 28.02.2018

2017 – 2018 **Specific research at BUT (FAST-J-17-4616)**  
Fečer T., Apeltauer T.; Šíření tepla v asfaltovém krytu vozovky,  
zahájení: 01.03.2017, ukončení: 28.02.2018

**Homepage**

<https://www.vutbr.cz/lide/tomas-fecer-135414>

## 9.4. Author Results

### 9.4.1. 2018 (RIV-F) Utility model

Horák P., Uher P., Plášek J., Formánek M., Fečer T.; *Výměník tepla*; Vysoké učení technické v Brně; Užiténý vzor 2019 (číslo patentu 32502)

ÚŘAD PRŮMYSLOVÉHO VLASTNICTVÍ  
Antonína Čermáka 2a, 160 68 Praha 6-Bubeneč  
tel: 220 383 111 fax: 224 324 718

Zde přihlašovatel uvede adresu, kam má  
být potvrzení o podání zasláno:

Ing. Libor M a r k e s  
Grohova 54  
602 00 BRNO

**POTVRZENÍ O PODÁNÍ PŘIHLÁŠKY UŽITNÉHO VZORU**

Úřad průmyslového vlastnictví potvrzuje, že dne .....  
byla podána přihláška užiténého vzoru o názvu  
(název doplní přihlašovatel)

Výměník tepla

se žádostí o zápis užiténého vzoru do rejstříku. Přihláška užiténého vzoru byla evidována  
pod spisovou značkou:

Úřad průmyslového vlastnictví  
10.10.2018  
Antonína Čermáka 2a  
160 68 Praha 6

PUV [ **PUV 2018 – 35443**  
10.10.2018 08:53:41

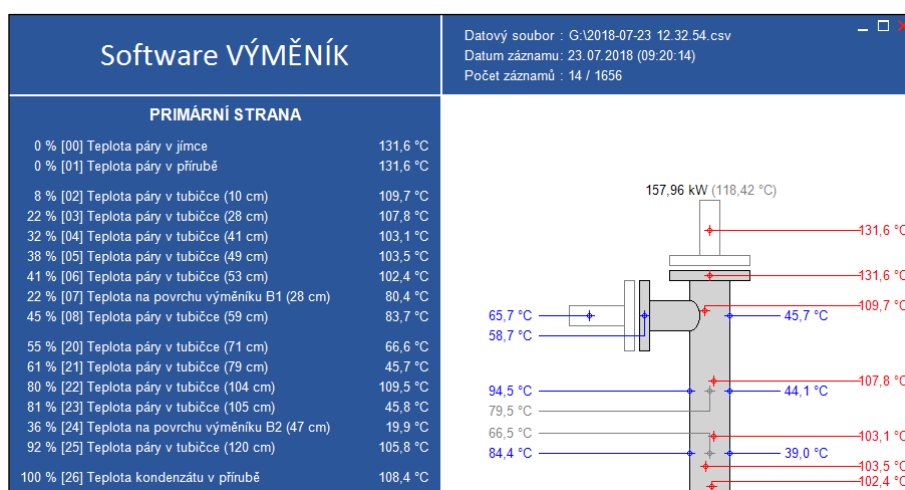
(podpis odpovědného pracovníka, datum, razítko)

Telefon: s provozbou 220 383 xxx (111 ústředna), fax: 224 324 718  
IČ 48135097



## 9.4.2. 2018 (RIV-R) Software Výměník

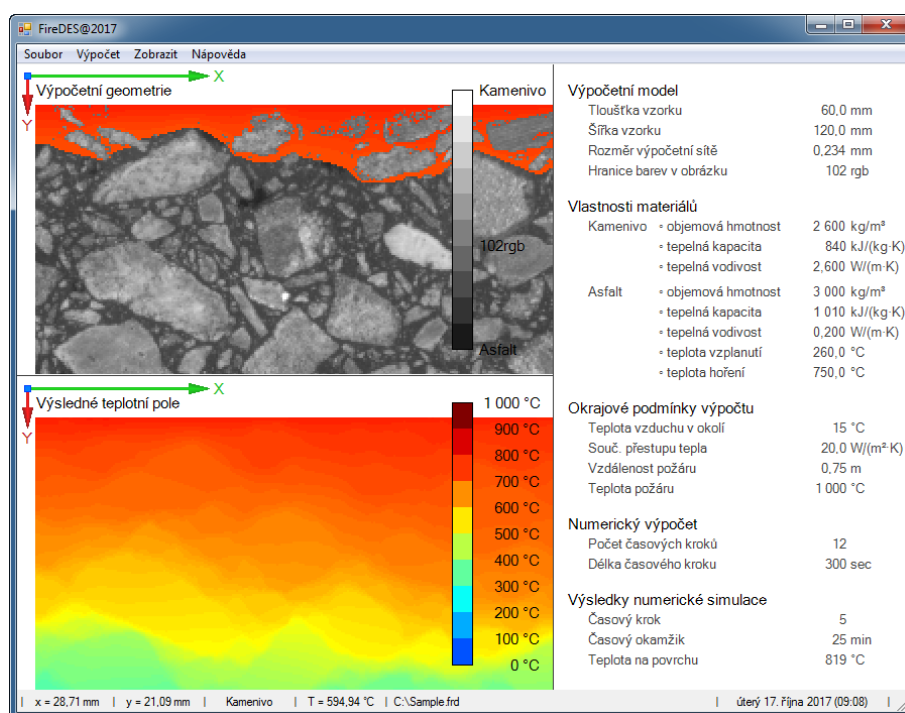
Software VÝMĚNÍK je desktopová aplikace určená pro záznam, zpracování a vyhodnocení měřených dat v reálném čase s využitím hardwarového rozhraní ústředny Ahlborn. Softwarová aplikace s názvem [vymenik.exe] je určena pro on-line měření více než 30 bodů uživatelsky definovaných v editovatelném souboru typu [\*.ini]. Tento software VÝMĚNÍK je vytvořen v plnohodnotném programovacím jazyku C# založeném na platformě Microsoft .NET, čímž je zaručen bezproblémový provoz softwaru na všech zařízeních s operačním systémem Windows. Software VÝMĚNÍK je již reálně ověřen více než 200 hodinovým provozem v souproudém i protiproudém zapojení trubkového výměníku pára/voda s ukázkou záznamu při plném provozu.



Software vzniknul jako unikátní výsledek aplikovaného technického výzkumu ve výzkumném centru AdMaS v rámci projektu LO1408 s názvem »AdMaS UP - Advanced Materials, Structures and Technologies« a podporou Specifického výzkumu FAST-J-18-5574 na Vysokém učení technickém v Brně. Autorem softwaru je prof. Ing. Jiří Hirš, CSc.; Dr. Ing. Milan Kubín; Ing. Lucie Horká; Ing. Tomáš Fečer a Ing. Josef Plášek, Ph.D.

### 9.4.3. 2018 (RIV-R) Software FireDES

Program FireDES verze 1.0 je desktopová aplikace určená pro nestacionární numerický výpočet 2D teplotního pole s proměnnou výpočetní geometrií v čase simulující odhořívání asfaltové suspenze mezi kameny. Výpočetní síť v rastru 512 x 256 buněk je importována z obrázkové bitmapy a vzniklá soustava 131 072 lineárních rovnic je řešena Gauss-Seidlovou iterační metodou. Výpočetní geometrie, stejně jako materiálové vlastnosti, okrajové podmínky a výsledné teplotní pole je uloženo do bitového souboru s příponou [\*].frd].



Program FireDES verze 1.0 vzniknul v rámci spolupráce VUT v Brně a firmy K.B.K. fire, s.r.o. v rámci projektu číslo TA04031642 s názvem »Asfalty v silničních tunelech«, realizovaného v programu ALFA Technologické agentury ČR. Autory softwaru jsou doc. Mgr. Tomáš APELTAUER, Ph.D.; Ing. Jiří APELTAUER; Bc. Aliaksandra MISHUK; Ing. Tomáš FEČER a Ing. Josef PLÁŠEK, Ph.D.

## 9.4.4. 2018 (RIV-D) Conference paper

Čekon M., Plášek J., Slávik R., Fečer T., Juráš P.; *An experimental and numerical model of a solar facade prototype with transparent insulation and selective absorber*; Conference proceeding by ASHRAE 2018; Chicago, USA: 2018; 398-405; ISSN: 2577-0446.



2018 Building Performance Analysis Conference and  
SimBuild co-organized by ASHRAE and IBPSA-USA  
Chicago, IL  
September 26-28, 2018

### AN EXPERIMENTAL AND NUMERICAL MODEL OF A SOLAR FACADE PROTOTYPE WITH TRANSPARENT INSULATION AND SELECTIVE ABSORBER

Miroslav Čekon<sup>1</sup>, Josef Plášek<sup>1</sup>, Richard Slávik<sup>1</sup>, Tomáš Fečer<sup>1</sup> and Peter Juráš<sup>2</sup>

<sup>1</sup>Centre AdMaS, Brno University of Technology, Brno, Czechia

<sup>2</sup>Faculty of Civil Engineering, University of Žilina, Žilina, Slovakia

#### ABSTRACT

The presented study focuses on the modelling of a Transparent Insulation Material (TIM) incorporated in a façade structure. An experimental prototype of a Transparent Insulation Façade (TIF) with and without a selective absorber was developed as part of the opaque building envelope. Experimental measurements were performed using a climatic chamber test with the aim of verifying theoretical models. A detailed comparative investigation of the thermal performance of both TIFs was conducted using numerical CFD methods. The proper consistency between the simulation results and the experimental data indicated that the simulation model was reliable for predicting the overall thermal performance of TIM based solar façade prototypes.

#### INTRODUCTION

The improved thermal insulation offered by integrating transparent insulation material (TIM) into building façades can ultimately affect the overall energy efficiency of the building. Different studies in the last two decades developed the solar walls with TIMs replacing the original glazing elements. Hence, the development of various innovative concepts of building envelopes, and their practical implementation, can be enhanced by applying the proper performance prediction theoretical models. Experimental tests in conjunction with numerical computations may validate and improve performance prediction models of building envelopes, such as novel solar thermal façade elements. This area needs to be studied to accurately predict the thermal and energy performance in the context of applying TIMs on a solar façade concept.

Current building energy simulation tools are not accurate enough for modelling these complex transparent insulation systems, often because of the simplified thermal and optical models used to solve heat transfer as well as light transmittance. Basically, one dimensional methods are used for both thermal transfer and solar transmittance through these systems (Sun et al. 2018). In practice, with the integration of a more complex structure within the air cavity of a double glazing unit, there will be a significant effect on the free convection,

long-wave radiative heat transfer and solar energy transmitted through the system that have not been typically considered. This was recently analyzed by Sun (2017) to comprehensively study all those aspects in glazing system with TIM for building energy saving and daylight comfort. They aimed to develop a comprehensive method to analyse these specific glazing systems (Sun et al. 2017). Specifically, in most of the previously conducted studies, long-wave radiation heat transfer, which accounts for two thirds of the total heat transfer across the air cavity (Gan 2001), is neglected within TIM-based structure during numerical modelling. In addition, when integrated in a building opaque element with multilayer structure that employ several low-e functionalities, this can result in a completely different situation and and give rise to a more complex task that needs to be considered.

Although, the thermal resistance of the glazing system varies with the change of the mean temperature of the glazing and the temperature difference between the two glazing panes, detailed investigations of the interstitial structure on the reduction of heat transfer in terms of both convection, which is driven predominately by temperature difference across the two glass panes, and radiation, which is driven predominately by glazing system mean temperature, under different environmental conditions that are commonly encountered in buildings are less well studied (Sun et al. 2016). The improved simulation methods have been implemented by Avedissian and Naylor (2008), who used a surface-to-surface model to include radiation, however they only used the model to calculate the  $U$ -value of the whole system instead of evaluating the effects of the internal structure on long-wave radiative heat transfer.

Brandl et al. (2015) developed a three-dimensional (3D) Computational Fluid Dynamics (CFD) model for the analysis of the thermal behaviour of a solar honeycomb (SHC) façade element using the cellulose honeycomb TIM in steady state conditions. Laboratory experiments were performed and the measured data were used for the validation of the 3D CFD models of the SHC element. Moreover, the impact of the SHC's material properties on the dynamic thermal behaviour was analysed with this CFD model. This was primarily focused on further

## 9.4.5. 2021 (RIV-J) Research paper

Horák P., Formánek M., Fečer T., Plášek J.; *Evaporation of refrigerant R134a, R404A, and R407C with low mass flux in smooth vertical tube*; International Journal of Heat and Mass Transfer 181 (2021) 121845; ISSN: 0017-9310; Publisher ELSEVIER © 2021 (IF = 5.584); [https://doi.org/10.1016/j.ijheatmasstransfer.2021.121845]

International Journal of Heat and Mass Transfer 181 (2021) 121845

---



Contents lists available at ScienceDirect

### International Journal of Heat and Mass Transfer

journal homepage: [www.elsevier.com/locate/hmt](http://www.elsevier.com/locate/hmt)



---

## Evaporation of refrigerant R134a, R404A and R407C with low mass flux in smooth vertical tube



P. Horák\*, M. Formánek, T. Fečer, J. Plášek

*Faculty of Civil Engineering, Brno University of Technology, Czech Republic*

---

**ARTICLE INFO**

*Article history:*  
Received 31 May 2021  
Revised 30 July 2021  
Accepted 11 August 2021

*Keywords:*  
Mass flux  
Heat flux  
Vapour quality  
Heat transfer coefficient  
Nusselt number

**ABSTRACT**

This experimental study analysis the low mass flux of refrigerant R134a, R404A, and R407C in the smooth vertical evaporator tube with an inner diameter of 32 mm. This downward-flow refrigerant with a mass flux of about  $9 \text{ kg}\cdot\text{m}^{-2}\cdot\text{s}^{-1}$  in the parallel/counter flow of heating water shows suppressed heat transfer by convective boiling and dominant heat transfer by nucleate boiling. This dominant heat transfer by nucleate boiling is dependent on the superheated wall of evaporator tube. The experimentally obtained Nusselt number correlates 92.2 % for R134a, 92.4 % for R404A, and 83.2 % for R407C with the predicted Nusselt number for mass flux over  $10 \text{ kg}\cdot\text{m}^{-2}\cdot\text{s}^{-1}$ . In summary, the untypically low mass flux of refrigerant about  $9 \text{ kg}\cdot\text{m}^{-2}\cdot\text{s}^{-1}$  is comparable with the current state of knowledge for low mass flux over  $10 \text{ kg}\cdot\text{m}^{-2}\cdot\text{s}^{-1}$ .

© 2021 Elsevier Ltd. All rights reserved.

---

**1. Introduction**

The refrigeration system is applied in advanced technology more and more often. The engineering design of refrigeration system is simplified usually on the application of boiling heat transfer coefficient. The prediction model of boiling heat transfer coefficient is published by Fang et al. [28], Kim and Mudawar [29], Sun and Mishima [30], Hamdar et al. [31], Li and Wu [32], and Fang et al. [38]. However, this boiling heat transfer coefficient includes complex heat transfer by nucleate boiling, convective boiling, and pre/post-dryout effect. The nucleate boiling is dependent on the superheated wall (i.e. heat flux), and the presence of active nucleation site. The heat transfer between the superheated wall and vapour core is performed in liquid film by convective boiling. This convective boiling is dependent on the mass flux and the vapour quality. The pre/post-dryout effect is associated with the annular flow when the liquid film is consumed, and the superheated wall is exposed directly to the vapour core. This pre/post-dryout effect is published by Klimenko [34], Wojtan et al. [35], and Lee and Mudawar [36].

The boiling heat transfer coefficient increases with the increasing mass flux and the increasing vapour quality as published Jung et al. [1], Bandhauer et al. [2] Arslan and Eskin [3], Adekunle et al. [4], Aroonrat and Wongwises [5], and Meyer et al. [6]. Meyer et al. [6], Ewim et al. [7], and Lips et al. [8,9] published condensation R134a with the mass flux in a range from 50 to

$600 \text{ kg}\cdot\text{m}^{-2}\cdot\text{s}^{-1}$  in the smooth inclined tube with an inner diameter of 8.38 mm, and the lowest boiling heat transfer coefficient from  $900$  to  $1500 \text{ W}\cdot\text{m}^{-2}\cdot\text{K}^{-1}$  is obtained for vertical tube with the downward flow of refrigerant. Akhavan-Behabadi et al. [10], and Mohseni et al. [11,12] published evaporation R134a with the mass flux in a range from  $46$  to  $170 \text{ kg}\cdot\text{m}^{-2}\cdot\text{s}^{-1}$  in the smooth inclined tube with an inner diameter of 8.9 mm, and the lowest boiling heat transfer coefficient from  $600$  to  $2500 \text{ W}\cdot\text{m}^{-2}\cdot\text{K}^{-1}$  is obtained for vertical tube with the downward flow of refrigerant. The dependence of boiling heat transfer coefficient on the heat flux for a fixed mass flux is studied by Greco and Vanoli [14].

The dependence of boiling heat transfer coefficient on the mass flux decreases for a lower mass flux (below or equal to  $100 \text{ kg}\cdot\text{m}^{-2}\cdot\text{s}^{-1}$ ) as reported Cavallini et al. [15]. This decreased dependence of boiling heat transfer coefficient on the mass flux is substituted by dependent on the temperature difference (superheated wall), according to Ewim et al. [7]. The low mass flux is studied by Meyer et al. [16] on  $50 \text{ kg}\cdot\text{m}^{-2}\cdot\text{s}^{-1}$ , Akhavan-Behabadi and Esmailpour [13] on  $46 \text{ kg}\cdot\text{m}^{-2}\cdot\text{s}^{-1}$ , Aprea et al. [17] on  $45.5 \text{ kg}\cdot\text{m}^{-2}\cdot\text{s}^{-1}$ , Lee and Son [18] on  $35.5 \text{ kg}\cdot\text{m}^{-2}\cdot\text{s}^{-1}$ , Dalkılıç et al. [19] on  $29 \text{ kg}\cdot\text{m}^{-2}\cdot\text{s}^{-1}$ , Arslan and Eskin [20] on  $20 \text{ kg}\cdot\text{m}^{-2}\cdot\text{s}^{-1}$ , and Hojati et al. [21] on  $16.5 \text{ kg}\cdot\text{m}^{-2}\cdot\text{s}^{-1}$ .

Therefore, this research study extension the current state of knowledge about the untypically low mass flux of refrigerant R134a, R404A and R407C in the smooth vertical tube with an inner diameter of 32 mm. This untypically low mass flux of about  $9 \text{ kg}\cdot\text{m}^{-2}\cdot\text{s}^{-1}$  in the vertical evaporator tube is analysed experimentally for the downward flow of refrigerant in the parallel/counter flow of heating water. This experimental analysis is based on the

---

\* Corresponding author.  
E-mail addresses: [plasek.j@vut.cz](mailto:plasek.j@vut.cz) (P. Horák), [plasek.j@vut.cz](mailto:plasek.j@vut.cz) (J. Plášek).


<https://doi.org/10.1016/j.ijheatmasstransfer.2021.121845>  
0017-9310/© 2021 Elsevier Ltd. All rights reserved.

## 9.4.6. 2021 (RIV-J) Research paper


Aganovic A., Cao G., Fečer T., Ljungqvist B., Lytsy B., Radtke A., Reinmüller B., Traversari R.; *Ventilation design conditions associated with airborne bacteria levels within the wound area during surgical procedures: a systematic review*; Journal of Hospital Infection 113 (2021) 85-95; ISSN: 0195-6701; IF = 3.926; [<https://doi.org/10.1016/j.jhin.2021.04.022>]

Journal of Hospital Infection 113 (2021) 85–95

Available online at [www.sciencedirect.com](http://www.sciencedirect.com)



Journal of Hospital Infection



journal homepage: [www.elsevier.com/locate/jhin](http://www.elsevier.com/locate/jhin)


Review

### Ventilation design conditions associated with airborne bacteria levels within the wound area during surgical procedures: a systematic review

A. Aganovic<sup>a,\*</sup>, G. Cao<sup>b</sup>, T. Fecer<sup>c</sup>, B. Ljungqvist<sup>d</sup>, B. Lytsy<sup>e</sup>, A. Radtke<sup>f</sup>, B. Reinmüller<sup>d</sup>, R. Traversari<sup>g</sup>

<sup>a</sup> Department of Automation and Process Engineering, The Arctic University of Norway, Norway  
<sup>b</sup> Department of Energy and Process Engineering, Norwegian University of Science and Technology - NTNU, Norway  
<sup>c</sup> Department of Computer Aided Engineering and Computer Science, Faculty of Civil Engineering, Brno University of Technology, Czech Republic  
<sup>d</sup> Department of Civil and Environmental Engineering, Chalmers University of Technology, Sweden  
<sup>e</sup> Department of Medical Sciences, Clinical Microbiology, Uppsala University, Sweden  
<sup>f</sup> Department of Clinical and Molecular Medicine, Norwegian University of Science and Technology, Norway  
<sup>g</sup> Netherlands Organization for Applied Scientific Research, Netherlands

---

<p><b>ARTICLE INFO</b></p> <p><i>Article history:</i> Received 23 February 2021 Accepted 21 April 2021 Available online 27 April 2021</p> <p><i>Keywords:</i> Ultra-clean air Intraoperative airborne contamination Ventilation system Unidirectional airflow (UDAF) Operating room</p> 	<p><b>SUMMARY</b></p> <p>Without confirmation of the ventilation design conditions (typology and airflow rate), the common practice of identifying unidirectional airflow (UDAF) systems as equivalent to ultra-clean air ventilation systems may be misleading, but also any claims about the ineffectiveness of UDAF systems should be doubted. The aim of this review was to assess and compare ventilation system design conditions for which ultra-clean air (mean &lt;10 cfu/m<sup>3</sup>) within 50 cm from the wound has been reported. Six medical databases were systematically searched to identify and select studies reporting intraoperative airborne levels expressed as cfu/m<sup>3</sup> close to the wound site, and ventilation system design conditions. Available data on confounding factors such as the number of persons present in the operating room, number of door openings, and clothing material were also included. Predictors for achieving mean airborne bacteria levels within &lt;10 cfu/m<sup>3</sup> were identified using a penalized multivariate logistic regression model. Twelve studies met the eligibility criteria and were included for analysis. UDAF systems considered had significantly higher air volume flows compared with turbulent ventilation (TV) systems considered. Ultra-clean environments were reported in all UDAF-ventilated (N = 7) rooms compared with four of 11 operating rooms equipped with TV. On multivariate analysis, the total number of air exchange rates (P=0.019; odds ratio (OR) 95% confidence interval (CI): 0.66–0.96) and type of clothing material (P=0.031; OR 95% CI: 0.01–0.71) were significantly associated with achieving mean levels of airborne bacteria &lt;10 cfu/m<sup>3</sup>. High-volume UDAF systems complying with DIN 1946-4:2008 standards for the airflow rate and ceiling diffuser size unconditionally achieve ultra-clean air close to the wound site. In conclusion, the studied articles demonstrate that high-volume UDAF systems perform as ultra-clean air systems</p>
---	---

\* Corresponding author. Address: Department of Automation and Process Engineering, The Arctic University of Norway, Klokkgårdsbakken 35, 9019 Tromsø, Norway.  
E-mail address: [amar.aganovic@uit.no](mailto:amar.aganovic@uit.no) (A. Aganovic).

<https://doi.org/10.1016/j.jhin.2021.04.022>  
0195-6701/© 2021 The Author(s). Published by Elsevier Ltd on behalf of The Healthcare Infection Society. This is an open access article under the CC BY license (<http://creativecommons.org/licenses/by/4.0/>).